NASA Contractor Report 189560
PSI-2090/TR-1140

p. 166

# PROPULSION SIMULATOR FOR MAGNETICALLY-SUSPENDED WIND TUNNEL MODELS

P. B. Joshi, M. R. Malonson, G. P. Sacco, and C. L. Goldey
Physical Sciences Inc.
Andover, MA

K. Garbutt and M. Goodyer
University of Southampton
Southampton, UK



Contract NAS1-18845
January 1992

National Aeronautics and Space Administration
**Langley Research Center**
Hampton, Virginia 23665-5225

(End of notice)

CONTENTS


| | | Page |
|---|---|---|
| 1 | INTRODUCTION | 1 |
| 2 | PROPULSION SIMULATOR DESIGN CONSIDERATIONS | 3 |
| 3 | SMALL-SCALE PROPULSION SIMULATOR DESIGN | 7 |
| 4 | RESULTS OF STATIC TESTING OF SMALL-SCALE SIMULATOR | 11 |
| 5 | LARGE-SCALE PROPULSION SIMULATOR DESIGN | 27 |
| 6 | RESULTS OF STATIC TESTING OF LARGE-SCALE SIMULATOR | 33 |
| 7 | THE UNIVERSITY OF SOUTHAMPTON MSBS | 39 |
| 8 | SYSTEM MODIFICATIONS | 41 |
| 9 | INITIAL SUSPENSION AND DEVELOPMENT | 43 |
| 10 | WIND TUNNEL TESTS | 45 |
| 11 | DATA ANALYSIS AND RESULTS | 47 |
| 12 | THRUST PROFILE AND MAGNETIC SUSPENSION | 49 |
| 13 | RESULTS AND CONCLUSIONS | 51 |
| 14 | RECOMMENDATIONS FOR FUTURE PROPULSION SIMULATOR WORK | 53 |
| 15 | REFERENCES | 55 |
| APPENDIX A: | MASS FLOW AND THRUST REQUIREMENTS FOR WIND TUNNEL MODELS | 59 |
| APPENDIX B: | SMALL-SCALE SIMULATOR TEST MATRIX | 61 |
| APPENDIX C: | LARGE-SCALE SIMULATOR TEST MATRIX | 65 |
| APPENDIX D: | LARGE-SCALE SIMULATOR THRUST AND MASS FLOW ANALYSIS | 67 |




i, ii blank

PAGE INTENTIONALLY BLANK

CONTENTS (Continued)


| | | Page |
|---|---|---|
| APPENDIX E: | PREHEATER THERMODYNAMIC MODEL | 73 |
| APPENDIX F: | SMALL-SCALE SIMULATOR INSTALLATION PROCEDURES | 77 |
| APPENDIX G: | LARGE-SCALE SIMULATOR INSTALLATION PROCESURES | 83 |
| APPENDIX H: | UNIVERSITY OF SOUTHAMPTON MSBS MODIFICATION FINAL REPORT | 87 |

FIGURES


| Figure | | Page |
|---|---|---|
| 1 | Schematic of propulsion simulation on a magnetically suspended model | 2 |
| 2 | Small-scale propulsion simulator design | 7 |
| 3 | Magnetic Mass Distribution in the small-scale simulator | 8 |
| 4 | Large and small piercing pin design for small-scale simulator | 9 |
| 5 | Cylinder and squib retainer arrangement in small-scale simulator | 9 |
| 6 | Schematic of small-scale simulator static testing | 11 |
| 7 | Thrust and pressure time history for baseline configuration without copper plug | 14 |
| 8 | Effect of three sets of 2 mm diameter copper spheres on thrust and pressure time history | 15 |
| 9 | Effect of horizontal simulator orientation on thrust and pressure time history | 16 |
| 10 | Effect of vertical down simulator orientation on thrust and pressure time history | 17 |
| 11 | Effect of increased $co_2$ mass flow rate on thrust and pressure time history | 19 |
| 12 | Effect of copper plug structure on thrust and pressure time history | 20 |
| 13 | Effect of "smaller" pin on thrust and pressure time history | 21 |
| 14 | Effect of exit nozzle diameter on thrust and pressure time history | 22 |
| 15 | Effect of removing copper plug on thrust and pressure time history of large nozzle diameter simulator | 23 |
| 16 | 0.295-in. Nozzle diameter with "small" pin: thrust and pressure time history | 24 |

FIGURES (Continued)


| Figure | | Page |
|---|---|---|
| 17 | Design of large-scale propulsion simulator | 28 |
| 18 | Large-scale propulsion simulator components | 29 |
| 19 | $CO_2$ filling scheme | 31 |
| 20 | Schematic of static test apparatus for large-scale propulsion simulator | 33 |
| 21 | Large-scale simulator static test | 34 |
| 22 | Repeatability of large-scale simulator thrust characteristics | 36 |
| 23 | Effect of under-filling $co_2$ reservoir on thrust characteristics | 37 |
| 24 | Multiple run operation of large-scale simulator | 38 |
| 25 | Electromagnetic configuration for university of southampton msbs | 40 |
| 26 | Axial force calibration at zero angle of attack | 44 |
| 27 | Rocket motor thrust profile (low thrust test) | 44 |
| 28 | Measured and extracted thrust profiles | 48 |
| 29 | Results of simplified prediction of model response to different step thrust impulses | 49 |

# 1. INTRODUCTION

The wind tunnel has been an indispensable tool for aeronautical research and aircraft configuration development for the past 80 years. During that period, tunnels have evolved in speed, increased in size, improved in flow quality, advanced in flow measurement techniques, and become sophisticated in the use of digital computers for data acquisition, reduction, and analysis. Throughout this advancement, the ability of the wind tunnel to faithfully simulate the aerodynamic forces and moments on a model, which can be related to the forces and moments on the full scale aircraft, has always been limited by uncertainties in measurements due to support and wall interference effects. Support interference can lead to significant errors in measured aerodynamic force and moment coefficients and static stability derivatives. These errors become very large at transonic speeds and/or high angles-of-attack. Magnetic suspension and balance systems (MSBS) were developed originally to eliminate the support interference problems. They also have the additional advantages of providing dynamic stability derivatives, two-body force measurements, and improved tunnel productivty. About 25 years ago wind tunnel development shifted emphasis from MSBSs to cryogenic tunnels which can duplicate the full-sale flight Mach and Reynolds numbers simultaneously. This capability has recently become available with the completion of the National Transonic Facility at NASA Langley Research Center (LaRC). Now, the community of experimentalists is advocating the development of MSBSs for large wind tunnels including the cryogenic tunnels. Further impetus for this development has been provided by advancements in the technologies of superconductivity, control systems, and computers.

One of the capabilities desired in magnetic suspension wind tunnels is the simulation of propulsion-induced aerodynamic forces and moments, which arise as a result of interactions between propulsive jets and the free stream. Such a simulation has always been a difficult task, even in conventional wind tunnels. The main reasons have been the problems of introducing high pressure air into the model, questions regarding proper scaling parameters, construction of models out of metric and non-metric sections, and accurately determining the force/moment contribution to the non-metric section. The model support is sometimes an advantage in that it provides a means of bringing air on-board either through ducts which can be secured to the support or through a passage drilled in the support. At times, however, the support can be a disadvantage in that it can prevent the discharge of air at the desired location, as would be the case for a sting support.

Propulsion simulation for magnetically suspended model presents special practical problems because there can be no physical connection between a compressed air reservoir and the model. Thus, propulsive gases must be generated on-board the model and then exhausted at desired locations on the model, Figure 1. The problem involves defining proper thrust (mass flow rate and velocity) requirements for the propulsive jet(s) and accomplishing gas generation within the volume of the model. Propulsion simulation in its entirety, whether for conventional or magnetically-suspended models, involves both engine intake and exhaust jet flows. Only the latter is addressed in the work presented here. Our rationale is that the first step in simulation of propulsion should be to introduce the effects of the exhaust jet and that the complexities of allowing properly matched inlet flows should be deferred to later stages of development.

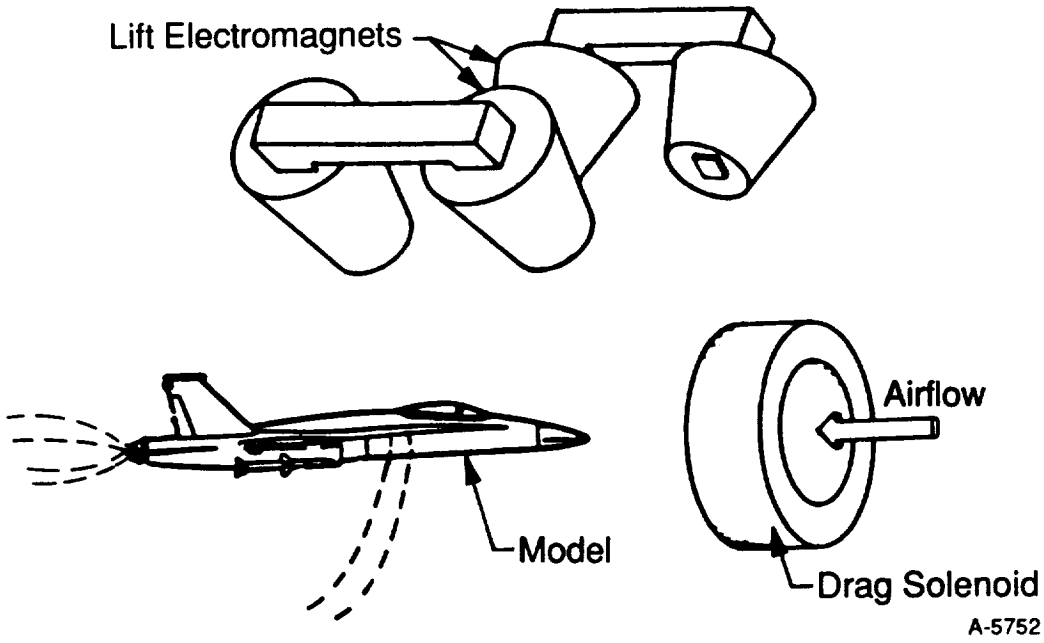


Figure 1. - Schematic of propulsion simulation on a magnetically suspended model.

Under Phase I of an investigation sponsored by NASA LaRC, the feasibility of generating exhaust jets of appropriate characteristics on-board magnetically-suspended models was examined. Four concepts of remotely-operated propulsion simulators were considered. Three conceptual designs involving conventional technologies such as compressed gas cylinders, liquid monopropellants, and solid propellants were developed. The fourth concept, a laser-assisted thruster, which can potentially simulate both inlet and exhaust flows, was found to require very high power levels (tens of kilowatts). This concept needs further research. The results of Phase I investigation, including a comparative evaluation of the four concepts, are discussed in ref. 1.

The objective of current Phase II investigation sponsored by NASA LaRC was to demonstrate the measurement of aerodynamic forces/moments, including the effects of exhaust jets, in MSBS wind tunnels. Two propulsion simulator models were developed, a small-scale and a large-scale unit, both employing compressed, liquified carbon dioxide as propellant. The small-scale unit was designed, fabricated, and statically-tested at Physical Sciences Inc. (PSI). It was tested in the 7-in. University of Southampton MSBS tunnel to measure forces/moments with jet on/off. The MSBS hardware and software was modified for this purpose to be compatible with the impulsive thrust forces associated with propulsive jets. The large-scale simulator was designed, fabricated, and statically-tested at PSI.

This report is in three parts. The first part presents design/development and static test data for the small-scale and large-scale simulators. The second part describes the modifications to the University of Southampton MSBS and results of the wind tunnel tests with the small-scale simulator. The third part of the report contains the figures referenced in Parts I and II. The paper concludes with recommendations for future developments including applications to conventional aeropropulsive testing.

## 2. PROPULSION SIMULATOR DESIGN CONSIDERATIONS

Before describing the small-scale simulator, it is appropriate to discuss the design requirements. Since the existing MSBS wind tunnels (ref. 2) allow the installation of relatively small models, a very limited volume is available for a propulsion device. Further, the magnetic core used for levitation also needs some space within the model, and the restrictions on the size of the propulsion simulator can indeed be significant. The largest operational MSBS wind tunnel in the U.S. at NASA LaRC has a 13-in. diameter test section. Another MSBS facility at University of Southampton, England, which is more versatile in that it has angle-of-attack variation capability, has only a 7-in. wide test section. In this wind tunnel, the model envelope would typically be 6 to 8-in. in length with 1 to 1.5-in. diameter centerbody. In the NASA tunnel, models 18-in. long by 3-in. diameter can be installed.

Since no external connections can be made to bring jet fluid to a model in an MSBS, the propellant must be carried on-board. The model volume limitations directly translate into the mass of the propellant which can be stored on-board. In turn, this limits the duration over which the exhaust jet can be maintained. For practical applications, this means frequent model refurbishing and thus potentially reduced tunnel productivity with propulsion simulation.

Because no physical connections exist with a magnetically-levitated model, it is necessary to control the propulsive model remotely. Therefore, the source of electrical energy required to open/close valves or initiate ignition must be carried on-board and triggered externally by such means as radio control or laser.

The characteristics of a particular MSBS also impose some restrictions on the propulsion simulator. These are the weight of the simulator module which can be suspended and the level of the thrust force. The restrictions arise due to the limitations on the amount of current which can be driven through the coils of the external electromagnets (Figure 1). Another consideration is that the model position changes due to the thrust rise (or fall) with time, when propulsion is turned on (or off). This movement must be controllable by the control system of the MSBS.

Finally, any propulsive gas generation technique must be compatible with the particular wind tunnel hardware involved and its operational requirements. Even small quantities of particulate matter or water vapor in the exhaust may not be acceptable in some facilities. Furthermore, there may be considerations of safety of personnel, requiring special precautions in some cases.

The design considerations are summarized in Table 1. The implementation of these requirements into the simulator design is discussed in Ref. 1.

Perhaps the simplest propulsion simulator is a compressed gas cylinder attached to a nozzle and turned on/off by means of a remotely-controlled valve. However, the mass of

TABLE 1. GENERAL DESIGN CONSIDERATIONS FOR PROPULSION SIMULATORS

| | |
|---|---|
| • Compactness | Smallest size possible for demonstration in current available MSBS tunnels |
| • High Density Propellant | Ability to carry the largest propellant mass in a given volume inside the model to maximize run time for a specified mass flow rate |
| • Relatively Lightweight | To minimize the size of magnetic core within the model and currents in external electromagnets |
| • Remote or Minimum Interference Activation | If remote activation is not feasible, the disturbance to flow field and magnetic field must be negligibly small |
| • Thrust Level | Compatible with particular MSBS capability |
| • Thrust versus Time Characteristics | Compatible with MSBS control system capability. Stable thrust duration must be sufficiently long so that data can be obtained after model becomes steady |
| • Safe Operation | Propellant material should be non-toxic, non-corrosive, with minimum of particulates |

gas which can be carried under reasonable pressures in volumes typical of a MSBS wind tunnel models, is so small that the resulting thrust time (or run time) will be of the order of tens of milliseconds. Furthermore, the gas container will have to be refilled under high pressure innumerable times, which makes this approach impractical. A way around this problem is to use gases that liquify easily under pressure at room temperature, so that a significantly larger mass can be stored in a given volume. Among common substances, the candidates are carbon dioxide ($CO_2$) and ammonia ($NH_3$). Table 2 lists the physical properties of these gases along with another substance, sulfur dioxide ($SO_2$) which has some desirable properties.

TABLE 2. PHYSICAL PROPERTIES OF PROPELLANT GASES

| Gas | Molecular Weight | Vapor Pressure at 70°F (psi) | Density of Liquid ($gm/cm^3$) | Heat of Vaporization (cal/gm) |
|---|---|---|---|---|
| $CO_2$ | 44 | 840 | 0.75 | 36 |
| $NH_3$ | 17 | 129 | 0.61 | 283 |
| $SO_2$ | 64 | 50 | 1.38 | 83 |

The ideal propellant gas should have a high density in liquid phase to pack as large a mass as possible in a given volume and a low molecular weight (see Appendix A). Low heat of vaporization is desired so that, as the liquid changes into vapor, it does not draw such a large amount of heat from itself and surrounding walls that it freezes. Low vapor pressure is also desirable, because it means that liquification occurs at lower pressure at a given temperature. Thus, the pressure regulation necessary to drop the pressure to say 45 to 60 psia ($P_{0j}/p_\infty$ = 3-4) is relatively straightforward. That is, compact regulators, necessary in the present application, are easy to find.

An examination of Table 2 shows that each gas has certain advantages and disadvantages. Ammonia has the lowest molecular weight and reasonably low vapor pressure, but it has extremely high heat of vaporization and the lowest density. Sulfur dioxide, on the other hand, has the lowest vapor pressure and highest density (38 percent above water), but the latter is offset by its high molecular weight. The heat of vaporization of $SO_2$ is considerably lower than that of $NH_3$. Carbon dioxide has a molecular weight between that of $NH_3$ and $SO_2$, the lowest heat of vaporization, and density slightly higher than that of ammonia. A disadvantage of $CO_2$ is its high vapor pressure (56 atm).

There are some practical advantages of $CO_2$ that make its choice as a propellant almost inevitable. It is commercially available in cartridges (or cylinders) which vary in weight from a few grams to hundreds of grams. The cylinders are very compact, a cylinder containing 16g of $CO_2$ measures 3.5 in. long $\times$ 0.865 in. diameter, a 60g cylinder measures 5.1 in. long $\times$ 1.6 in. diameter. As these cylinders have wide commercial applications (air guns, life vests, inflatable boats, beverage industry), they are available in any desired quantity at a very low cost. For example, the price of a 16g $CO_2$ cylinder is less than \$2. Another advantage of these cylinders is that they are available in stainless steel (which is non-magnetic) or as magnetizable steel. This is potentially useful because the mass of the cylinder itself can serve as a part of the magnetic core. $CO_2$ cylinders can be obtained as customized components from Sparklet Devices, Inc.

$CO_2$ also has some operational advantages over $NH_3$ and $SO_2$. In practice, the mass flow rate of the gases will be small ($<100$ g/s) compared to that in the wind tunnel ($\sim 2$ kg/s in University of Southampton 7-in. tunnel and 7 kg/s in NASA LaRC 13-in. tunnel) and the duration will be typically less than 5s for one thrusted run. Thus the propellant gases will get quickly mixed, diluted, and dispersed in the wind tunnel-free stream. In open circuit tunnels, of course, the products will leave the test section and not be circulated. $CO_2$ is a clean, non-contaminating, non-corrosive, and safe gas. $NH_3$ and $SO_2$ on the other hand are somewhat corrosive, and can be irritants to eyes and lungs, if released accidentally. The use of these gases then entails special precautions not necessary to $CO_2$.

Some disadvantages of the compressed gas concept are that miniaturized, remotely operated valves are required to turn the jet on/off, and further, a battery power supply and switch must be incorporated in the model. An inherent limitation of the concept is that the total temperature of the jet is close to room temperature. Therefore, a hot jet is not possible unless heat is added before exhausting the gas, which represents an additional complication.

The problem of cooling of the cylinder as the liquid vaporizes can be minimized by surrounding the cylinder with an annular magnetic core which can provide the necessary thermal mass.

It is shown in Appendix A that the thrust and mass flow ranges for a propulsive jet on a typical 1/40-scale model of a fighter aircraft are 2.5 to 3.2 kgf and 0.08 to 0.01 kg/s of $CO_2$ gas, respectively.

The primary objective of the present work was to demonstrate the operation of a thrusting, propulsive model in an MSBS, and to measure the resulting forces/moments. The University of Southampton wind tunnel to be used for testing has a 7-in. octagonal test section. The small test section size and the desire to achieve high angles of attack ($\sim$45 deg), limits the model size. This limitation, in turn, restricts the number and the size of flow control components (a pressure regulator, an on/off solenoid valve, for example) that can be incorporated into the model. It was decided, therefore, to design and build two models: a small-scale simulator for demonstration in an MSBS and a large-scale simulator for static testing only. The small-scale model was developed principally to (1) demonstrate generation of an exhaust jet using $CO_2$ propellant, (2) guide in the design of the large-scale unit, and (3) verify the control and force/moment measurement of a thrusted model in the Southampton MSBS. The larger model was developed to: 1) generate exhaust jets of desired characteristics; and 2) demonstrate the feasibility of propulsion simulation on larger wind tunnel models representative of practical applications.

The large-scale simulator was a designed to generate a jet with pressure ratio, mass flow, and thrust requirements outlined in Appendix A. This design permits intermittent, on/off operation of the jet. By contrast, the small-scale simulator was designed to be such that the propellant and some components must be replaced after every jet "run". No attempt was made to tailor the jet characteristics to the requirements of Appendix A for the small-scale device.

## 3. SMALL-SCALE PROPULSION SIMULATOR DESIGN

Figure 2 shows the small-scale simulator design which is a 1-1/8-in. diameter cylinder, 8-in. long, with hemispherical ends. The principal components are a 16g, liquified $CO_2$ cylinder (manufactured by Sparklet Devices), a cap-piercing hardened pin and squib mechanism (adapted from a design by Special Devices, Inc. (SDI)), battery and electronics assembly housed in the nose, three removable sets of copper spheres, and a nozzle. These components are housed inside a tube, 1/8-in. thick, made from an electromagnetic alloy formulated by Connecticut Metals, Inc. (CMI). The total weight of the simulator is about 600g with approximately 500g of magnetizable materials. The latter includes the material of the $CO_2$ cylinder and other miscellaneous components such as retainer rings, fasteners, spacers, etc. Figure 3 shows the distribution of the magnetizable mass in the simulator.

The simulator consists of three major subassemblies: nose section, center section, and nozzle section. The nose section, which screws onto the center section, contains the battery (Kodak K28A) used as a power source for firing the squib (made by Cartridge Actuated Devices, Inc.) and the electronics assembly. The latter consists of a light-activated switch (EG&G, VTIC1110), a small mirror, and a silicon controlled rectifier, all mounted on a 0.06-in. thick circuit board. The battery is held inside a retaining clamp onto which the circuit board is mounted. An optical filter is embedded in the wall of the nose section. The filter allows HeNe laser wavelength (632.8 nm) to pass to the light activated switch. A pair of 22 AWG wires runs from the circuit board to the squib in the center section.

The center section of the simulator contains the $CO_2$ cartridge with its threaded neck screwed into a cylinder retainer which is held in place by a squib retainer. The pin-squib mechanism (made by SDI) is screwed into the threaded hole at the center of the squib retainer. The SDI design was modified such that inexpensive squibs made by Cartridge

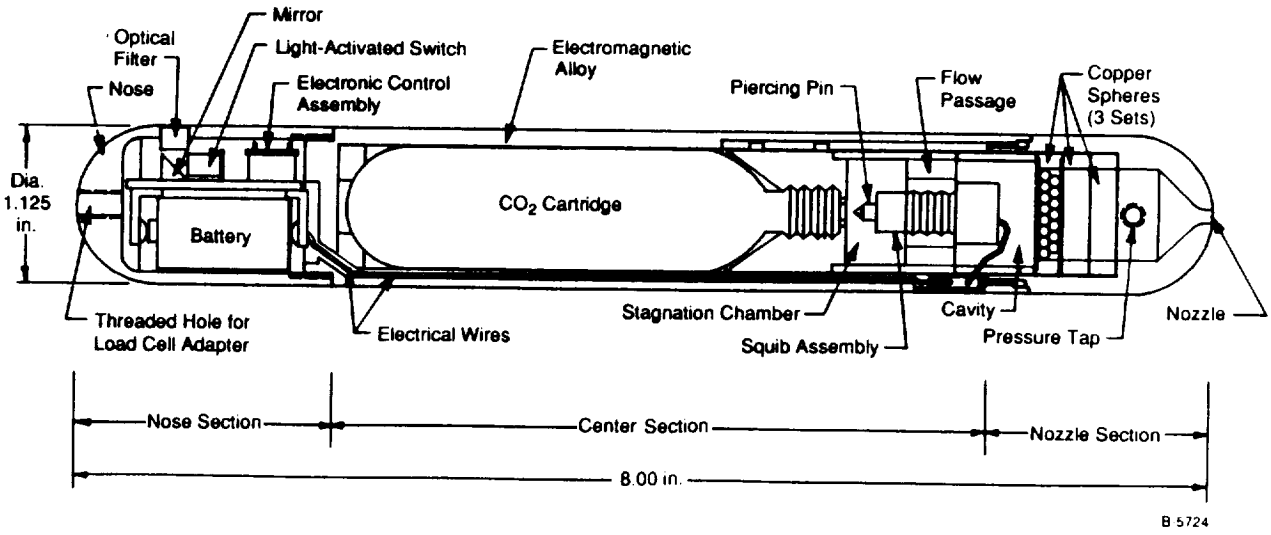


Figure 2. - Small-scale propulsion simulator design.

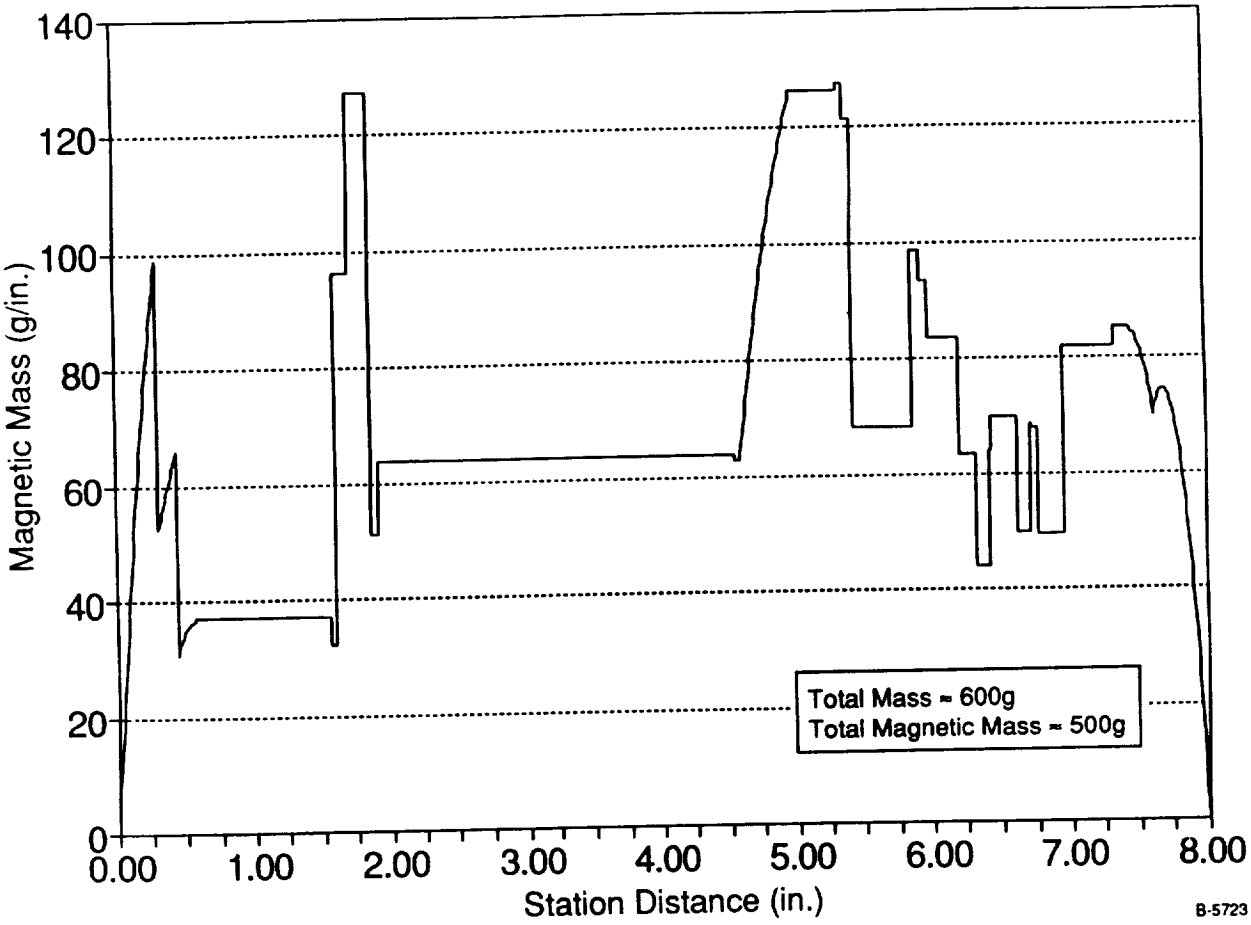


Figure 3. - Magnetic mass distribution in the small-scale simulator.

Actuated Devices could be incorporated into it. Had this modification not been done, the complete SDI pin/squib mechanism would have required replacement after each firing, costing about $150. Our design modification makes it possible to replace the squib only, for approximately $5 to $10. Earlier in the program, the "standard" piercing pin in the SDI component was used. This pin (also called "large" pin) as shown in Figure 4(a), had an internal hollow passage 0.050-in. diameter to draw $CO_2$ from the cylinder. Two holes, 0.050-in. diameter, in the 0.045-in. thick walls of the standard pin, expel the $CO_2$ into a stagnation chamber. The gas then flows from the chamber into a cavity surrounding the squib assembly through four oval passages drilled into the squib retainer (Figure 5). Another pin, with smaller outside and inside diameters, and with smaller ports for expelling $CO_2$, was also used during development, Figure 4(b). Both pins were case-hardened to ensure reliable penetration of the diaphragm of the $CO_2$ cylinder. Moreover, hardening also improved the usable life of the firing pin. Two holes (not shown in Figure 2) are drilled into the wall of the center section for measuring pressure in the stagnation chamber and in the cavity upstream of the nozzle section. The two 22 AWG wires connecting the squib to the electronics in the nose section pass through a lengthwise groove machined in the wall of the center section.

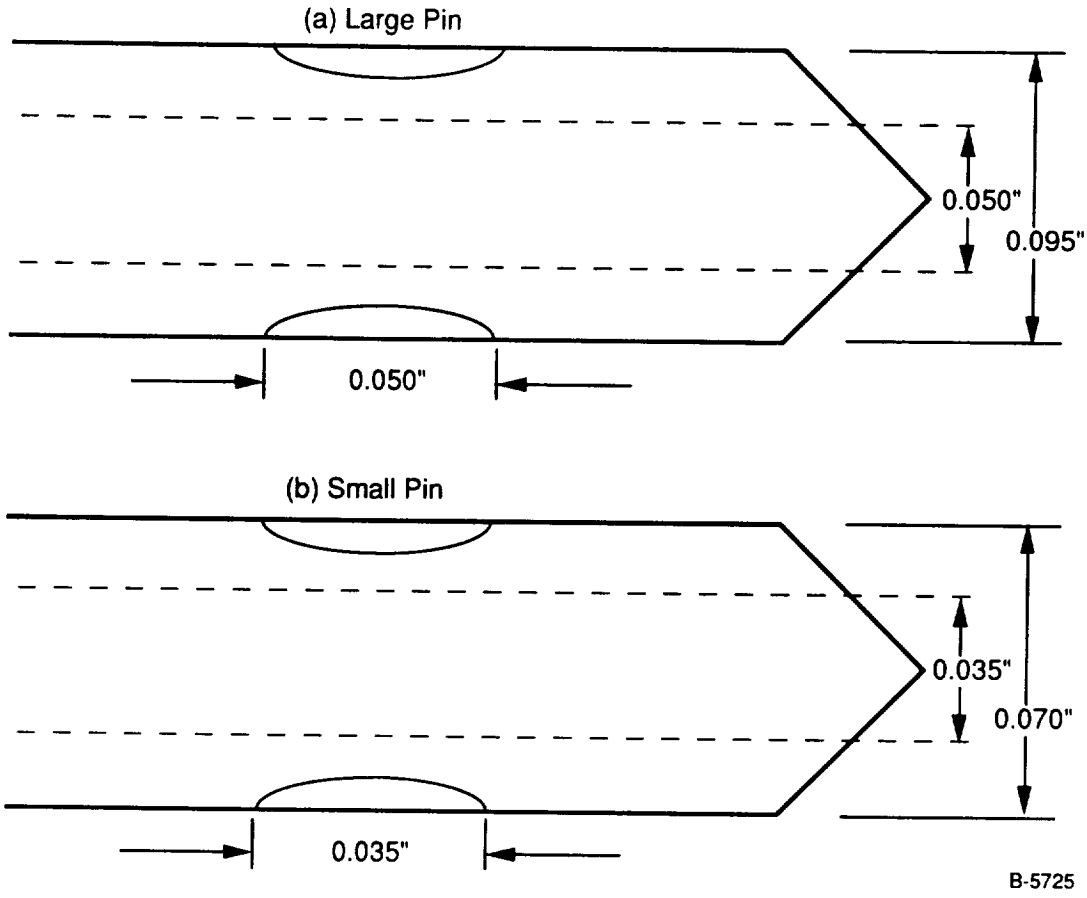


Figure 4. - Large and small piercing pin design for small-scale simulator.

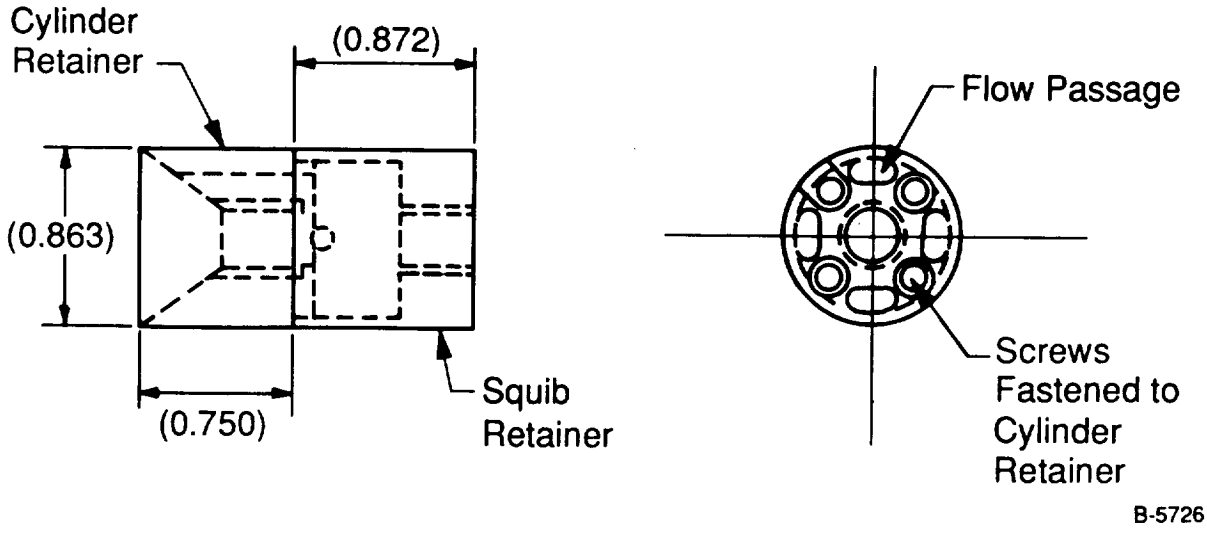


Figure 5. - Cylinder and squib retainer arrangement in small-scale simulator.

The nozzle section screws onto the back end of the center section of the simulator. It contains three baffle assemblies which can be loaded with copper spheres of 1 or 2 mm diameter. Each assembly consists of a copper housing (a ring as shown in Figure 2) with a copper wire mesh at each end for retaining the spheres. Each assembly can be individually removed and replaced by a ring made of the CMI electromagnetic alloy. The purpose of the three copper plugs was to introduce a drop in total pressure as the $CO_2$ negotiated a tortuous path, and secondly, to vaporize any fine solid particles of $CO_2$ which may be present in the flow. As will be discussed later, the copper plugs were not always effective. A convergent passage was drilled into the nozzle with a baseline diameter of 0.098 in. A separate nozzle section with exit diameters of 0.298 in. was also used. Both nozzle sections were tested. The larger nozzle, used on a 1/40-scale model, corresponds to 12-in. full-scale throat diameter. A pressure tap was drilled into the nozzle wall downstream of the copper plugs and upstream of the exit orifice.

The operation of the small-scale simulator consists of shining a HeNe laser beam onto the optical filter in the nose section. The light switch is activated and the SCR then draws approximately 1 amp current from the battery to fire the squib. Explosion of the squib drives the pin (which moves against O-ring friction) into the diaphragm which caps the $CO_2$ cylinder. Only about 45 psi pressure is needed to rupture the diaphragm and the squib supplies 70 to 150 psi from the gaseous products of explosion. After penetration the pin stays in place due to the friction of the O-ring inside the housing of the SDI squib assembly. $CO_2$ liquid-gas mixture flows through the center passage in the pin and escapes through the two holes drilled in the walls (Figure 4). Upon passage through the squib retainer (Figure 5), the $CO_2$ flows through the copper plug(s) into the nozzle chamber and out through the orifice producing a jet.

## 4. RESULTS OF STATIC TESTING OF SMALL-SCALE SIMULATOR

As mentioned under Design Considerations, the small-scale model was developed primarily to verify the control of and force/moment measurement on an impulsively-thrusted model in an MSBS and to guide in the design of the large-scale unit. Toward these objectives, a series of static tests was conducted. The tests were designed to yield thrust versus time history and pressure versus time history, the latter at three locations within the simulator. The thrust versus time data are necessary for design of the MSBS control system so that the model stays in place as it reacts to the propulsive jet turning on/off. The pressure data, which are diagnostic in nature, provide important insight into the effectiveness of the copper plug(s) in creating a pressure drop and into the gas dynamic processes within the simulator.

The schematic of the static-test set-up is shown in Figure 6. A load cell manufactured by Sensotec was used to obtain force (i.e., thrust) data. The pressure

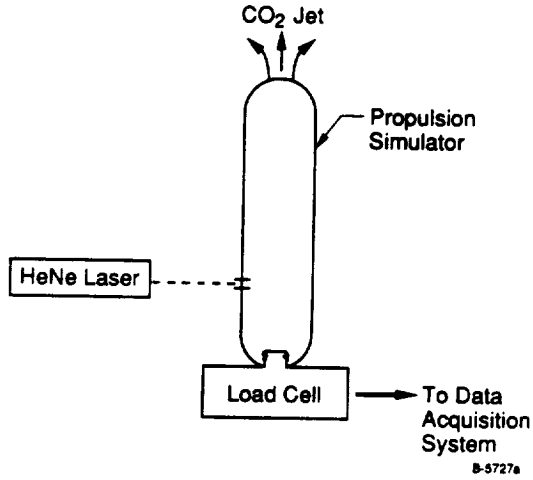


(a) Thrust Measurements

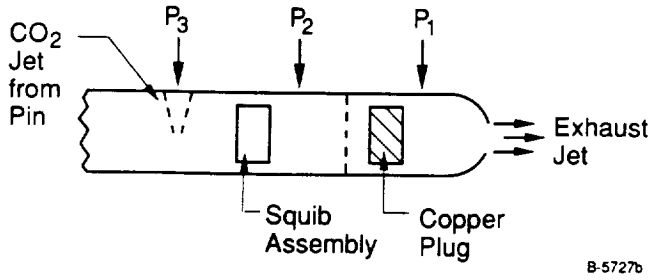


(b) Pressure Measurement

Figure 6. - Schematic of small-scale simulator static testing.

transducers were supplied by D.J. Instruments and located as shown in Figure 6(b). The pressure $P_2$ and $P_1$ give a measure of the effectiveness of the copper spheres in creating a pressure drop. The pressures $P_2$ and $P_3$ give a measure of the gas dynamic processes and losses due to jet impingement on the cylindrical walls of the simulator. The load cell and transducer signals were sampled at 1 kHz. Visual observations of the jet just outside the nozzle exit plane indicated whether or not mist was present. The presence of mist shows that the copper spheres were not very effective in vaporizing the tiny solid particles formed during the expansion of $CO_2$ from compressed liquid to vapor.

The test variables were:

- Simulator orientation:

In the vertically-up orientation shown in Figure 6(a), vapor rather than liquid is being drawn through the pin upon its penetration into the $CO_2$ cylinder. In a vertically-down configuration, one expects the liquid to be drawn through the pin, and the vaporization to take place in the stagnation chamber (pressure $P_3$ in Figure 6(a)). Of course, in practice, the simulator will be used mostly in a horizontal position or with the jet pointing downward, except in few instances of negative angle-of-attack. The effects of simulator orientation, therefore, are expected to be important. Static tests were conducted in all three orientations.

- Copper plug structure:

The copper plug(s) were introduced in the small-scale simulator to act as a pressure-drop device and also to aid in vaporizing small solid particles in the $CO_2$ stream. The data on effectiveness of the plug in performing these functions were necessary to guide the design of the large-scale simulator. For example, a pressure regulator and/or a heater (i.e., vaporizer) were considered, as the copper plugs were found not to be very effective.

- Pin design:

The internal passage diameter of the piercing pin (Figure 4) determines the maximum possible mass flow rate through the propulsive device and thus its internal pressure and thrust versus time characteristics. Tests were conducted using a so-called "standard" or "large" pin, Figure 4(a), and a "small" pin, Figure 4(b).

- Nozzle diameter:

The nozzle diameter determines the actual mass flow rate through the simulator and thus thrust level duration. Further, the nozzle area is an important design parameter of the aircraft configuration being tested. Two values of diameter, 0.098 and 0.295, were used in the static tests.

Selected data from the simulator tests are presented in Figures 7 through 16. Each figure contains thrust and pressure versus time history. The three pressures, $P_1$, $P_2$, and $P_3$ are given on the same plot. Appendix B contains the small-scale simulator test matrix.

Figure 7 shows thrust and pressure curves for the baseline simulator configuration without any copper plugs. After an initial spike which reaches 4 lbf, the thrust rises to a maximum of about 1.9 lbf in about 0.1s and decreases gradually over the next 1.2s. An average thrust of about 1 lbf over a duration of 0.5s is achieved. The rise in thrust is due to the increase of pressure as the $CO_2$ fills up the simulator volume. The fall in thrust thereafter is directly due to the dropping stagnation pressure inside the simulator as the $CO_2$ escapes through the nozzle. The thrust behavior correlates well with the pressure history in Figure 7(b). The pressures $P_2$ and $P_3$ are coincident in this figure. Unfortunately, the $P_1$ transducer was overpressurized and saturated during this run. The initial spike in Figure 7(a) is a ubiquitous feature of most thrust data. It represents the impact of the piercing pin on the diaphragm of the $CO_2$ cylinder. The duration of this spike is a few milliseconds. It should also be pointed out the time elapsed from the instant that the laser triggers the light-activated switch to the instant the pin impacts the cylinder is of the order of 20 to 50 ms. This interval includes the electronics reaction time and the firing of the squib.

Figure 8 shows thrust and pressure histories when three sets of copper plugs, each packed with 2 mm diameter copper spheres, are placed upstream of the nozzle. A comparison of Figures 7 and 8 shows that the thrust curves are nearly the same and the pressures are also substantially similar. Thus, for the simulator with a large (or standard) piercing pin, the copper plug has little effect on the flow and pressures inside the simulator.

Figures 9 and 10 show the effect of simulator orientation on thrust and pressure characteristics. In Figure 9, the simulator was horizontal and incorporated the same copper plugs as the configuration in Figure 8. The peak thrust in the horizontal orientation is slightly higher and falls off somewhat faster than the vertically-up orientation of Figure 8. The data in Figure 9 is also more noisy and is believed to be an artifact of the simulator cantilevered from the load cell. The pressures in Figure 9(b) are seen to be greater than those in Figure 8(b), which explains the thrust behavior. Figure 10 shows data for the simulator firing the jet vertically down. The copper plugs are the same as for Figures 8 and 9. A comparison between Figure 8 and Figure 10 reveals that the thrust is substantially higher when liquid $CO_2$ is drawn because greater mass of $CO_2$ enters the stagnation chamber in a given time. Further, the thrust maintains its higher level for about 0.5s before beginning to drop-off rapidly. This behavior suggests that the liquid $CO_2$ escaping into the stagnation chamber of the simulator (Figure 2) vaporizes. During this process, liquid-vapor equilibrium is maintained, and the pressure tends to remain constant. However, the pressure drops as the $CO_2$ vapor leaves through the nozzle. The net effect of these two opposing processes is to reduce the rate at which pressure and thrust drop. A comparison of Figures 10(b) and 8(b) shows higher pressure for the vertically-down orientation. Also, the behavior of pressure with respect to time in Figure 10(b) explains the thrust history in Figure 10(a).

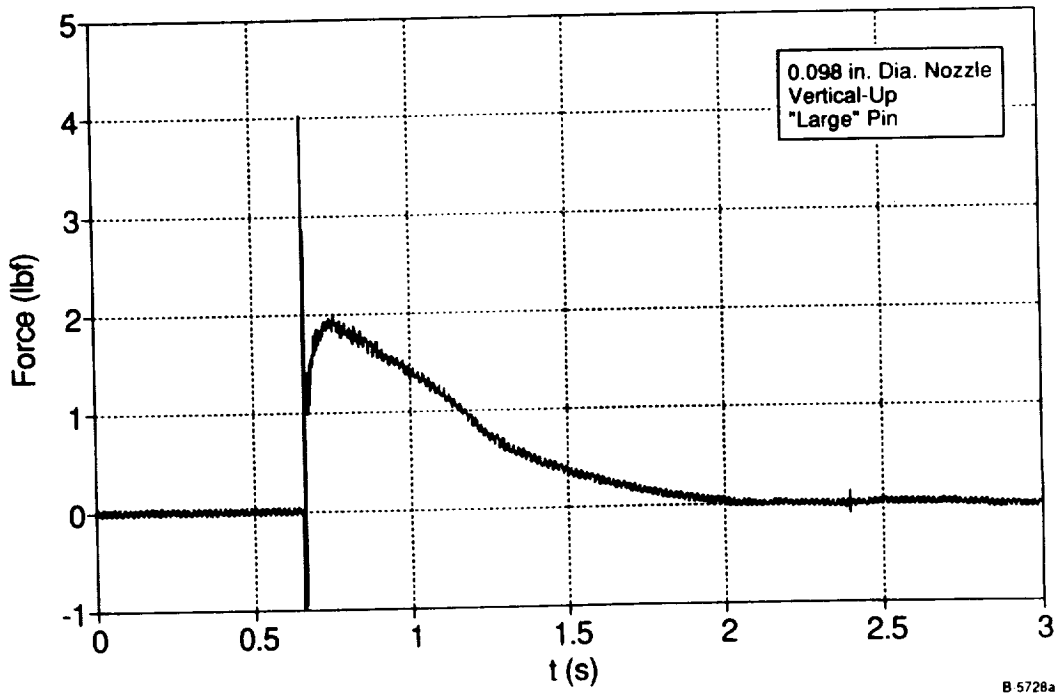


(a) Thrust versus Time

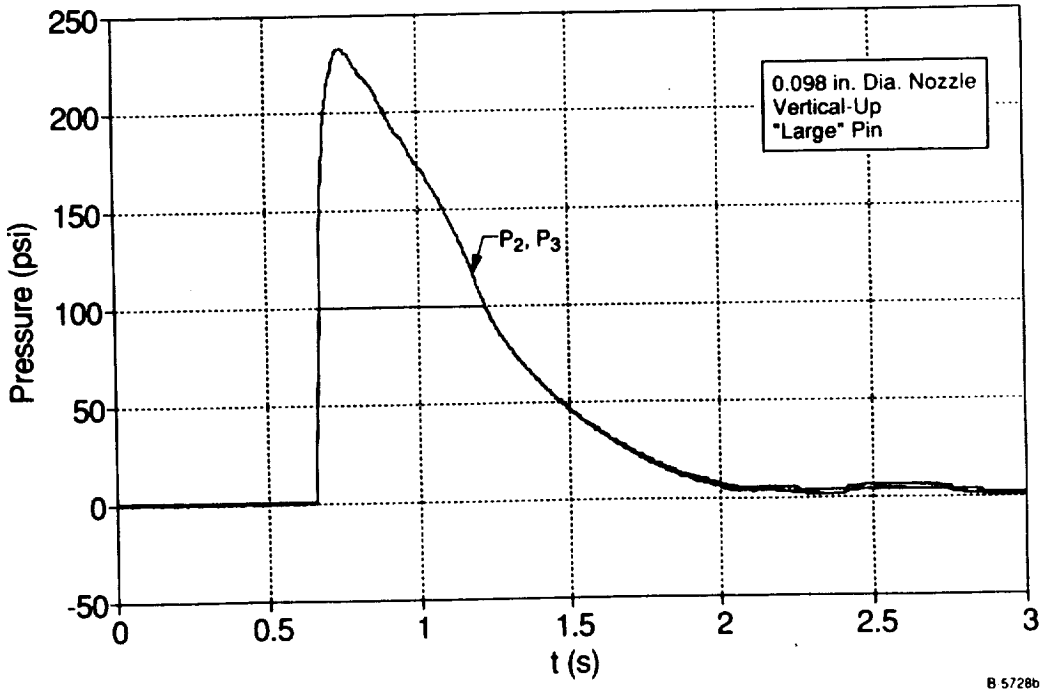


(b) Pressure versus Time

Figure 7. - Thrust and pressure time history for baseline configuration without copper plug (large pin, 0.098-in. diameter nozzle, vertical up orientation).

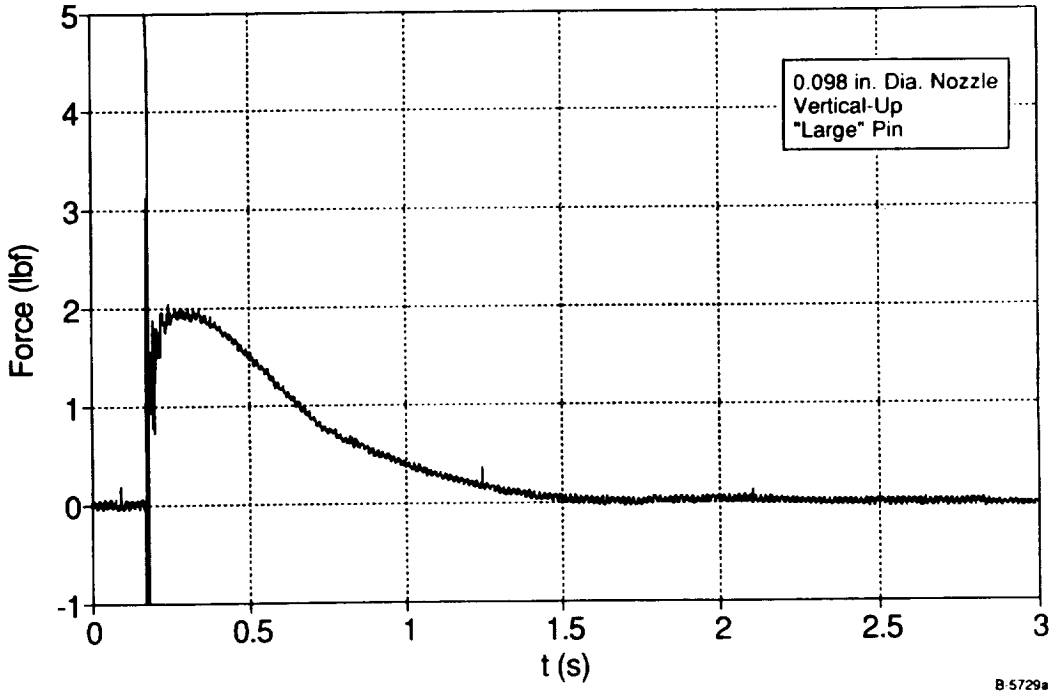


(a) Thrust versus Time

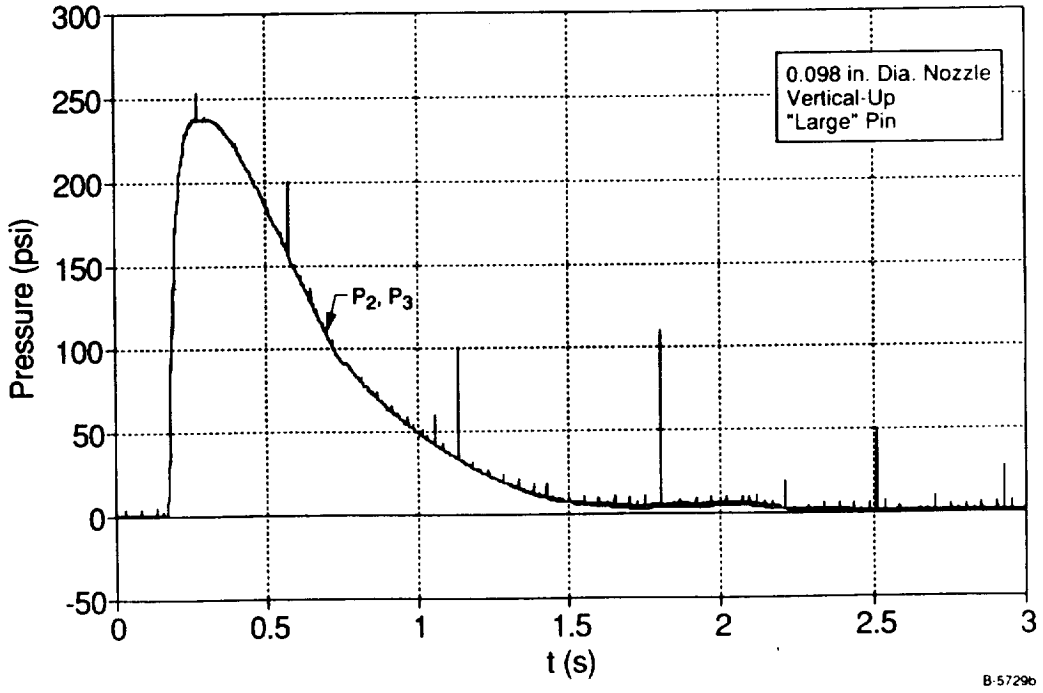


(b) Pressure versus Time

Figure 8. - Effect of three sets of 2 mm diameter copper spheres son thrust and pressure time history (large pin, 0.098-in. diameter nozzle, vertical up simulator orientation).

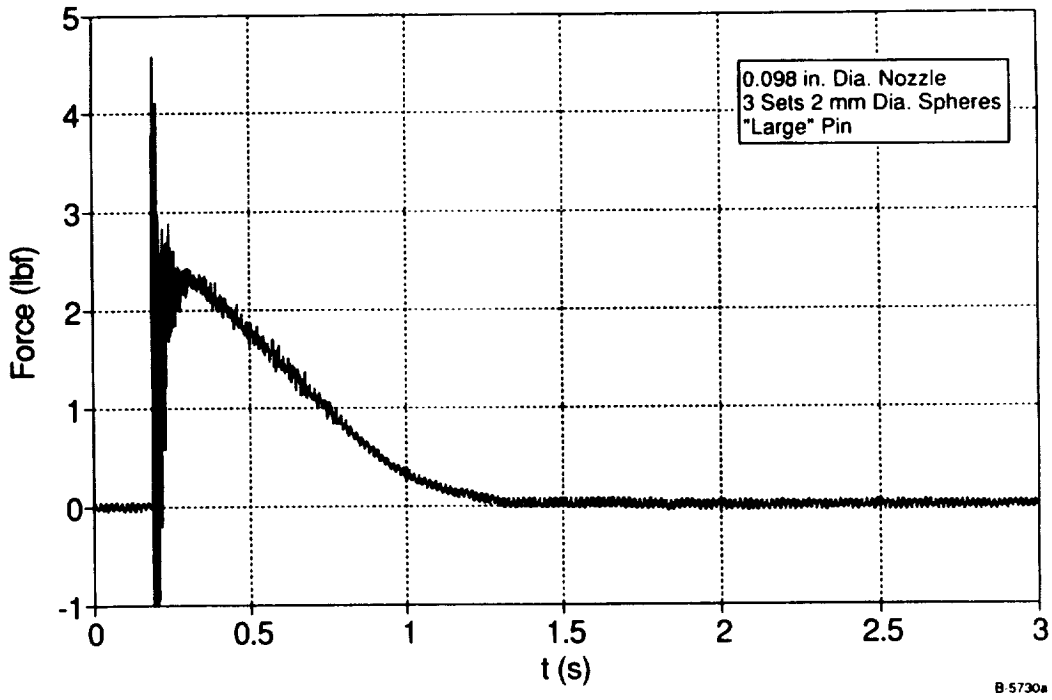


(a) Thrust versus Time

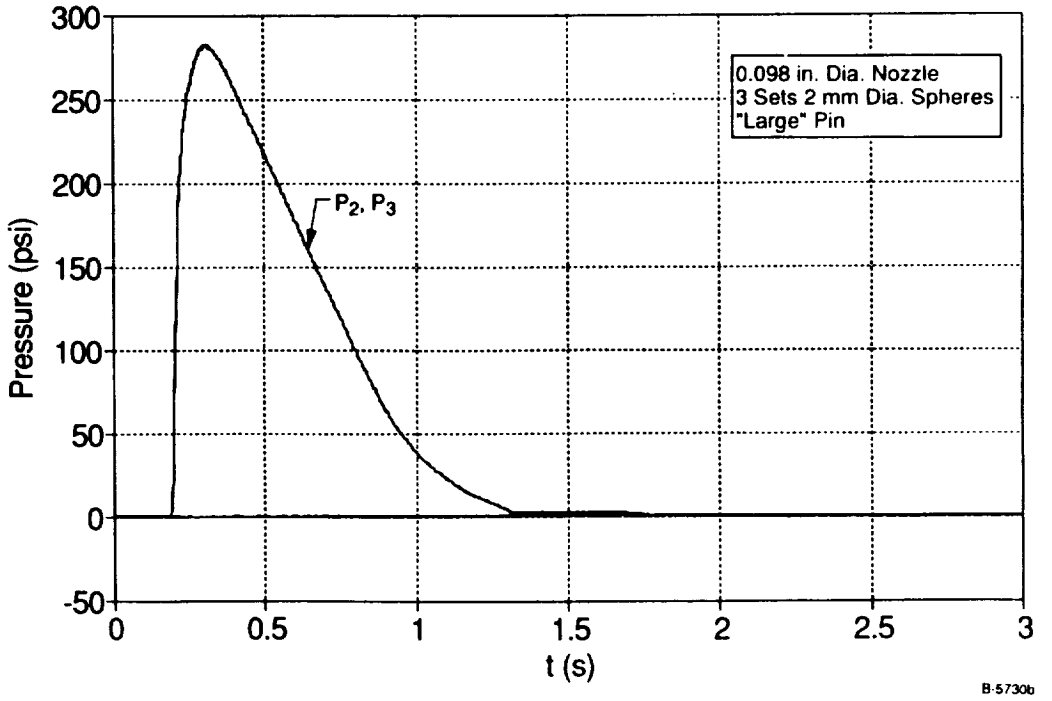


(b) Pressure versus Time

Figure 9. Effect of horizontal simulator orientation on thrust and pressure time history (large pin, 0.098-in. diameter nozzle, three sets of 2 mm copper spheres).

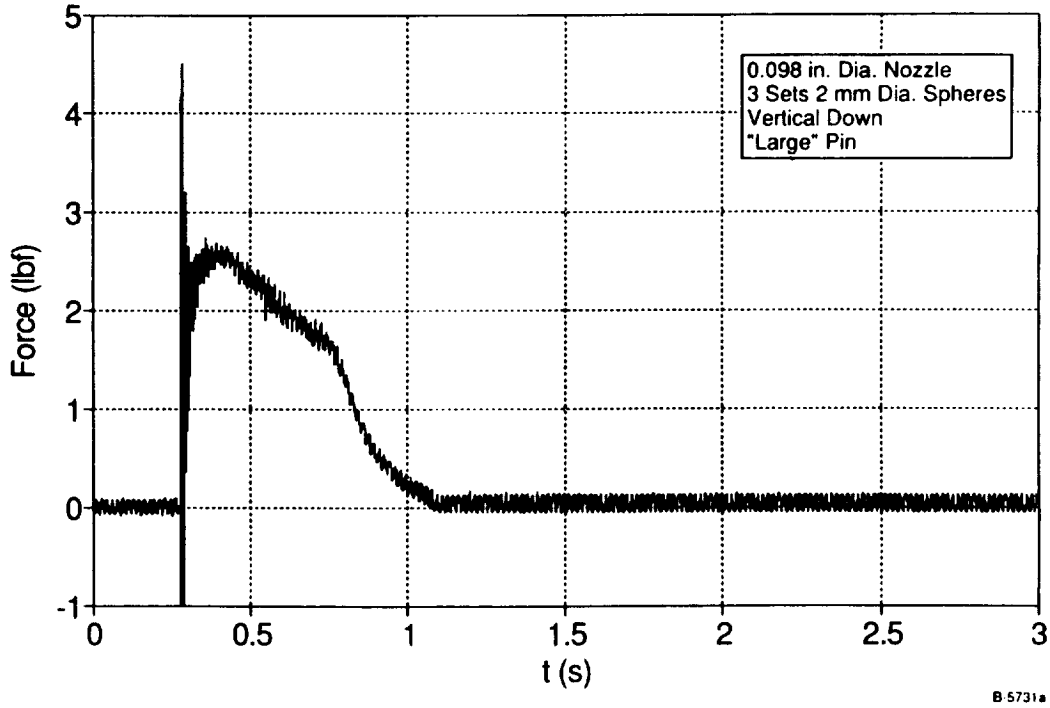


(a) Thrust versus Time

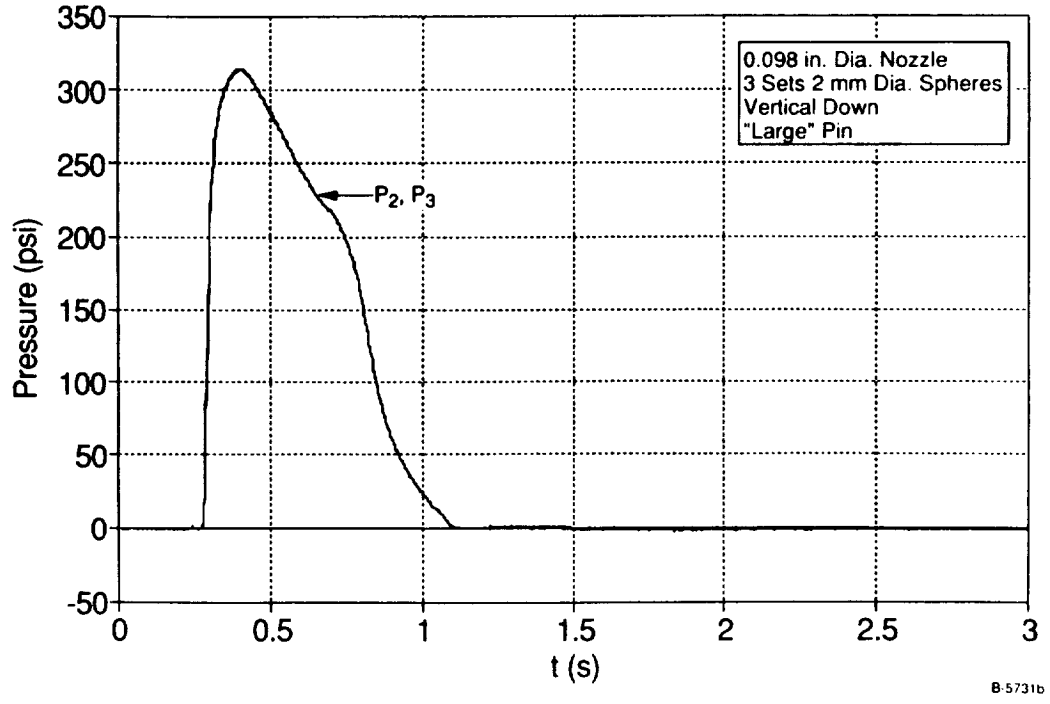


(b) Pressure versus Time

Figure 10. Effect of vertical down simulator orientation on thrust and pressure time history (large pin, 0.098-in.diameter nozzle, three sets of 2 mm copper spheres)

Figure 11 shows an interesting observation when the $CO_2$ mass flow rate into the stagnation chamber is extremely high. This condition occurred when the piercing pin was pushed back (due to the wear of an O-ring in the squib assembly) by the high pressure $CO_2$, resulting in efflux through a larger area (0.095-in. diameter) than the normal two-hole configuration (0.05-in. diameter each), Figure 4. The consequence is very high peak thrust, ~5 lbf which drops off rapidly, Figure 11(a). The pressure has now reached a very high value, almost 600 psi, Figure 11(b).

Figure 12 illustrates the effect of changing the copper plug arrangement to one set of 1 mm diameter copper spheres and tightly packed bronze wool replacing the other two sets. Comparison with Figure 8 shows the thrust and pressure histories to be very similar in both cases. Thus, the structure of the plug has very little effect on the flow processes within the simulator. Note in Figure 12(b) that the three pressures, $P_1$, $P_2$, and $P_3$ at different locations (Figure 6) are very close. This indicates that with the 0.098-in. diameter exit nozzle, the simulator behaves essentially like a closed vessel which is pressurized by the $CO_2$, maintaining pressure equilibrium throughout its volume. This would explain the ineffectiveness of the copper plug observed thus far.

Figure 13 shows the effect of reducing the mass flow rate from the $CO_2$ cylinder by using the "small" pin design of Figure 4(b). Comparison with Figure 12, which presents data for the large pin in Figure 4(a), reveals lower thrust level and longer duration with the small pin, as one would expect. The peak thrust is approximately 1.4 lbf and the average thrust is about 0.75 lbf over 0.75s. The pressures with the small pin (Figure 13(b)) are correspondingly lower in comparison with the large pin (Figure 12(b)).

Figure 14 through 16 contain data of the case of a larger nozzle diameter (0.295 in.) with both the large and small piercing pins. With the standard, large pin, the thrust in Figure 14(a) may be compared with Figure 12(a). As one would expect, with a larger nozzle, the pressures are lower (Figures 14(b) versus 12(b)) and the thrust is lower, but it drops off at a slower rate. The slower rate is due to reduced mass flow rate through the nozzle, resulting from lower (i.e., subsonic) pressure ratio relative to the ambient. The effect of removing the copper plug with the 0.295-in. diameter nozzle on the simulator is to decrease significantly the thrust as seen from Figure 15(a), indicating that the plug, rather than the nozzle, was the controlling area for the mass flow rate. The pressures throughout the simulator volume, especially upstream of the nozzle, are low (and noisy), Figure 15(b). Finally, Figure 16 illustrates the thrust and pressure histories for the simulator configuration with a 0.295-in. diameter nozzle, "small" pin, and a plug made of one set of 1 mm diameter copper spheres plus bronze wool. When compared with "large" pin data of Figure 14, the thrust (and pressures) are lower with the small pin.

During the series of static tests, visual observations of the $CO_2$ jet from the nozzle indicated presence of white mist frequently, even with the copper plugs and bronze wool in place. Thus the effectiveness of the copper spheres in vaporizing solid particles upon contact is questionable. It is possible that the particles are so fine that they follow the gas streamlines without actually making contact with the spheres.

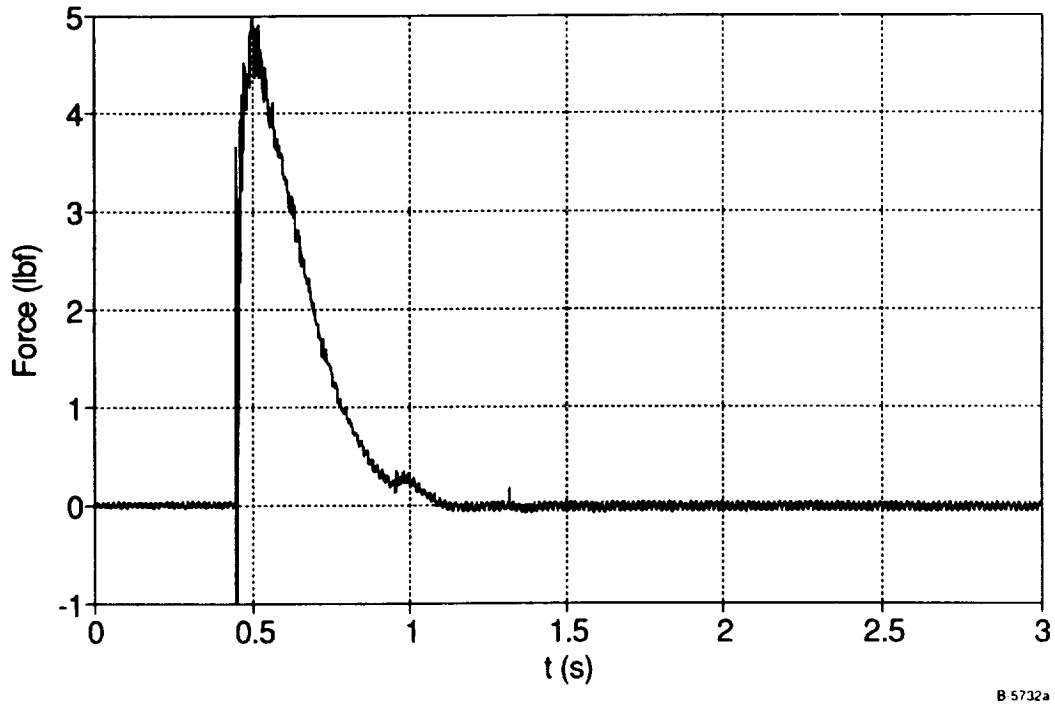


(a) Thrust versus Time

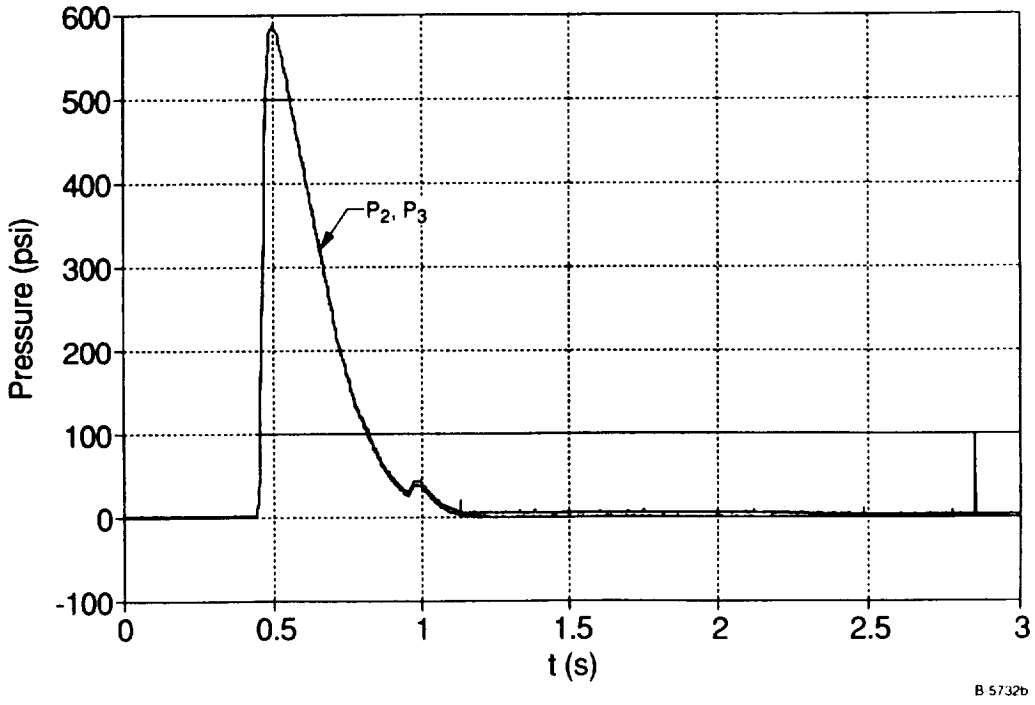


(b) Pressure versus Time

Figure 11. - Effect of increased $CO_2$ mass flow rate on thrust and pressure time history (large pin, 0.098-in. diameter nozzle, three sets of 2 mm copper spheres, vertical up simulator orientation).

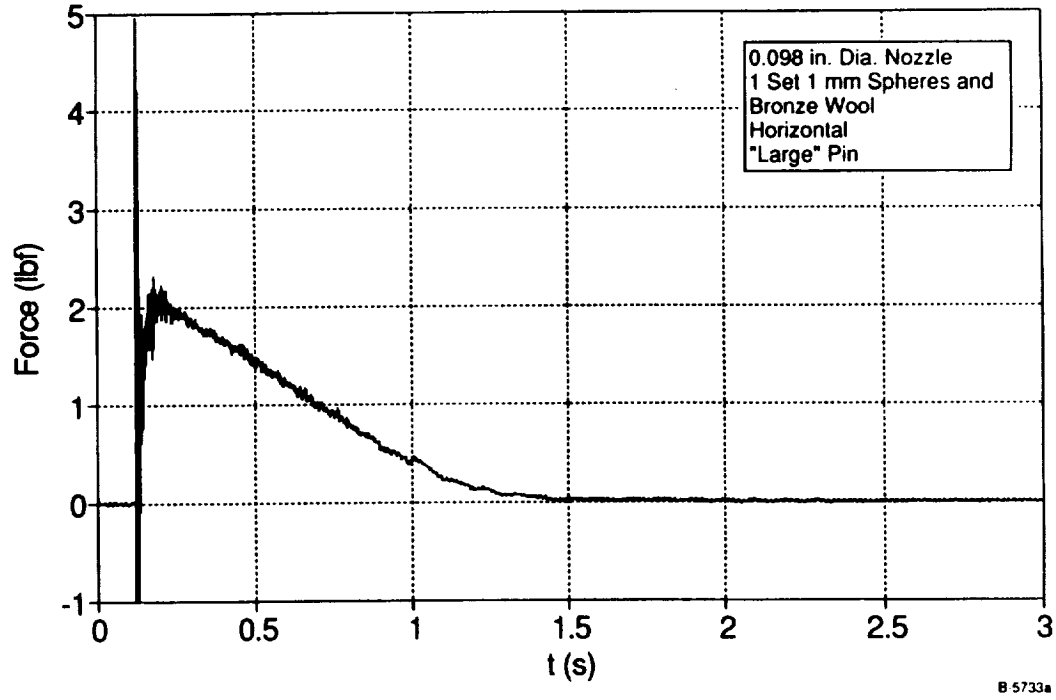


(a) Thrust versus Time

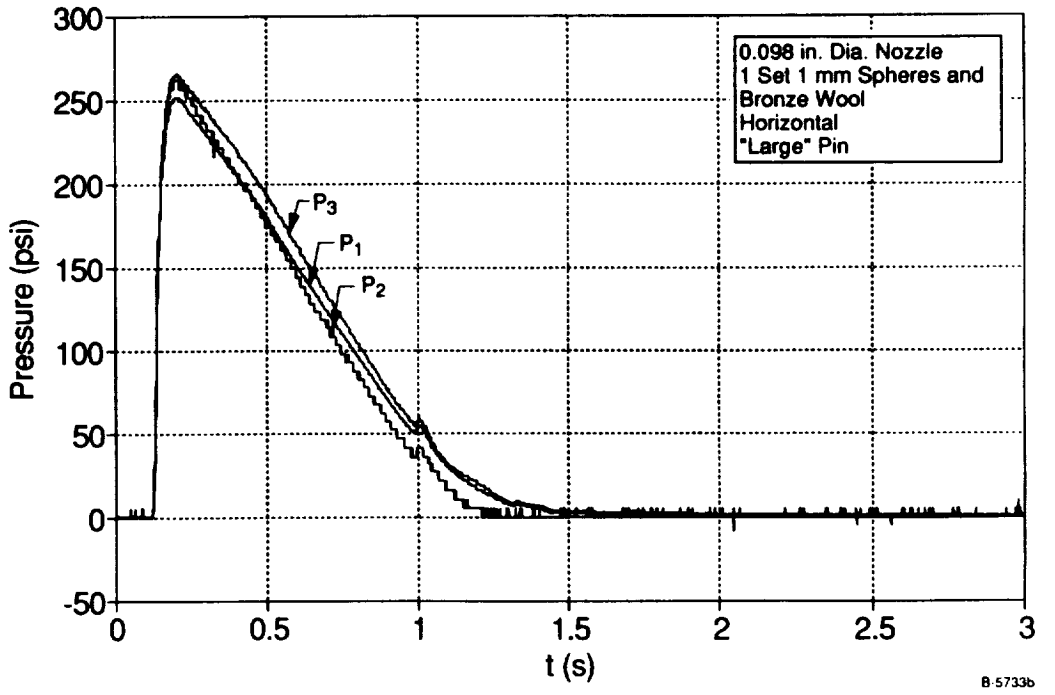


(b) Pressure versus Time

Figure 12. - Effect of copper plug structure on thrust and pressure time history (large pin, 0.098-in. diameter nozzle, one set of 1 mm copper spheres, plus bronze wool, horizontal orientation).

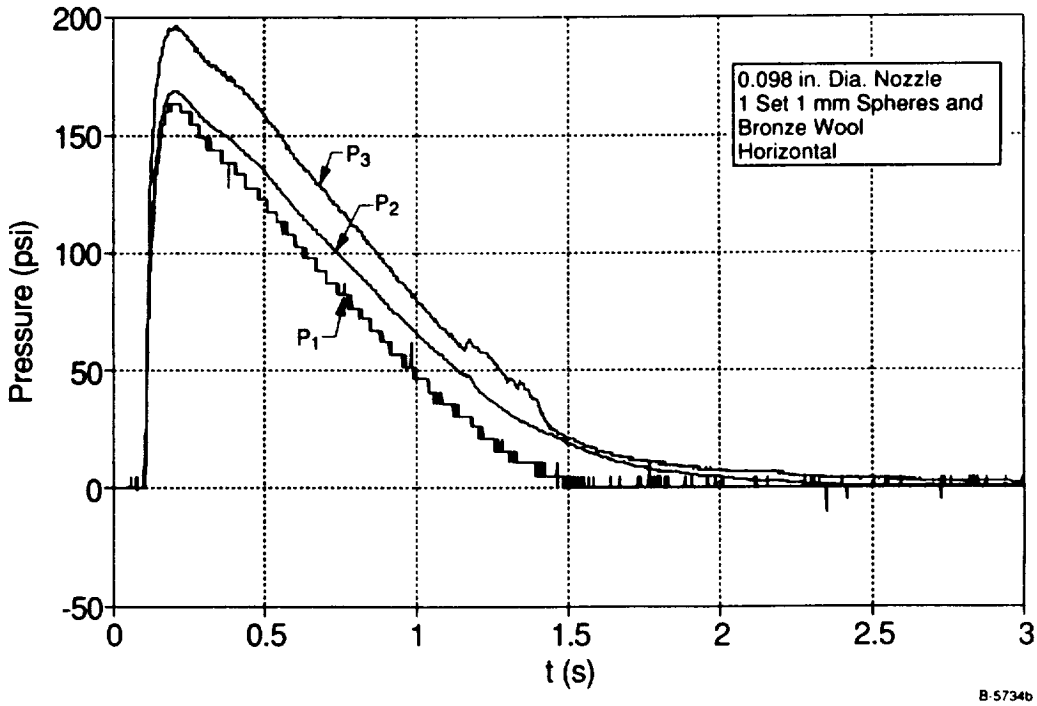


(a) Thrust versus Time

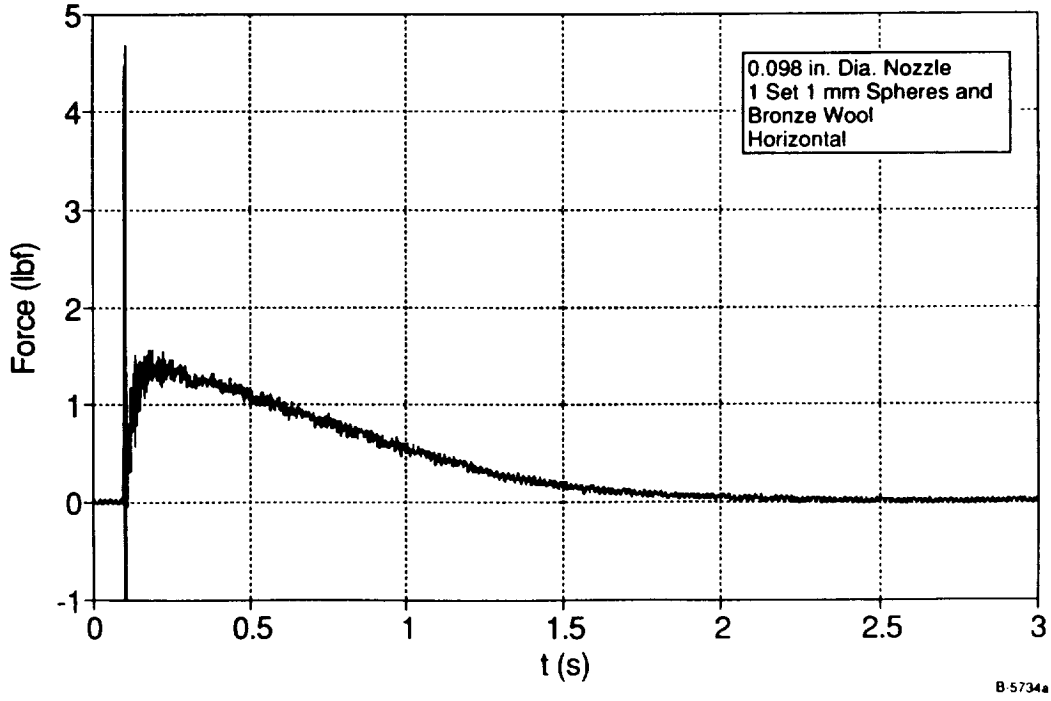


(b) Pressure versus Time

Figure 13. - Effect of "smaller" pin on thrust and pressure time history (0.098-in. diameter nozzle, one set of 1 mm copper spheres, plus bronze wool, horizontal orientation).

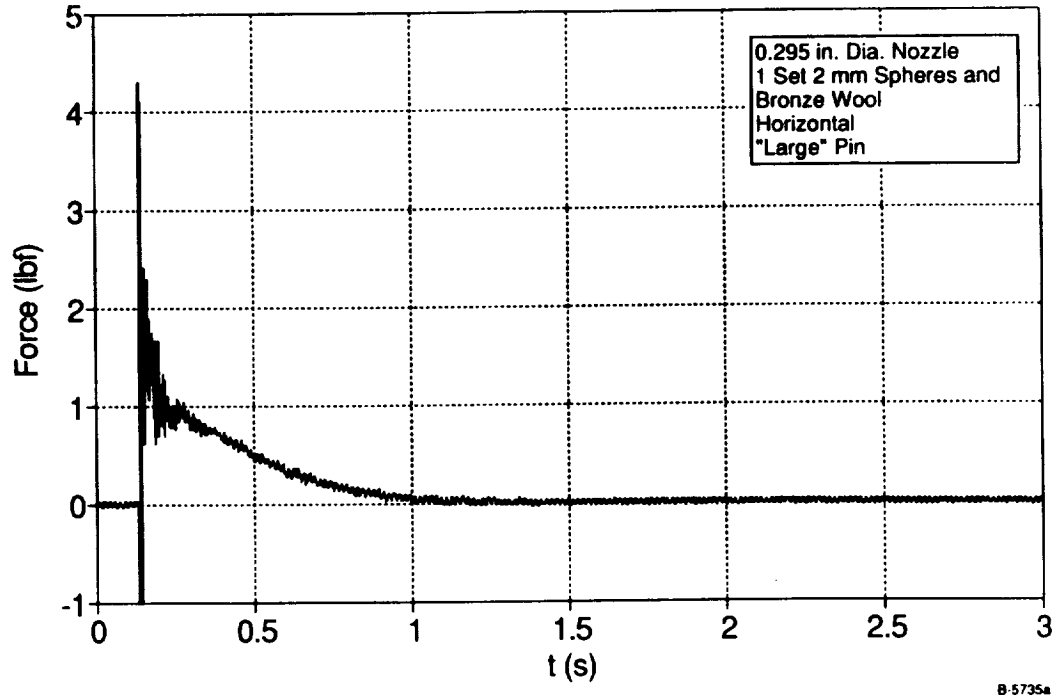


(a) Thrust versus Time

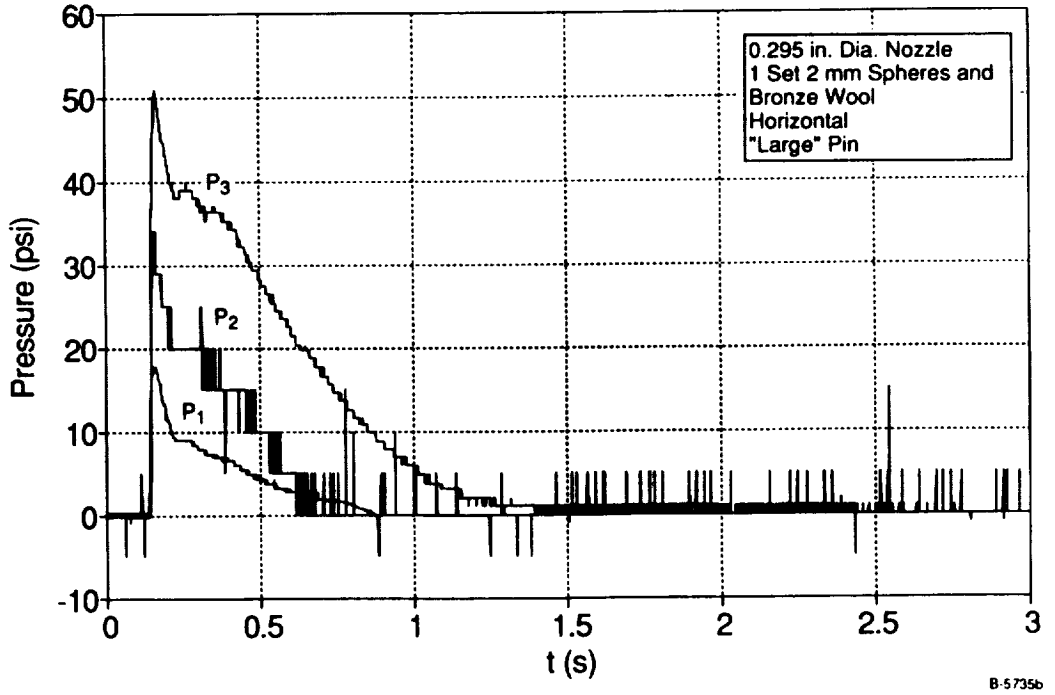


(b) Pressure versus Time

Figure 14. - Effect of exit nozzle diameter on thrust and pressure time history (large pin, 0.295-in. diameter nozzle, one set of 1 mm copper spheres, plus bronze wool, horizontal orientation).

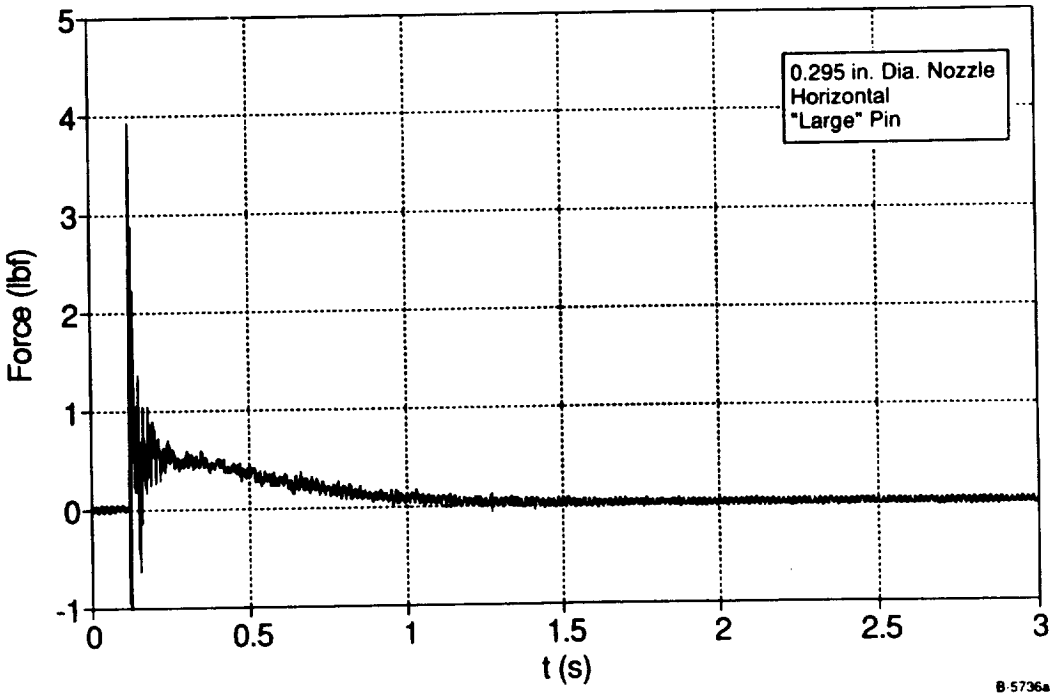


(a) Thrust versus Time

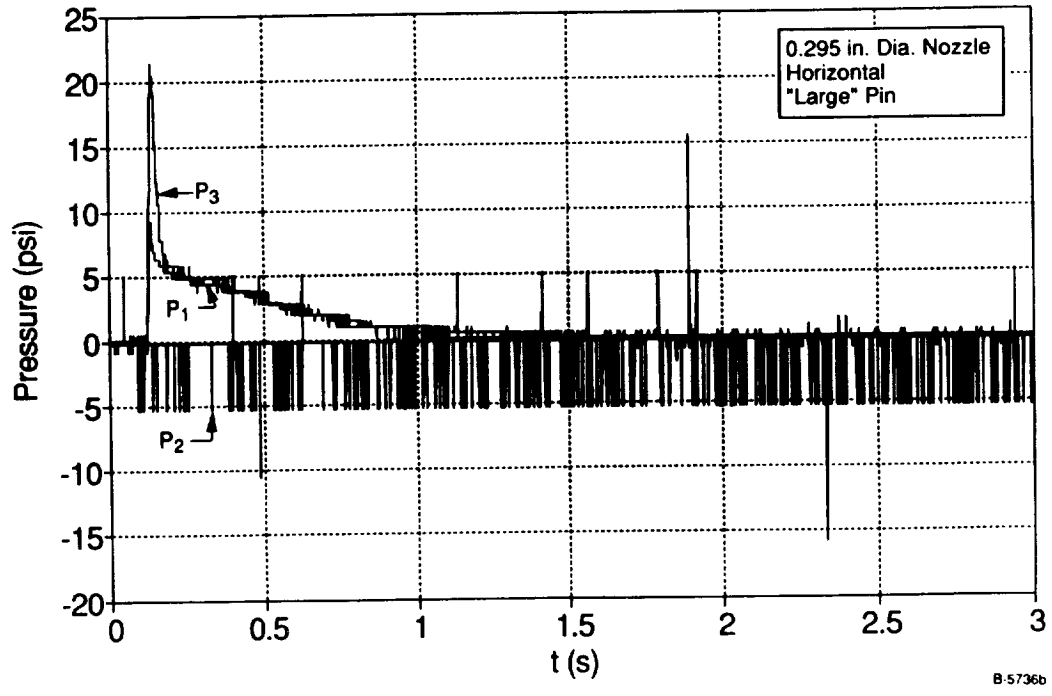


(b) Pressure versus Time

Figure 15. - Effect of removing copper plug on thrust and pressure time history of large nozzle diameter simulator (0.295-in. nozzle diameter, horizontal orientation, large pin).

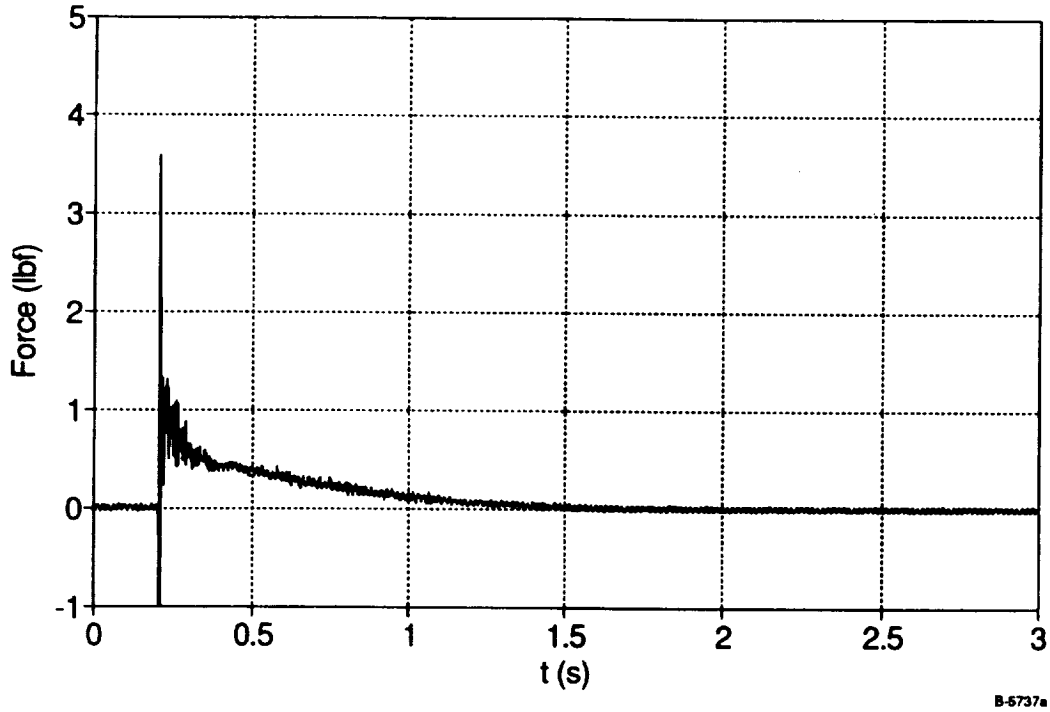


(a) Thrust versus Time

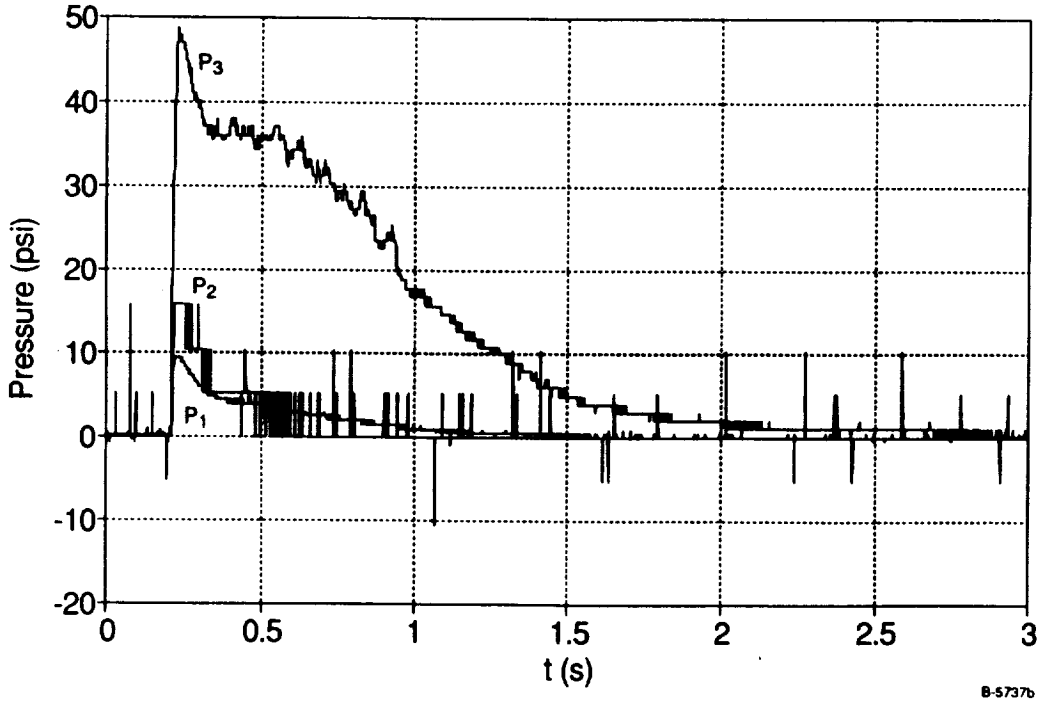


(b) Pressure versus Time

Figure 16. - 0.295-in. Nozzle diameter with "small" pin: thrust and pressure time history (one set of 1 mm diameter copper spheres plus bronze wool, horizontal orientation).

It can be summarized from results of the small-scale simulator that a working device was developed for wind tunnel test in the University of Southampton MSBS. It was difficult to insure high degree of repeatability of thrust for several reasons. First, the tolerance on the thickness of the caps of the commercially-available $CO_2$ cylinders was unknown. Secondly, the explosive capacity of the squibs was not uniform. These uncertainties made the mechanics of cap piercing not too repeatable. Furthermore, upon piercing the cap, the metallic piece of the material sometimes remained attached to the pin, restricting the mass flow through it. Also, as the pin wore out after repeated fixings, the piercing characteristics changed, contributing further to non-repeatability.

# 5. LARGE-SCALE PROPULSION SIMULATOR DESIGN

As mentioned earlier, the large-scale simulator design was based upon the lessons learned from the small-scale simulator experience. The large-scale device was intended only for static testing on a thrust stand. It is apparent from the review of the small-scale test data that a pressure control component and a means of vaporizing small solid $CO_2$ particles must be incorporated into the large-scale design. Furthermore, one must be able to turn the simulator on/off during wind tunnel testing. The thrust and mass flow requirements are as defined in Appendix A.

Taking the above requirements into account, the simulator design shown in Figure 17 was developed. The overall envelope is 2.5 in. dia. x 15 in. long. A copper reservoir holds about 200g of $CO_2$ when full, resulting in a total simulator weight of 5.5 Kg. Liquid, rather than vapor, carbon dioxide is drawn from the reservoir via an eductor tube to attain high mass flows ($\sim$40 g/s was achieved). The flow of liquid $CO_2$ is turned on/off by a miniature solenoid valve made by General Valve Corporation. It is operated by an on-board battery via a light-activated switch. $CO_2$ liquid flows through 5 coiled copper tubes which form a compact pre-heater block. It vaporizes and expands in the process, dropping its pressure. The pre-heater employs a cartridge heater which is run on external AC power prior to a propulsion test run. The power connector can be on the model or at the wall. It will be removed before a test run. The flow from the pre-heater enters a short settling/stagnation chamber and exits through a contoured nozzle. The nozzle was designed to be removable and replaceable. The pressure ratio was varied by varying the throat area.

As will be shown in Section 6, the simulator developed a thrust of 1.25 Kgf for approximately 4s. A maximum nozzle pressure ratio of four was attained.

The following paragraphs describe the main components of the large-scale simulator.

a) $CO_2$ Reservoir

The $CO_2$ reservoir, shown schematically in Figure 18(a), consists of a nickel-plated copper cylinder, 7 in. long, 2.5 in. O.D., 0.25 in. wall thickness; with a stainless steel plug threaded into its open end and sealed to the cylinder by a buna-N o-ring. The reservoir has a capacity of 200g of liquid $CO_2$. It was designed to withstand a pressure of 2000 psi, with a factor of safety of 4 to ultimate, and was proof-tested to 2500 psi. The copper cylinder has sufficient thermal mass to maintain the temperature, and therefore pressure, of the liquid $CO_2$ during the run. Furthermore, $\sqrt{\alpha t}$ , i.e., the square root of the product of the thermal diffusivity of copper and the run time, equals 2.1 cm, a factor of three greater than the wall thickness. Therefore, the $CO_2$ is able to draw heat from the entire thickness of the cylinder. The stainless steel cap contains a filling duct with a check valve (Kepner, 6000 psi max, 2 psi cracking); a burst disk (Frangible Disks, 1875 psi burst) to prevent over-pressurization; and a 0.093 in. dia. duct (eductor tube) to carry liquid $CO_2$ from the bottom of the cylinder to the solenoid valve.

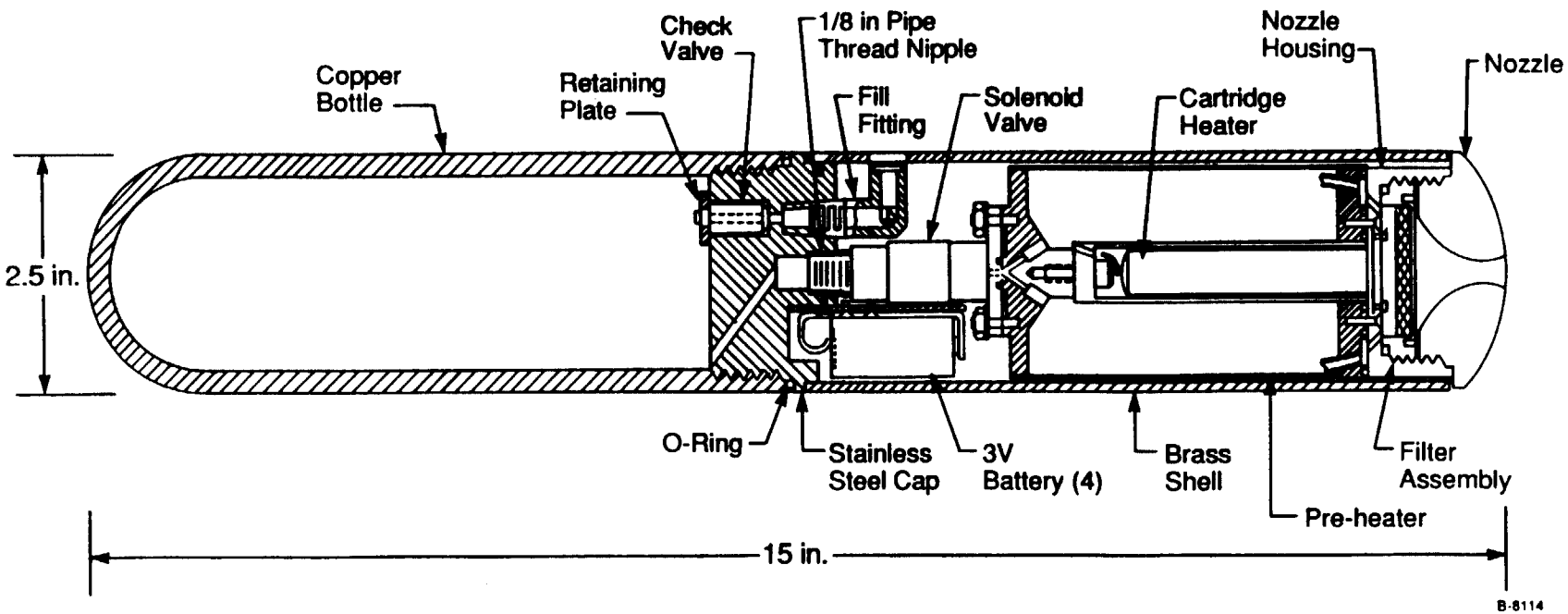


Figure 17. - Design of large-scale propulsion simulator.

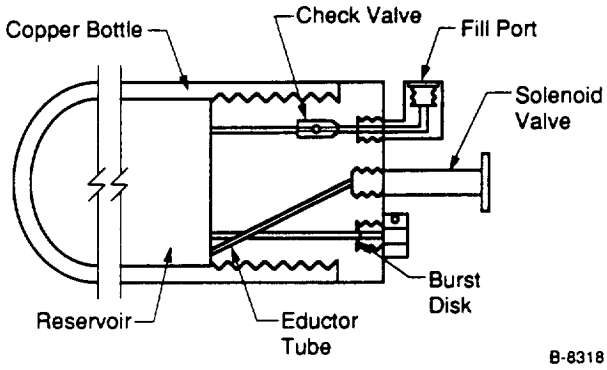


(a) $CO_2$ Reservoir

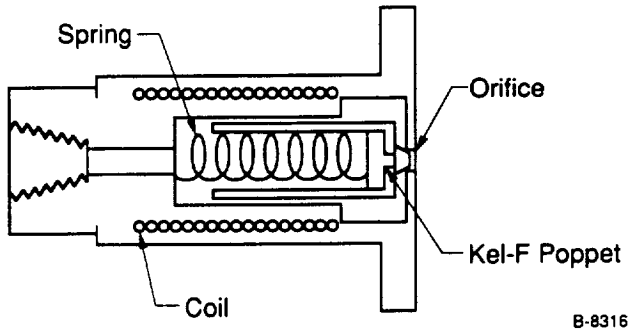


(b) Solenoid Valve

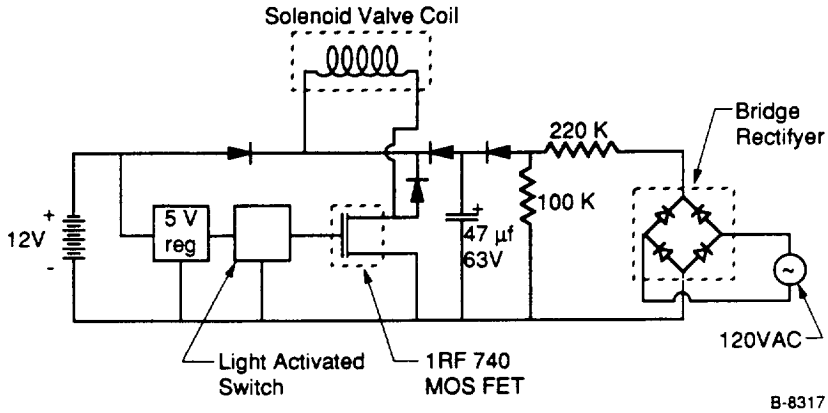


(c) Triggering Circuit

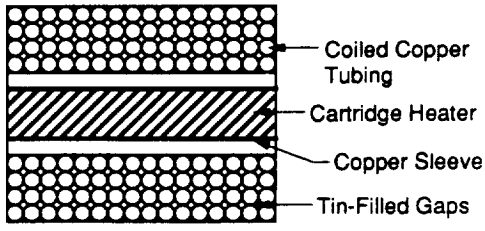


(d) Preheater/Pressure Reducer

Figure 18. Large-scale propulsion simulator components.

b) Solenoid Valve

The solenoid valve, shown schematically in Figure 18(b), was manufactured by General Valve Corporation. Its dimensions are 1.6 in. long x 0.7 in. dia., and it weighs approximately 80g. It has a maximum operating pressure of 900 psi and is sealed by buna-N O-rings. The coil is rated for 6V and draws 2 amps during steady state operation. The valve operates by pulling a Kel-F poppet off of a 0.060 in. dia. orifice when the coil is activated. The valve is able to pass 40 g/s of liquid $CO_2$ through the orifice with an upstream pressure of 840 psig.

c) Triggering Circuit

The triggering circuit is shown in Figure 18(c). Basically, it consists of four 3V batteries in series with the valve coil, with power switched by an IRF740 MOSFET, which in turn is activated by an EG&G light activated switch. Twelve volts are used because during operation the coil draws enough current to drop the battery voltage to the rated voltage of 6V. Also in series with the coil is a 47 $\mu$f 63V electrolytic capacitor. Before each run, this capacitor is charged to 50V via external AC power and a bridge rectifier. (The capacitor charges in approximately 30s.) This capacitor sends an extra boost of current through the coil when the switch is first closed which helps to pull the valve open. Blocking diodes prevent communication between the capacitor and the batteries and prevent the capacitor from discharging to ground when AC power is removed. The light activated switch and a 5V regulator drain about 6 mA of current when the circuit is "off".

d) Preheater

After exiting the solenoid valve, the liquid $CO_2$ passes through a pre-heater to vaporize it and increase its enthalpy before entering the nozzle. The pre-heater transfers enough heat to the flow to increase its enthalpy by 180 kJ/kg, which is sufficient to prevent condensation when the $CO_2$ expands to 1 atm. It also drops the pressure of the flow to 70 psig in the nozzle chamber, although this pressure drop is a function of the mass flow (controlled by the solenoid valve) and the nozzle area, rather than the pre-heater characteristics. The pre-heater is shown schematically in Figure 18(d). It consists of five copper tubes (through which the $CO_2$ passes), each 90 in. long and 0.065 in. I.D., coiled around a copper sleeve into a 3 in. long x 2.25 in. diameter cylinder. The gaps between tubes were filled with tin to increase the thermal mass of the assembly and to increase the thermal conductivity between tubes. At the center of the copper sleeve is a 400W cartridge heater. The entire assembly weighs 1400g. Before each run, 120 VAC is applied to the cartridge heater which heats the pre-heater assembly to 75°C in 90s. During a 4s run of the simulator, the pre-heater cools to ~0°C. A one-dimensional flow and heat transfer model, included in Appendix E, predicts that at a mass flow rate of 40 g/s, the pre-heater will transfer 180 J/g to the flow. This prediction is entirely consistent with the observed temperature drop of the pre-heater.

e) $CO_2$ Filling

The $CO_2$ reservoir was filled with liquid $CO_2$ using the apparatus shown in Figure 19. A flex hose attached at one end to a $CO_2$ supply bottle was connected to the simulator via a fill fitting mated to the fill port of the simulator and a quick connect. The check valve in the reservoir cap prevented backfilling. In order to fill the reservoir to a higher density of $CO_2$ than was in the supply bottle (without pumping), the reservoir had to be cooler than the supply. This necessitated either heating the supply bottle or cooling the simulator. We chose to heat the supply bottle (with heating tape) as this was quicker and easier than cooling the simulator and kept the simulator at room temperature. A thermistor was placed on the outside of the reservoir, and the density (and therefore mass) of the $CO_2$ in the reservoir was determined by measuring the temperature and pressure. This determination was verified by weighing the simulator before and after filling.

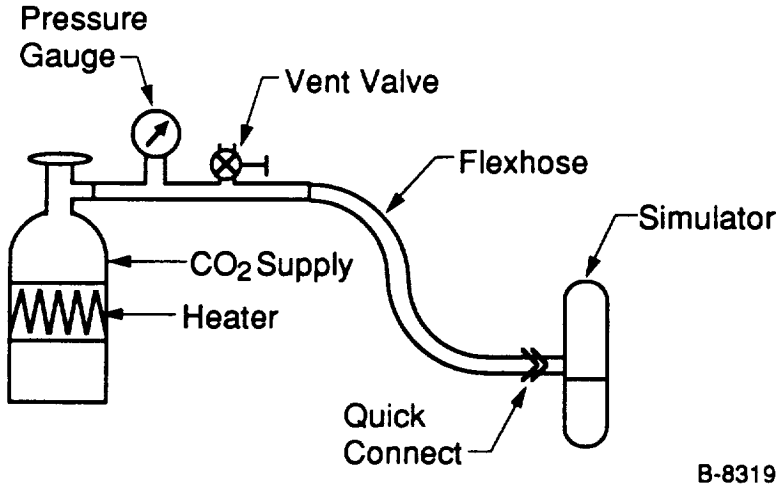


Figure 19. - $CO_2$ filling scheme.

## 6. RESULTS OF STATIC TESTING OF LARGE-SCALE SIMULATOR

Figure 20 shows the schematic of the large-scale simulator static test stand. The tests were conducted according to the matrix shown in Appendix C. The objective of these tests was to demonstrate the repeatability of the thrust, multiple jet operation, and a reasonably flat thrust versus time profile. The measurements were thrust, pressure in the $CO_2$ reservoir, and pressure at the center of the nozzle exit plane, as a function of time.

Figure 21(a) shows typical static test data for the large-scale simulator. The thrust profile is essentially flat at 2.75 lbf (1.25 Kgf) for about 4s. The time required to attain 90 percent of full thrust is approximately 0.4s. The gradual drop-off is due to $CO_2$ vapor after all the liquid $CO_2$ has changed phase. Plotted in Figure 21(c) is the exit plane pressure on the nozzle centerline. These data have been corrected for the normal shock in front of the pitot tube in Figure 20. The shock occurs because the nozzle used in the test was supersonic with an area ratio of 1.19.

Both Figures 21(a) and 21(c) show an initial "bump" which lasts for about 1s. Corresponding to this, there is an increase in pressure of the $CO_2$ vapor in the reservoir, following a sharp initial drop as the solenoid valve is opened, Figure 21(b). The increase in pressure occurs as a result of the heat transfer from the copper wall of the reservoir to the $CO_2$ vapor. The sharp drop in pressure is believed to be due to "over-compression" of the $CO_2$ liquid during the filling process. It will be shown later in this section that slight under-filling of the reservoir avoids the initial sharp pressure drop and the subsequent bump in the thrust profile.

It is noted in Figure 21(b), that there is a distinct change in the slope of the $CO_2$ reservoir pressure curve after 5.5s. This is the point by which sufficient liquid has been drawn from the reservoir so that only vapor remains therein. As this vapor leaves the

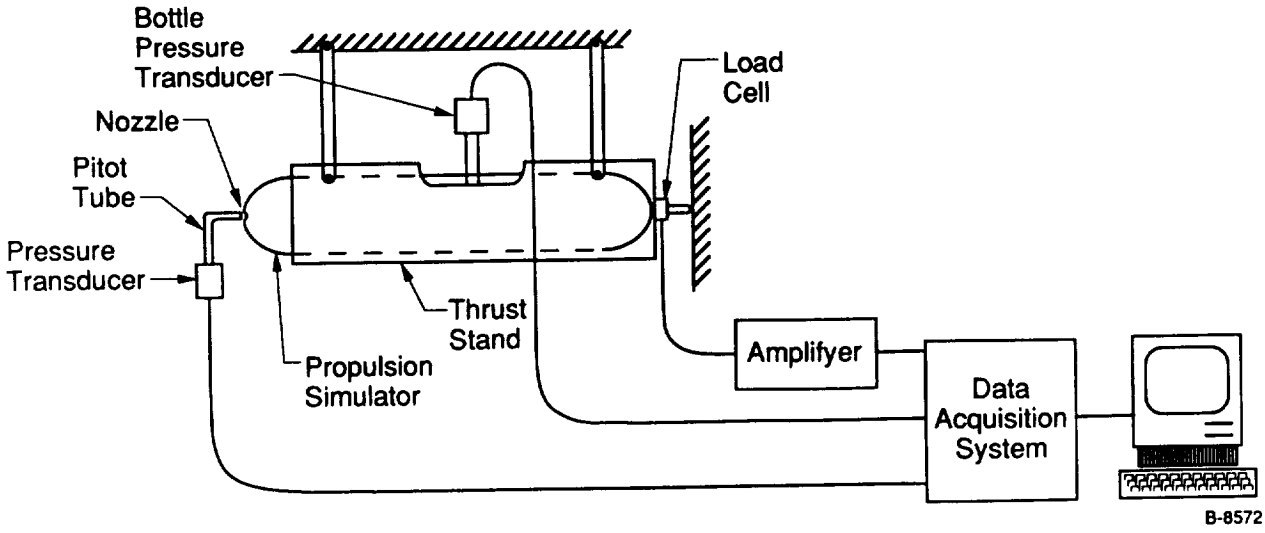


Figure 20. - Schematic of static test apparatus for large-scale propulsion simulator.

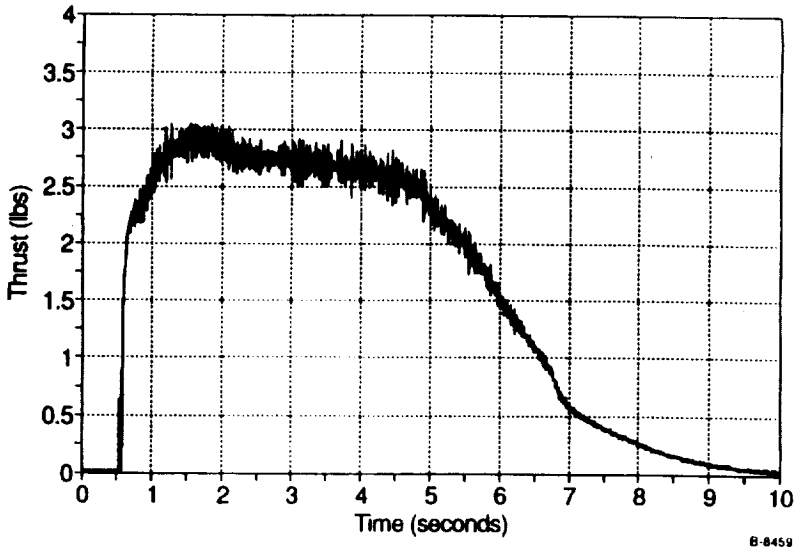


(a) Thrust versus Time

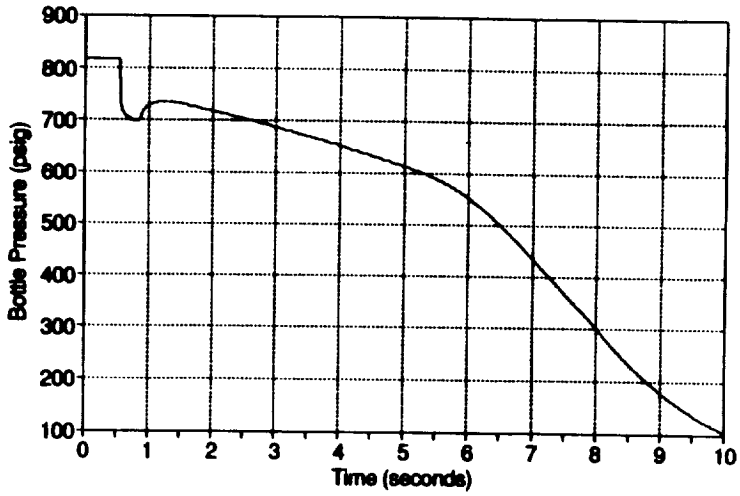


(b) Bottle Pressure versus Time

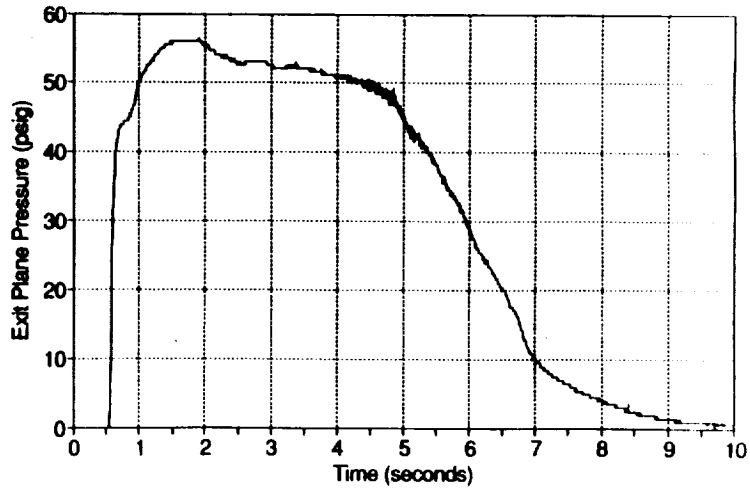


(c) Exit Phase Pressure versus Time

Figure 21. - Large-scale simulator static test (Run 48).

reservoir, the pressure drops rapidly, and the mass flow rate through the system is significantly reduced, leading to a rapid drop in thrust as seen in Figure 21(a). Prior to t=5.5s, there is always some liquid inside the reservoir which continually vaporizes. As liquid $CO_2$ is drawn, the pressure and temperature of the vapor above it reduces. As heat is received from the copper walls, the temperature of the $CO_2$ liquid/vapor system rises, resulting in vaporization of the liquid. Ideally, this process should keep a constant pressure in the reservoir, provided the temperature of $CO_2$ system remains roughly constant. In reality, this does not happen, and the pressure does keep dropping between 1 and 5.5s, as seen from Figure 21(b). However, the rate of pressure drop is sufficiently slow that the thrust variations are small, as seen in Figure 21(a).

Figure 22 shows repeatability of the thrust characteristics of the large-scale simulator. It is noted that the data of Figure 22 are substantially the same as Figure 21.

In Figure 23, the effect of under-filling the $CO_2$ reservoir on the thrust versus time curve is shown. It is seen from Figure 23(b) that the drop in $CO_2$ pressure upon activating the solenoid is much more gradual compared to over-filled case (Figure 21(b)). Also, there is no increase in the $CO_2$ pressure, unlike in Figure 21(b), following the initial drop in pressure. The result is that there is no bump in the thrust profile as was seen in Figure 21(a). This demonstrates that slight under-filling of the reservoir can produce a smoother thrust profile.

Figure 24 shows the on/off capability of the large-scale simulator. This feature is necessary for producing jet pulses so that multiple runs can be made after filling the $CO_2$ reservoir. Note the absence of the bump in the thrust profile seen earlier for the over-filled reservoir.

An analysis of the thrust produced by the large-scale simulator is provided in Appendix D. It is shown that the pressure ratio and thrust are directly proportional to the area of the flow orifice ($A_s$) of the solenoid. In the static tests, nozzle pressure ratio of the order of 4 to 5 were obtained (Figures 21(a) and 22(a), after accounting for the normal shock at the pitot tube). The pressure ratio can be lowered by increasing the nozzle throat area. The measured thrust of 1.25 Kgf is lower than the ideal thrust calculation (1.6 Kgf) given in Appendix D. The lower thrust (1.25 Kgf) and mass flow (40 g/s) when compared to the requirements of Appendix A (3 Kgf a 80 to 100 g/s), resulted from the flow restriction in the solenoid valve ($d_s$ = 0.060 in.). This particular valve, made by General Valve Co., was selected as an inexpensive, miniaturized device. In principle, a specially-designed valve with a larger orifice can be incorporated in the current simulator design to yield the required 80 g/s mass flow. The current pre-heater can also handle mass flows of this magnitude.

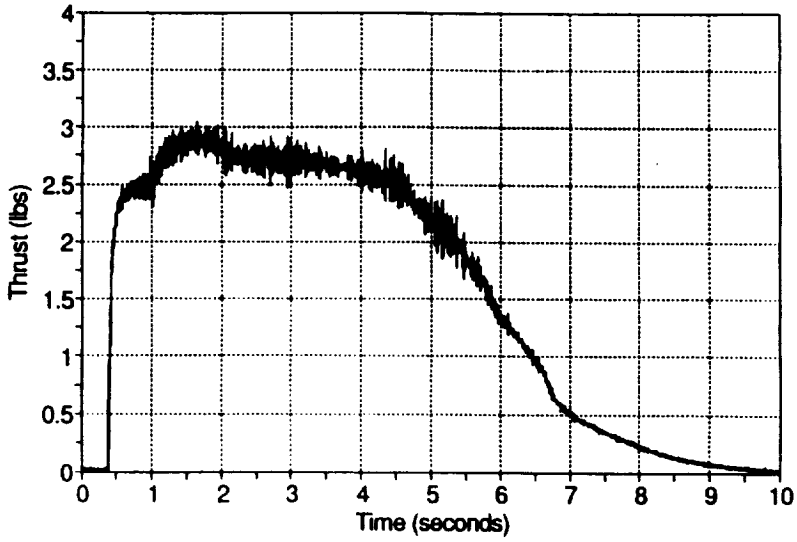


(a) Thrust versus Time

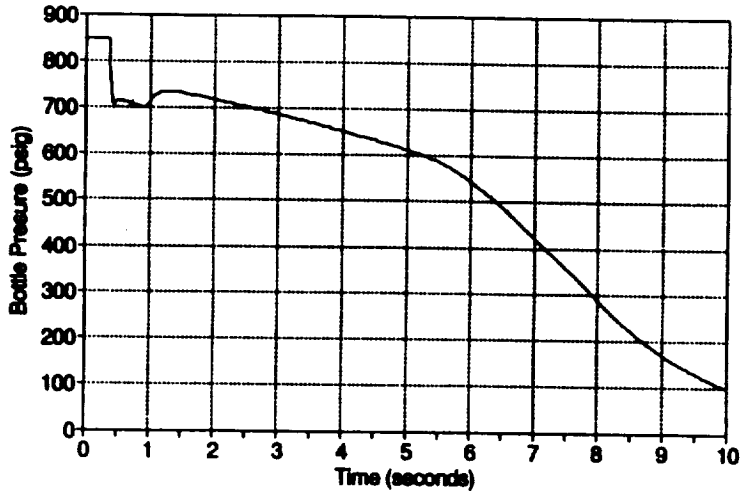


(b) Bottle Pressure versus Time

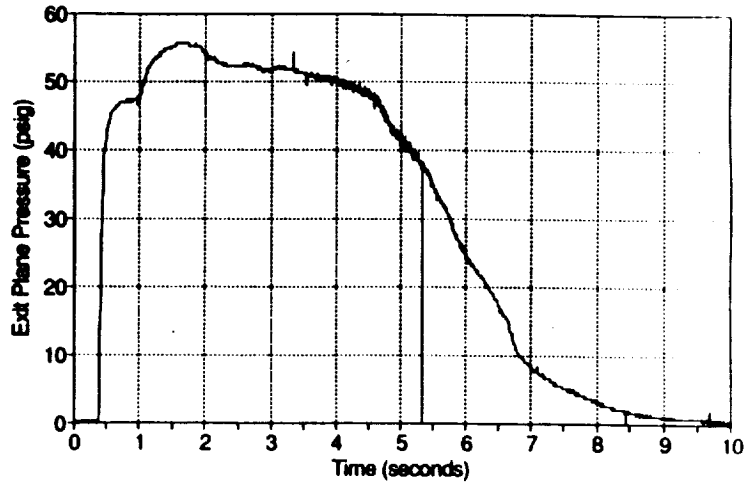


(c) Exit Phase Pressure versus Time

Figure 22. - Repeatability of large-scale simulator thrust characteristics (Run 49).

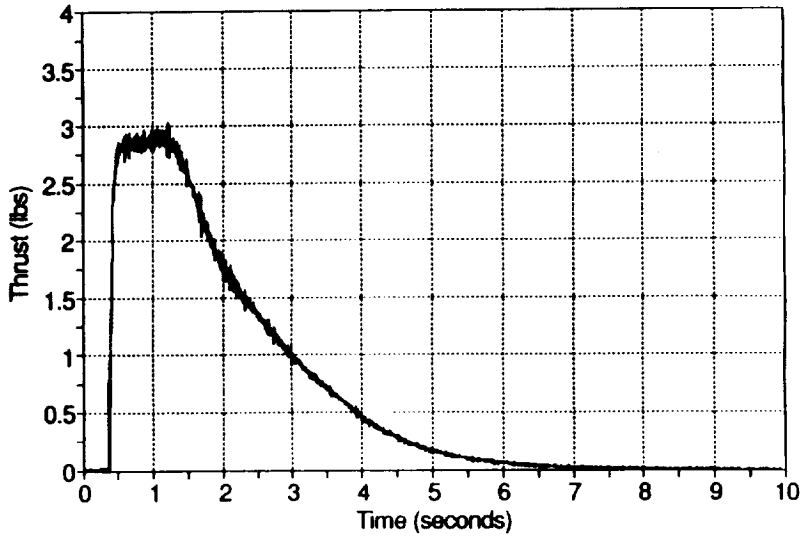


(a) Thrust versus Time

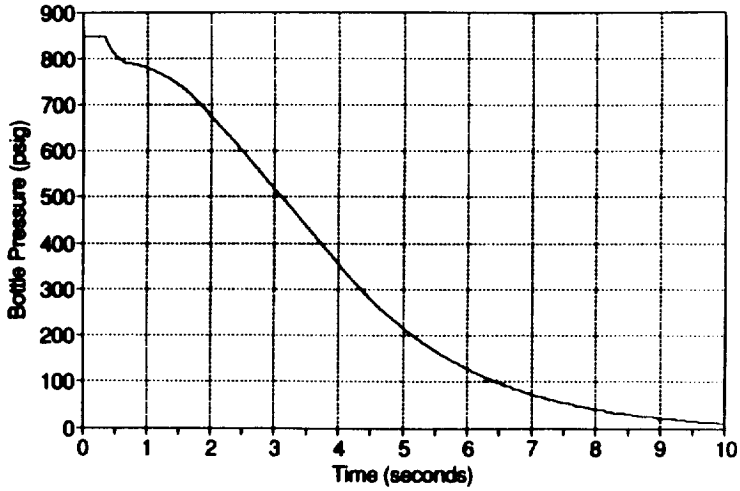


(b) Bottle Pressure versus Time

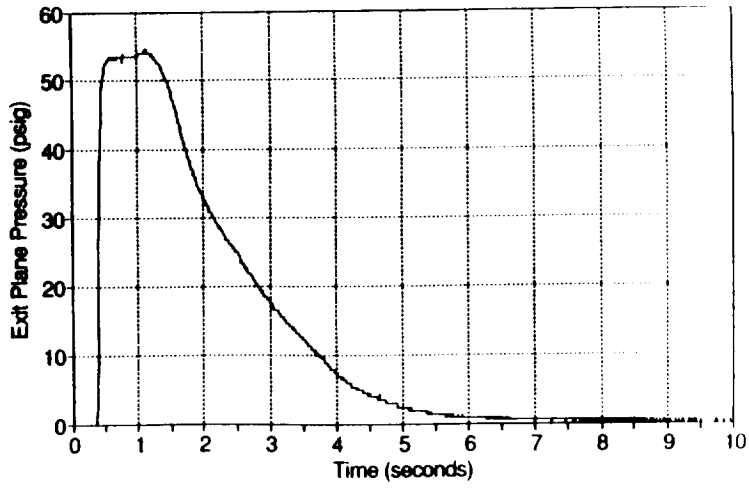


(c) Exit Phase Pressure versus Time

Figure 23. - Effect of underfilling $CO_2$ reservoir on thrust characteristics (Run 50).

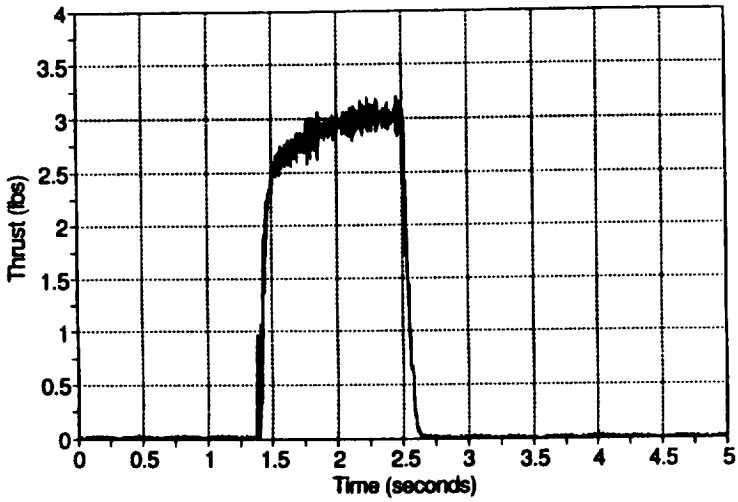


(a) Pulse 1

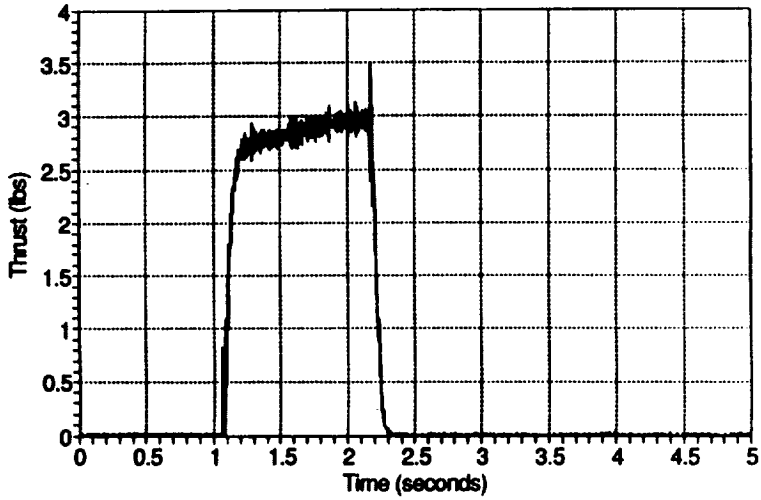


(b) Pulse 2

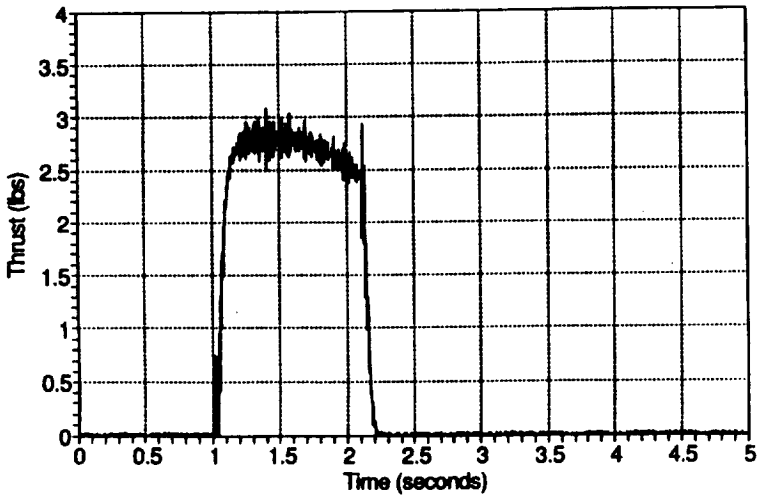


(c) Pulse 3

Figure 24. - Multiple run operation of large-scale simulator.

## 7. THE UNIVERSITY OF SOUTHAMPTON MSBS

The modifications to the University of Southampton magnetic suspension and balance system for propulsive testing are described in detail in the Final Report contained in Appendix H. Sections 7 through 12 present a summary version of the University of Southampton report.

In order to increase the versatility of the Magnetic Suspension and Balance System (MSBS) applied to the testing of wind tunnel models, development of techniques for simulation of propulsion systems is under way. The purpose of the work described in this report was to begin to address the issue of developing exhaust flow simulators. The outcome was a set of simulators, two of which were brought to the stage of operating on board models levitated in a wind tunnel. The levitated model featured a supply of gas, discharged on command for a brief period to produce a jet exhausting at the rear.

The simulator development was carried out under NASA SBIR 87-1 whereby two styles of gas generator were developed. These were a carbon dioxide thruster with the gas stored under pressure as liquid $CO_2$, and a rocket thruster using a solid propellant as the gas generator.

To enable suspension and testing of the propulsion simulators at the University of Southampton, a number of modifications were required to the suspension system, the wind tunnel hardware and to the control system.

The present electromagnet configuration is shown in Figure 25(a) '+' layout is used, symmetrical apart from the skew in the lateral electromagnets. This was introduced to provide a side force at high angles of attack. Position sensing is achieved via five linear photodiode arrays and a system of laser light sheets (ref. 3). A PDP11/84 computer is currently used for control of the MSBS. Dual-phase advance control algorithms with proportional and integral feedback are employed (ref. 4).

The initial aim of the wind tunnel experiments was to test at speeds up to Mach 0.2, and at angles of attack up to 20 deg.

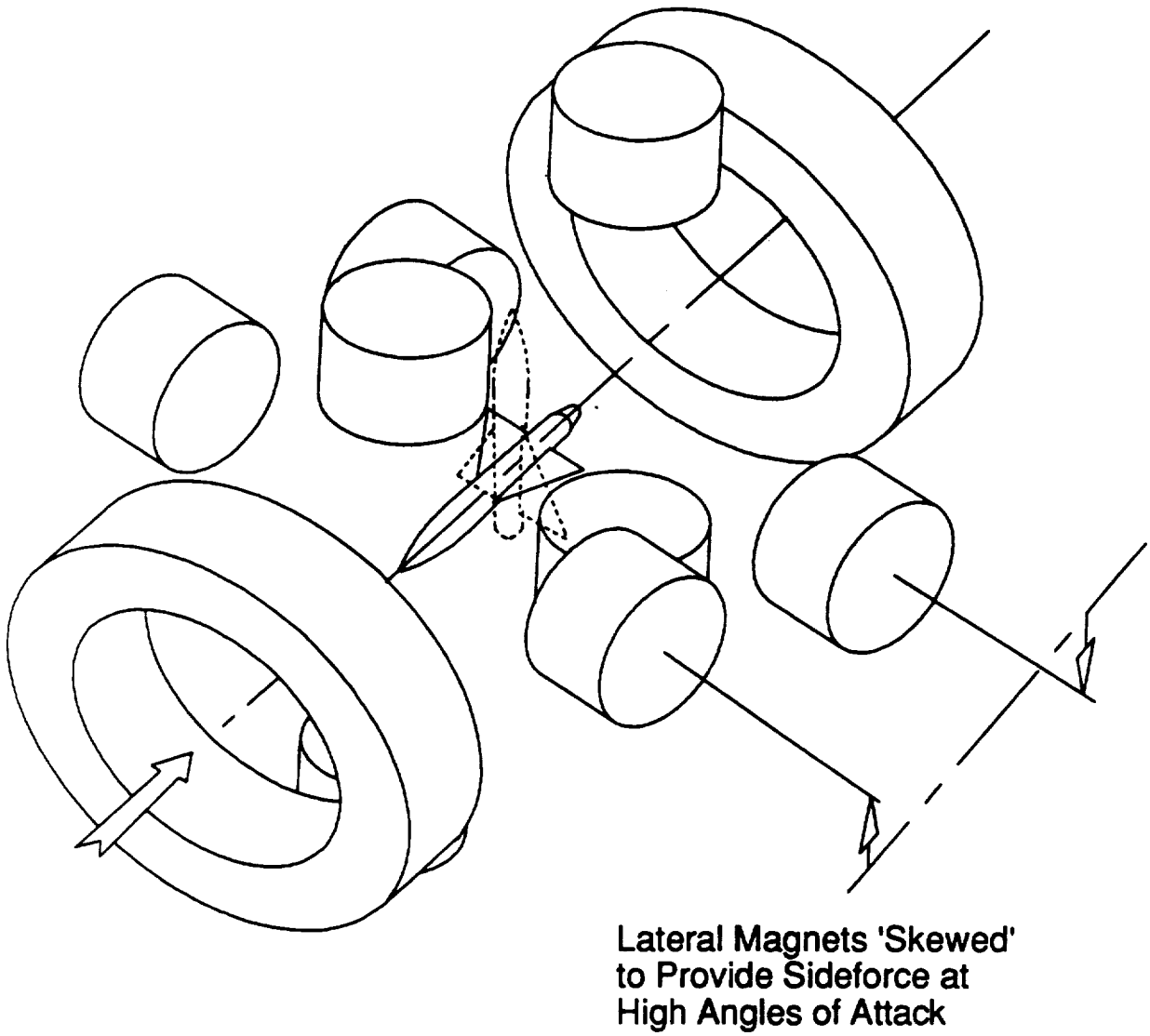


Figure 25. - Electromagnetic configuration for University of Southampton MSBS.

# 8. SYSTEM MODIFICATIONS

It was necessary to alter the path of the axial position sensing laser light sheet, to avoid its corruption by the model's exhaust efflux. A change was made from tail to nose scanning, after consultation with PSI over a suitable nose geometry.

A PC was integrated into the control loop to act as a data logger, and eventual replacement for the PDP11 control computer. This allowed development of more sophisticated data analysis and presentation software than had previously been feasible at Southampton.

The high angle of attack control system was modified to allow suspension of iron models. It had originally been developed for use with models with permanent magnet cores. The change was necessary because machining the relatively complex components of propulsion simulators would have been very difficult with permanent magnet alloys. To magnetize the model a steady field component is added to the suspension field. The magnetizing field is generated by contributions from all ten electromagnets, and rotates to match the instantaneous angle of attack. The unique capability of the Southampton MSBS to suspend models over a 110 degree angle of attack range is thus retained.

It was found that a field strength of around 0.02 T was required to adequately magnetize the propulsion simulator, this rather high value being a result of its self-demagnetizing geometry. A number of additional minor system modifications were made.

## 9. INITIAL SUSPENSION AND DEVELOPMENT

Following initial suspension of the propulsion simulators, attempts were made to optimize the controller in each degree of freedom. Particular attention was paid to quality of suspension. Difficulties were expected in control of the simulators under the influence of force transients associated with the thruster firing. It was demonstrated that the optimum input constants to the dual-phase advancer were angle of attack dependent, rather than being constant for all angles of attack as had been previously been assumed.

Further optimization was necessary to maximize the ability of the system to resist externally applied forces in the axial direction. This was achieved primarily by ensuring that the electromagnets used for axial force generation made the minimum practicable contribution to magnetization of the model. The level of magnetization was also adjusted to give the best compromise between strong magnetization and peak force generation.

Force and moment calibrations were performed to allow extraction of axial force data at zero angle of attack, and additionally for heave force and pitching moment data at angles up to twenty degrees. Conventional calibration techniques were employed, using small weights and low friction pulleys to apply forces to the suspended model, whilst recording the changes in electromagnet currents. Figure 26 shows the results of an axial force calibration, plotting magnet currents against externally applied load. The result is linear except at the extremes, where electromagnet current limits cause a non-linear region.

At zero degrees only the two axial magnets are used to oppose the drag force, so just their two currents are recorded during the calibration process. For other attitudes a technique was developed whereby several currents were recorded during heave, pitch and axial calibrations. Run-data was processed to find the changes in these currents during a suspended thruster firing, and matrix inversion used to deduce heave force, axial force and pitching moment simultaneously.

Peak axial force capability was found to be around 4.5 N at zero angle of attack, falling to 4.0 N at twenty degrees.

Bench tests of the carbon dioxide thruster showed the peak thrust to be significantly above these values, and initial wind tunnel testing was delayed while a series of nozzle modifications gradually reduced the thrust peak to below 4 N. The rocket thruster used initially also displayed a thrust profile with an initial peak. In a later version the profile is more constant, as shown in Figure 27.

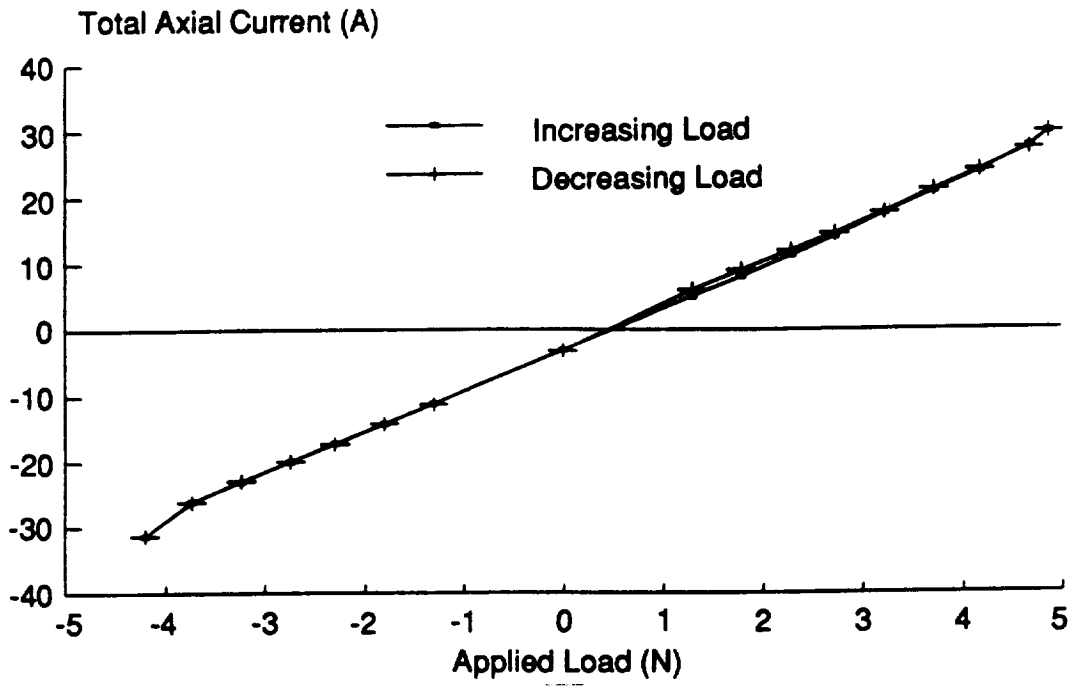


Figure 26. - Axial force calibration at zero angle of attack.

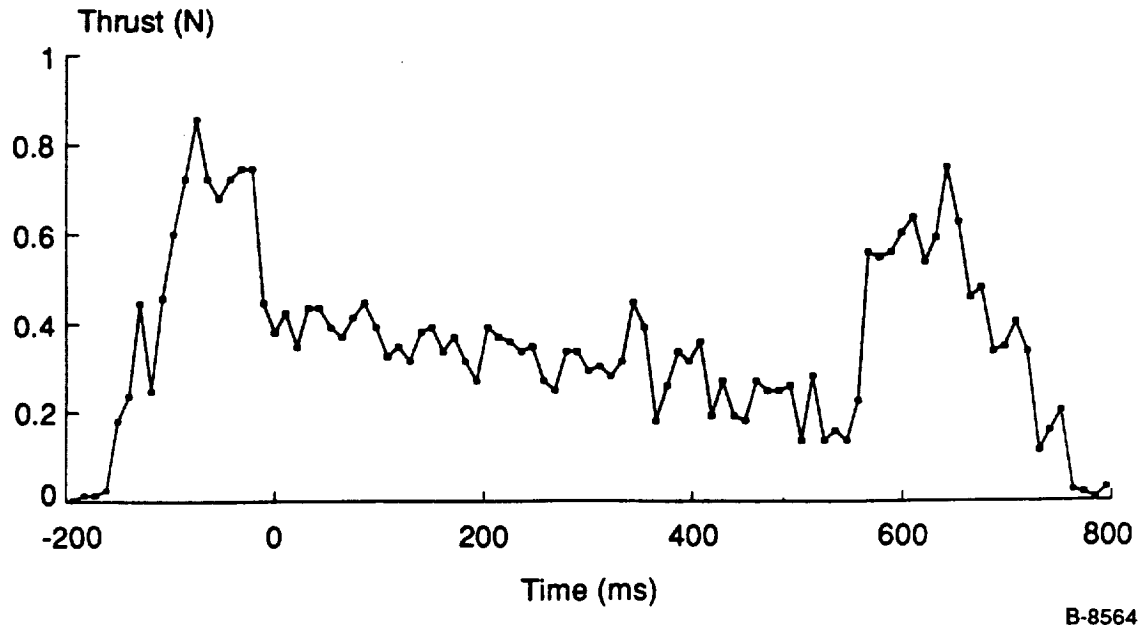


Figure 27. - Rocket motor thrust profile (low thrust test).

# 10. WIND TUNNEL TESTS

A series of firings of the carbon dioxide propulsion simulator was performed in the Southampton MSBS, at zero wind speed and up to Mach 0.1, and attitudes of zero, ten and twenty degrees angle of attack. Initially the success rate was only about 50%, with the model regularly falling out of suspension because of the high and erratic thrusts produced. Operating experience and further thrust reductions led to a much higher success rate. The rocket thruster has also been fired in suspension, and wind tunnel tests with this propulsion simulator will be performed in the near future.

# 11. DATA ANALYSIS AND RESULTS

The unsteady thrust profile and short run time of the carbon dioxide propulsion simulator provided particular problems for data analysis. As there was no period following a firing where the model was stationary during the thrust cycle, analysis of run-data had to address the motion transients. Software was developed to attempt to find the external forces and moments experienced by the suspended model, by considering its motion in addition to the electromagnet currents. Factors accounted for included the model's inertia, cross coupling in the position sensors, changes in level of magnetization and the relationship between calibration constant and axial position.

The aim was to extract a thrust profile similar to that demonstrated in bench tests, possibly going on to examine changes in drag coefficient caused by the presence of the exhaust plume. Unfortunately the variability of thrust produced by the carbon dioxide jet was such that no accurate measurements of this type were possible. In addition, the transient analysis did not prove satisfactory, giving external force data which did not agree closely enough with bench test results. In Figure 28, the bench test data shows an exponential thrust decay after the initial peak, while the data extracted from a test in suspension includes an oscillatory component, associated with model motion.

The force and moment results obtained with the model levitated were inconclusive. However the emphasis of the tests was placed on proof of concept and on overcoming some of the practical difficulties inherent in these experiments, rather than aiming to demonstrate an aerodynamic effect of the exhaust plume.

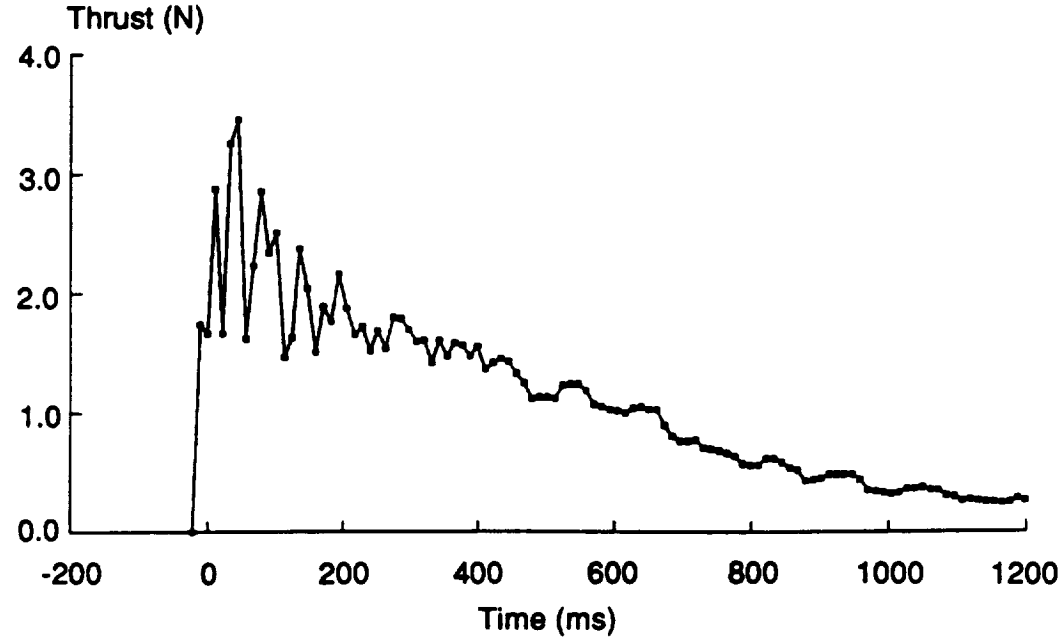


(a) Static Test Thrust Profile

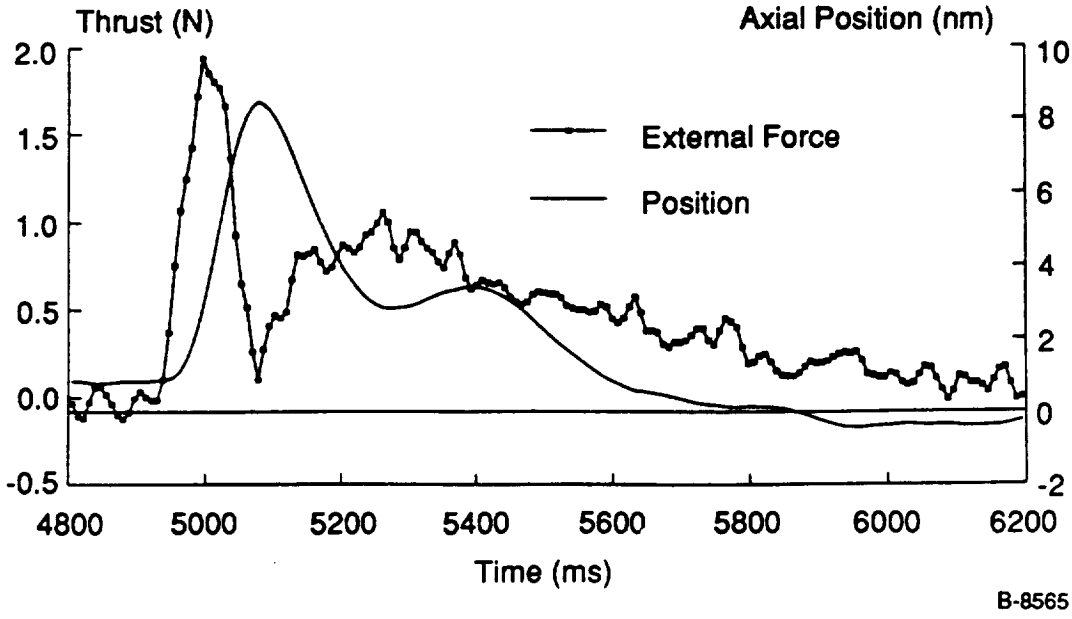


(b) Thrust Profile as Extracted from Current and Position Data

Figure 28. - Measured and extracted thrust profiles.

## 12. THRUST PROFILE AND MAGNETIC SUSPENSION

Control problems experienced using the PSI propulsion simulator were attributed to the very rapid increase in thrust to peak level when fired - the ramp lasting around 1 ms. Tests showed that the response to a demand for a step change in electromagnet current takes around 45 ms with the hardware presently in use at Southampton. The time measured to achieve peak restraining force during a suspended firing of the carbon dioxide thruster was also 45 ms, demonstrating a hardware, rather than a control software, limitation in responding to a sharply increasing thrust.

Loss of control during firing was always preceded by excessive axial motion of the model, causing it to obscure the axial position sensor. A simple analysis showed that the lag between thruster firing and application of maximum restraining force made the amount of axial travel highly sensitive to variations in peak thrust. Results of this analysis are shown in Figure 29. For a low peak thrust the axial travel of the model is minimal. As the peak approaches the maximum restraining force the travel increases rapidly.

It is concluded that for reliable suspension during propulsion simulation in an MSBS, a thrust profile with a ramp to peak thrust of a similar time span to the minimum system response is necessary. Alternatively an unconventional model control system might be invoked.

The emphasis of this project was on proving that a model which carried a substantial thruster (peak thrust close to model weight) could be flown, fired and retained in controlled suspension. This aim was satisfied. It remains to develop the equipment and analysis further to the point where accurate force measurement is possible.

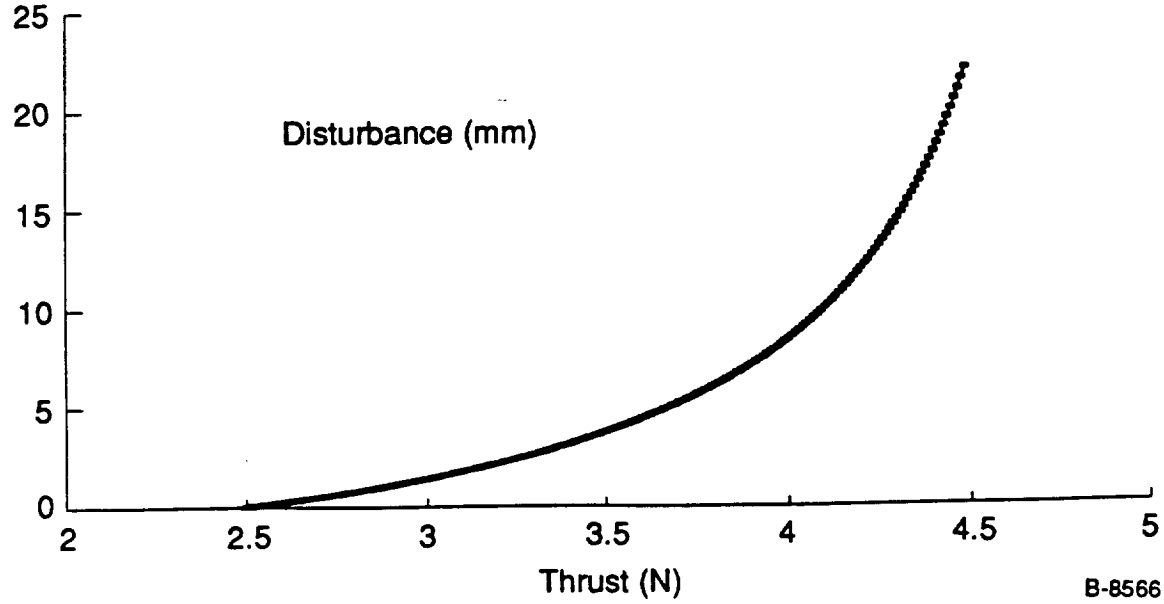


Figure 29. - Results of simplified prediction of model response to different step thrust impulses

# 13. RESULTS AND CONCLUSIONS

- The applicability of a wind tunnel employing Magnetic Suspension and Balance System (MSBS) to propulsive testing was demonstrated.
  - A small-scale propulsive device (1 in. diameter x 8 in. long), which generated a carbon dioxide jet, was designed, built, and statically-tested to measure its thrust characteristics. It was successfully tested in the University of Southampton MSBS at angles-of-attack up to 20 deg.
  - The MSBS at Southampton was modified to keep the model stable under the action of the impulsive force generated by a thrusting model.
- A large-scale propulsive device (2.5 in. diameter x 15 in. long), which generated a carbon dioxide jet, was designed, built, and statically-tested to measure its thrust characteristic.
  - A stable flat thrust profile was obtained over a period of 4s.
  - Nozzle pressure ratios (NPR) of up to 5 were obtained. The device allows variation of NPR by varying the nozzle throat area.
  - The propulsion simulator was demonstrated to operate in a pulse mode via a miniaturized solenoid valve.
  - The thrust and mass flow of the current design are limited by the largest orifice (0.060 in. diameter) in the commercially-available miniature solenoid valve. This limitation can be removed by using a specially designed miniature solenoid valve.

## 14. RECOMMENDATIONS FOR FUTURE PROPULSION SIMULATOR WORK

The present work has developed a propulsive device which can generate an exhaust jet with appropriate characteristics, such as thrust, mass flow, and pressure ratio. Although the initial motivation for this work was application to magnetic suspension, the propulsion simulators can be employed in conventional wind tunnel test applications as well. In fact, conventional testing has less stringent requirements. For example, the electronics can be located external to the simulator, preheater can stay on continuously, etc. In particular, with the following modifications, the large-scale device can be made highly useful for conventional applications.

- Modify solenoid for larger mass flows
  - Increase orifice diameter to $\geq 2$ mm
  - Modify coil to overcome greater force
  - Recharge capacitor to higher voltage

- Operational changes
  - Automatic shut off for pre-heater
  - Power on during run

- Develop model of thermo-fluid dynamics of the simulator to understand transients and to improve short pulse operation.

The small-scale simulator developed in the current program is especially suitable for high-speed (supersonic), blow down testing. The device is compact so that it can be easily incorporated into a high-speed model; and its short thrust time ($< 1$s) is compatible with blow down run times (typically few seconds). With the following modifications, the small-scale simulator can be adapted to high-speed testing.

- Replace off-the-shelf $CO_2$ cartridges by specially-made copper bottle to store $> 16$g of $CO_2$ and for effective heat transfer to the vapor inside the bottle.

- Replace current firing pin/squib mechanism by General Valve Solenoid.

- Locate battery-plus-electronics external to the simulator, outside the test section or as a small module attached to the support.

- Use stack of pre-heated copper balls to avoid condensation with the above modifications; it appears possible to package the simulator in an envelope 1.25 in. diameter x 10 in. long.

## 15. REFERENCES


1. Joshi, P.B., et al., "Propulsion Simulation for Magnetically-Suspended Wind Tunnel Models," Physical Sciences Inc., PSI-2055/TR-859, NASA CR-182093, October 1990.

2. Tuttle, M.H., Kilgore, R.A., and Boyden, R.P., "Magnetic Suspension and Balance Systems, A Selected, Annotated, Bibliography," NASA TM 84661, July 1983.

3. Parker, D.H., "Techniques For Extreme Attitude Suspension of a Wind Tunnel Model in a Magnetic Suspension and Balance System. University of Southampton Ph.D. Thesis, April 1989.

4. Britcher, C.P., "The Southampton University Magnetic Suspension and Balance System - a Partial User Guide. AASU Memo 83/8, April 1984.

## ACKNOWLEDGEMENTS

This work was supported by NASA Langley Research Center under Contract No. NAS1-18845. The authors wish to acknowledge the comments and contributions of Dr. Evan Pugh at Physical Sciences Inc. during this investigation.

## APPENDIX A

### Mass Flow and Thrust Requirements for Wind Tunnel Models

Reference 1 shows that the characteristics of current jet engines require

$$\frac{\dot{m}}{A}\sqrt{RT_{oj}} \approx 1000 - 1200 \text{ lbm/in}^2\text{-s} \cdot \text{ft/s} \tag{A-1}$$

$$\frac{T}{A} \approx 40 - 50 \text{ lbf/in}^2 \tag{A-2}$$

$$\frac{P_{oj}}{p_\infty} \approx 2.5 - 4.5 \tag{A-3}$$

where:

| | | |
|---|---|---|
| $\dot{m}$ | = | mass flow rate lbm/s |
| A | = | nozzle throat area |
| R | = | $R_{univ}$/mol wt |
| | = | gas constant of propellant, ft-lbf/lbm °R |
| $T_{oj}$ | = | stagnation temperature of exhaust, °R |
| T | = | thrust, lbf |
| $P_{oj}$ | = | stagnation pressure of exhaust, lbf/in$^2$ |
| $p_\infty$ | = | ambient pressure, lbf/in$^2$. |

To keep $\dot{m}$ small (for maximum "run" time out of a given storage volume), $T_{oj}$ must be high and molecular weight low - i.e., higher jet velocity. The area A is determined by geometrical scaling of the model. The pressure ratio is determined by similarity of jet expansion characteristics.

It is of interest to determine the mass flow rates of typical propellant gases from the requirements stated above. For this purpose an exit area for the jet, A, must be chosen. The 1/40-scale throat area for an F-404 engine at maximum power is approximately 0.14 in.$^2$ or 0.43-in. diameter. Table A-1 shows the required mass rates for typical gases, carbon dioxide and helium, at room temperature (300°K) and at 1200°K. It is clear that helium at high temperature has the smallest mass flow rate. However, in a typical 5s run, approximately 60g or 15 moles of helium will be needed. For this amount of helium to be carried in a cylinder approximately 1-in. diameter and 5-in. long, the required pressure will be in excess of 5000 atm or density greater than 1 gm/cm$^3$! As discussed in the main text,

Table A-1. Typical Mass Flow Rate and Thrust Requirements

| Gas | Molecular Weight | Mass Flow Rate*, g/s | | Thrust (kgf) |
|---|---|---|---|---|
| | | @ $T^o$ = 300°K | @ $T^o$ = 1200°K | |
| $CO_2$ | 44 | 80-100 | 40-50 | 2.5-3.2 |
| He | 4 | 25-30 | 12-15 | 2.5-3.2 |
| *A = 0.14 $in.^2$ (0.43-in. diameter) with parameters as specified by Eqs. (A-1) to (A-3). | | | | |

carbon dioxide is a more attractive propellant in spite of its greater molecular weight because it can be carried in liquified form under pressure.

The mass flow requirements in Table A-1 must be adjusted if a smaller jet area must be chosen due to model size constraints dictated by common MSBS wind tunnels. A 1/40-scale F-16 (which has the F-404 engine) has a wing span of 9.3 in. and can be accommodated in the 13-in. NASA LaRC MSBS tunnel, but not in the University of Southampton tunnel.

## APPENDIX B

Small-Scale Simulator Test Matrix

| Test No. | Configuration | | | Pin Size | Comment |
|---|---|---|---|---|---|
| | Orientation | Cu Plug | Nozzle Diameter (in.) | | |
| 1 | Vertical (up) | 2 mm-1 set | 0.098 | Large | No pressure data |
| 2 | Vertical (up) | 2 mm-1 set | 0.098 | Large | Cylinder didn't open - pin OD was larger than center section of bottle diaphragm |
| 3 | Vertical (up) | None | 0.098 | Large | Good |
| 4 | Vertical (up) | 2 mm-1 set | 0.098 | Large | Dull pin |
| 5 | Vertical (up) | 2 mm-1 set | 0.098 | Large | Repeat of 4 |
| 6 | Vertical (up) | 2 mm-1 set | 0.098 | Large | Hardened pin - OD too large |
| 7 | Vertical (up) | 2 mm-1 set | 0.098 | Large | Pin OD turned down by 0.005 in. - worked |
| 8 | Vertical (up) | 2 mm-3 sets | 0.098 | Large | Good shot |
| 9 | Vertical (up) | 2 mm-3 sets | 0.098 | Large | Blocked pin orifice |
| 10 | Vertical (up) | 2 mm-3 sets | 0.098 | Large | Pin pushed out of $CO_2$ cylinder, overpressurization, $P_1$ transducer failed |
| 11 | Vertical (up) | 2 mm-3 sets | 0.098 | Large | Good shot, no $P_1$ data |
| 12 | Horizontal | 2 mm-3 sets | 0.098 | Large | Good shot, not much $CO_2$ cloud |
| 13 | Horizontal | 2 mm-3 sets | 0.098 | Large | Good shot, repeat of 12 |
| 14 | Vertical (down) | 2 mm-3 sets | 0.098 | Large | Good shot, repeat of 13 |
| 15 | Vertical (down) | 2 mm-3 sets | 0.098 | Large | Good shot, repeat of 14 |

| Test No. | Configuration | | | Pin Size | Comment |
|---|---|---|---|---|---|
| | Orientation | Cu Plug | Nozzle Diameter (in.) | | |
| 16 | Horizontal | 2 mm-1 set<br>1 mm-2 sets | 0.098 | Large | Pin pushed out of bottle, $P_1$ working |
| 17 | Horizontal | 2 mm-1 set<br>1 mm-2 sets | 0.098 | Large | Good shot, redo 16 |
| 18 | Horizontal | 2 mm-1 set<br>1 mm-2 sets | 0.098 | Large | Good shot, repeat of 17 |
| 19 | Horizontal | 2 mm-1 set<br>1 mm-2 sets | 0.098 | Large | Good shot, repeat of 18. P3 adjusted to measure total pressure |
| 20 | Horizontal | 1 mm-1 set<br>bronze wool | 0.098 | Large | Good |
| 21 | Horizontal | 1 mm-1 set<br>bronze wool | 0.098 | Large | Good |
| 22 | Horizontal | 1 mm-1 set<br>bronze wool | 0.098 | Small | Pin pushed out of bottle - OD of pin same as large pin |
| 23 | Horizontal | 1 mm-1 set<br>bronze wool | 0.098 | Small | Redo 23 - good run. OD reduced. Note $P_2$v$P_3$ pressure drop, longer run at flatter thrust |
| 24 | Horizontal | 1 mm-1 set<br>bronze wool | 0.098 | Small | Repeat of 24 |
| 25 | Horizontal | 2 mm-1 set<br>bronze wool | 0.295 | Large | Very high thrust, short run 0.2s, $P_2 \approx P_3$, $P_1$ low - substantial drop through plug |
| 26 | Horizontal | 2 mm-1 set<br>bronze wool | 0.295 | Large | Redo 25, good |
| 27 | Horizontal | 2 mm-1 set<br>bronze wool | 0.295 | Large | Repeat 26 |

| Test No. | Configuration | | | Pin Size | Comment |
|---|---|---|---|---|---|
| | Orientation | Cu Plug | Nozzle Diameter (in.) | | |
| 28 | Horizontal | None | 0.295 | Large | Initial "ringing" in thrust profile. Pressures too low, in transducer noise, 60 cycle noise on force |
| 29 | Horizontal | None | 0.295 | Large | Redo 28, same result |
| 30 | Horizontal | 1 mm-1 set bronze wool | 0.295 | Small | Low thrust level, longer run |
| 31 | Horizontal | 1 mm-1 set bronze wool | 0.295 | Small | Repeat of 30 |

Notes:

1. The $P_1$ pressure transducer saturated during Test 8 and failed during Test 10. It was replaced in Test 16.

2. Following Test 19, the orientation of the $CO_2$ jet from the pin was adjusted such that it impinged directly on the $P_3$ pressure port, providing a more reliable measure of stagnation pressure.

3. Pressure transducer ranges were:

   $P_3$: 1000 psi
   $P_2$: 500 psi for runs < Test 16
   : 5000 psi for runs ≥ Test 16
   $P_1$: 100 psi for runs < Test 16
   : 500 psi for runs ≥ Test 16

## APPENDIX C

Large-Scale Simulator Test Matrix

| Test No. | Description | Acquired Data | | | Comments |
|---|---|---|---|---|---|
| | | Thrust | Bottle Pressure | Exit Plane Pressure | |
| 45 | 5s run | x | x | | Simulator filled with gaseous $CO_2$ at 840 psi. Pre-heater cold |
| 46 | 5s run | x | x | | No pitot tube at nozzle exit plane |
| 47 | 5s run | x | x | x | |
| 48 | 5s run | x | x | x | Repeat of Test 47 |
| 49 | 5s run | x | x | x | Repeat of Test 47 |
| 50 | 5s run | x | x | x | Reservoir under-filled |
| 51 | 1s pulse | x | x | x | |
| 52 | 1s pulse | x | | x | No refill after Test 51. No bottle pressure data due to data acquisition failure |
| 53 | 1s pulse | x | x | x | No refill after Test 52. Pitot tube was off axis at exit plane of nozzle |
| 54 | 1s pulse | x | | x | No refill after Test 53. No bottle pressure data due to data acquisition failure. |
| 55 | Reservoir purge | x | x | x | No refill after Test 54 |
| Note: Tests 1 - 44 were tests of the small-scale propulsion simulator which are summarized in Apendix B. | | | | | |

# APPENDIX D

## Large-Scale Simulator Thrust and Mass Flow Analysis

- Mass flow through nozzle:

$$\dot{m}_n = c_{d_n} A_n^* \sqrt{\frac{\gamma}{RT_{o_n}}} P_{o_n} \left(\frac{2}{r+1}\right)^{\frac{\gamma+1}{2(\gamma-1)}}$$

- Mass flow out of reservoir (through solenoid valve)

$$\dot{m}_s = c_{d_s} A_s \sqrt{\frac{2(P_{o_r} - P_{o_n} - \Delta P)}{\rho_r}}$$

$\rho_r = \rho_r(P_{o_r}, T_{o_r})$ Equilibrium vapor pressure curve

$\Delta P$ = Pressure drop through preheater

- Since $\dot{m}_n = \dot{m}_s$ under steady-state and $P_{o_n} << P_{o_r}$ ,

$$P_{o_n} \approx \frac{c_{d_s}}{c_{d_n}} \left(\frac{A_s}{A_n^*}\right) \sqrt{\frac{2RT_{o_n}}{\gamma}} \left(\frac{\gamma+1}{2}\right)^{\frac{\gamma+1}{2(\gamma-1)}} \rho_r^{1/2} (P_{or} - \Delta P)^{1/2}$$

- Assume

$T_{o_n} = T_{o_r} \approx 283°K$, then $P_{o_r} = 45.2$ atm

$\rho_r = 861$ kgm/m$^3$

$d_s$ = solenoid orifice dia = 0.152 cm

$c_{d_s} = 0.7$

$d_n^*$ = nozzle throat dia = 0.689 cm

$c_{d_n} = 0.9$

$\Delta P \approx 34$ atm (estimated)

then,

$P_{o_n} \approx 5.6$ atm (82 psia)

Measured exit plan pressure ≈ 70 psia

$\therefore P_{o_n} \approx 75$ psia

or NPR ≈ 5

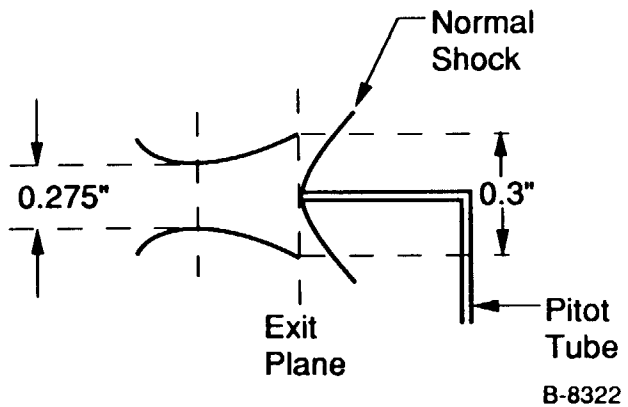


$A_e/A_n^* = 1.19 \Rightarrow Me = 1.5$ for $CO_2$

$P_{o_e}/P_{o_n} = 0.93$

- Thrust Calculation

$$T = \dot{m}_n u_e + A_e (p_e - p_\infty)$$

$$u_e = M_e \sqrt{\gamma R T_e}\,, \quad T_o / T_e = \left(1 + \frac{\gamma - 1}{2} M_e^2\right)$$

Typically, $\dot{m}_n \leq 40$ g/s

then,

$T \approx 1.6$ kgf (3.5 lbf)

## APPENDIX E

### Preheater Thermodynamic Model

The $CO_2$ in the simulator reservoir is saturated liquid at approximately 20°C. This has a specific enthalpy of 180 kJ/kg. As is evident from the Molier diagram (Figure E-1), if this liquid was expanded into 1 atm without any increase in enthalpy, it would immediately freeze. In order to prevent freezing, the enthalpy must be increased to at least 370 kJ/kg. Heat must be added to the $CO_2$ to increase its enthalpy before it leaves the nozzle. Our design uses a preheater, consisting of a heated cylinder of coiled copper tubes through which the $CO_2$ passes, to facilitate this heat transfer.

Our preheater consists of five copper tubes of 0.125 in. O.D. and 0.065 in. I.D., each 92 in. (2.3m) long, coiled into a cylinder with an O.D. of 2.25 in. and 3 in. long. The coiled tubes are sandwiched between two brass plates, and the gaps between tubes are filled with tin to increase the thermal mass and improve heat transfer from tube to tube. The cylinder is heated from the inside by a 400W cartridge heater, and is heated to 75°C before the simulator is fired.

When liquid $CO_2$ passes through a heated tube, two phenomena occur simultaneously. Heat is transferred to the $CO_2$ due to the temperature difference between the wall and the $CO_2$, causing the liquid to vaporize. Also, the pressure of the flowing $CO_2$ drops due to friction. This also causes $CO_2$ to vaporize. These two phenomena are respectively described by the following equations:

$$\Delta h = \frac{4\bar{q}\Delta L}{DG} \tag{E-1}$$

and

$$\Delta L = - \frac{D}{2f}\left[\frac{\Delta P}{G^2\bar{v}_m} + \frac{\Delta v_m}{\bar{v}_m}\right] \tag{E-2}$$

where $\Delta L$ is an increment of length along the tube, $\Delta h$ is the change in specific enthalpy over the increment, D is the diameter of the tube, G is the mass velocity of the flow, $\bar{q}$ is the average heat flux over the increment, f is the friction coefficient of the tube, $\Delta p$ is the change in pressure over the increment, $\bar{v}_m$ is the average specific volume over the increment, and $\Delta v_m$ is the change in specific volume over the increment. Heat flux, $\dot{q}$, is given by:

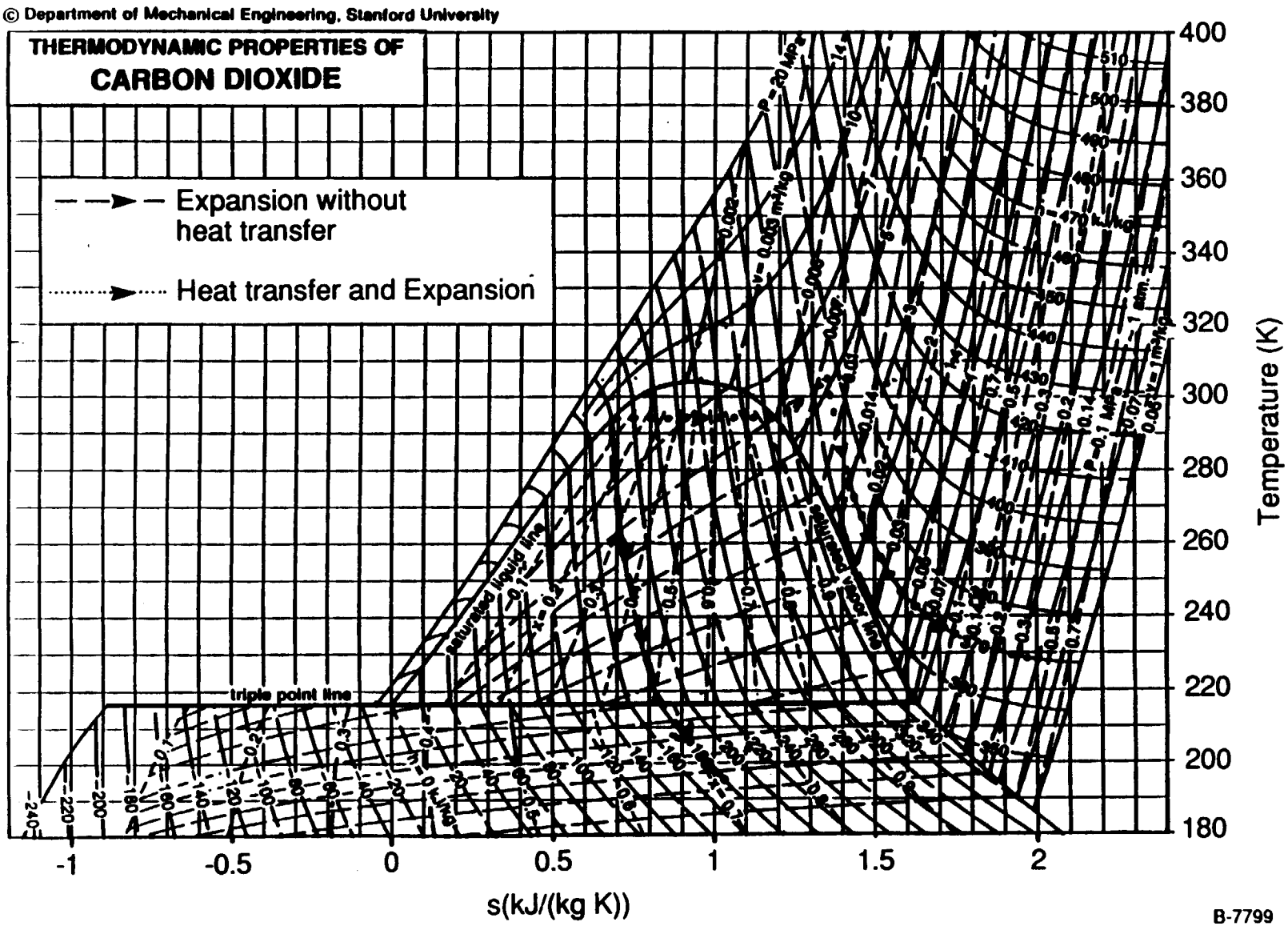


Figure E-1. - Molier diagram for $CO_2$.

$$\dot{q} = 0.023\frac{k}{D}(Re)^{0.8}(Pr)^{0.4}(T_w - T_{CO_2}) \qquad \text{(E-3)}$$

where k is the thermal conductivity of $CO_2$, $T_w$ is the wall temperature, $T_{CO_2}$ is the flow temperature, $Re = DG/\mu$, and $Pr = \mu C_p/k$.

For two phase flow, these equations, along with the p, v, T, h relations for $CO_2$, can be used iteratively to calculate pressure and enthalpy versus length along the tube. However, for a hot wall ($T_w - T_{CO_2} > 10°C$) and a reasonable value for the friction coefficient, the pressure drop is negligible for a large enthalpy increase. In terms of the Molier diagram (Figure E-1), saturated liquid is converted to saturated vapor by a constant pressure (and temperature) heat transfer process. For this process, Eq. (E-1) alone can be used to calculate enthalpy as a function of length along the tube. After the point at which the $CO_2$ is converted to saturated vapor, the pressure drops significantly with increasing enthalpy, so both Eqs. (E-1) and (E-2) must be used to calculate enthalpy versus length.

Figure E-2 shows the specific enthalpy of $CO_2$ versus length along the tube for different tube wall temperatures at a mass flow rate of 8 g/s per tube (40 g/s through five tubes). This figure shows that a tube length of 2.3m is long enough to provide the enthalpy required.

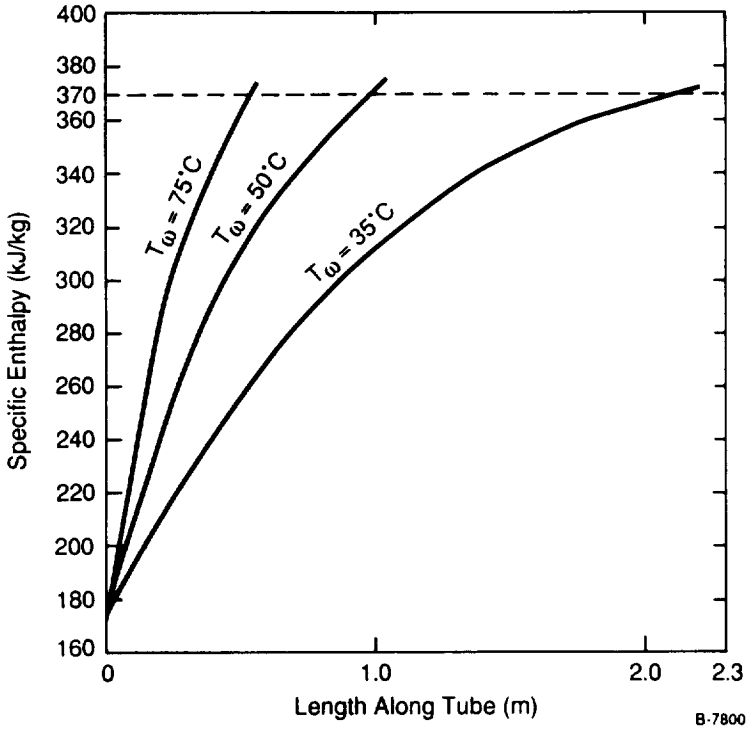


Figure E-2. - Specific enthalpy versus length along tube.

It must be shown, however, that there is sufficient thermal mass in the preheater to provide this enthalpy to the $CO_2$ for a reasonable period of time. The preheater contains 620g of copper tubing, 470g of tin, and 300g of brass. This has a total thermal mass of 480 J/°C, which, when heated to 75°C, can provide 26 kJ of heat before dropping below 20°C. This must provide 7600 J/s to the $CO_2$, so it can maintain the necessary heat transfer for 3.5s.

Tests have shown that the simulator blows $CO_2$ at 40 g/s for approximately 4.5s before snow is observed, and the final temperature of the preheater after a run is about 0°C. Therefore, the model is conservative, and the actual preheater continues to provide heat to the $CO_2$ for about 1s after its temperature drops below 20°C.

## APPENDIX F

### Small-Scale Simulator Installation Procedures

NOTE: The installation procedures should be followed with reference to Figure F-1.

1) Put on safety glasses

2) Unscrew the HeNe OPTICAL FILTER (ITEM #1) from the NOSE (ITEM #2).

NOTES:
A. Do not attempt to remove the NOSE without first removing the OPTICAL FILTER.

3) Unscrew the NOSE (ITEM #2) from the BODY (ITEM #3).

4) Install BATTERY (ITEM #4) in orientation for correct polarity.

NOTES:
A. Only use KODAK PHOTOLIFE K28A 6 VOLTS alkaline.

B. A single battery will last for approximately five (5) experiments. When the voltage of the battery drops below 5.5 Volts it will no longer fire the squib and should be replaced.

C. When the battery is installed the circuit is powered up and there is a current drain on the battery. Installing the battery for a long period of time (hours) before an experiment should be avoided.

5) Screw the NOSE (ITEM #2) back onto the BODY (ITEM #3).

6) Re-install the HeNe OPTICAL FILTER (ITEM #1) in the NOSE (ITEM #2).

NOTES:
A. The HeNe optical filter is optimized to transmit HeNe laser light (632.8 nm) and reject other wavelengths. It should be noted, however, that while light from overhead fluorescent light fixtures will be sufficiently rejected and will not turn the switch on, a bright light fixture or camera flash in close proximity and in direct view of the optical system will.

7) Put black electrical tape over the HeNe OPTICAL FILTER (ITEM #1).

7a) Check voltage across the two BINDING POSTS (ITEM #8) after installing a new battery. Voltage should be approximately 0.6V.

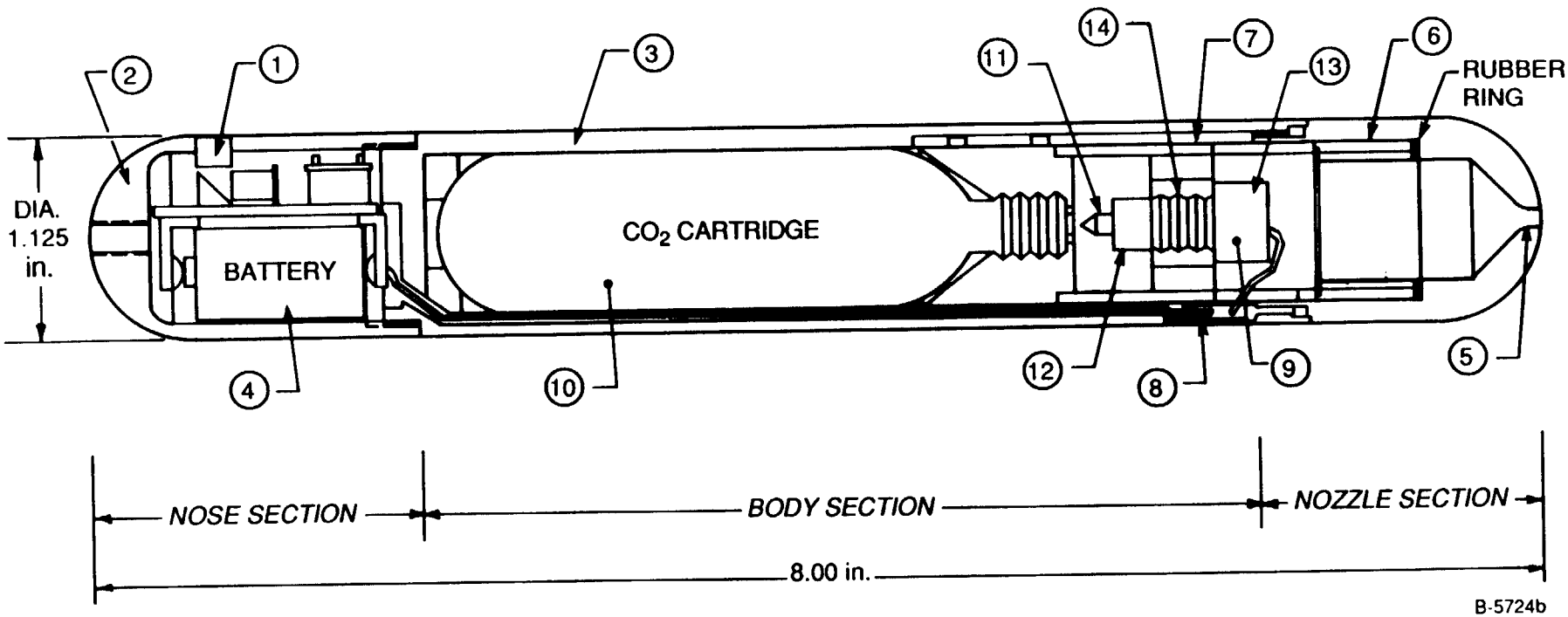


Figure F-1. - Small-scale propulsion simulator design.

NOTES:

A. The electrical tape is used as a safety such that stray light will not be able to trigger the switch.

8) Unscrew the NOZZLE (ITEM #5) from the rear of the BODY (ITEM #3).

9) Remove the RING (ITEM #6) from inside the NOZZLE (ITEM #5).

10) Remove the RETAINER (ITEM #7) from inside the BODY (ITEM #3).

11) Loosen the two set screws from the BINDING POSTS (ITEM #8) where the SQUIB (ITEM #9) wires are attached using the provided wrench. Slide the wires out of the cross holes in the BINDING POSTS (ITEM #8).

12) Slide the $CO_2$ CYLINDER (ITEM #10)/SQUIB (ITEM #9)/PIN (ITEM #11) assembly out of the BODY (ITEM #3).

13) Unscrew the used $CO_2$ CYLINDER (ITEM #10) from the HOLDER (ITEM #12).

14) Unscrew the CAP (ITEM #13) which contains the SQUIB (ITEM #9) using the provided tool.

15) Remove the used SQUIB (ITEM #9), using a pair of pliers, if necessary.

NOTES:

A. After a couple of experiments (2-3) the squib products accumulate on the inside of the squib retainer. This debris can be cleaned out using methanol and the provided cotton swabs.

16) Unscrew the SQUIB RETAINER (ITEM #14) from the HOLDER (ITEM #12) using the provided tool.

NOTES:

A. A squib retainer should last for approximately eight (8) experiments and then should be replaced. The end where the pin comes out will start to deform after numerous experiments and affect the pin/cylinder alignment.

17) Push the extended PIN (ITEM #11) back into the SQUIB RETAINER (ITEM #14) until it's shoulder is even with the end of the SQUIB RETAINER (ITEM #14).

NOTES:

A. Each pin provided should stay sharp enough to be used in approximately ten (10) experiments.

18) Screw the PIN (ITEM #11)/SQUIB RETAINER (ITEM #14) combination into the HOLDER (ITEM #12). Tighten to a few inch-lbs using the provided tool.

19) Insert a new SQUIB (ITEM #9) into the SQUIB RETAINER (ITEM #14) making sure the SQUIB (ITEM #9) black plug is in snug. Make sure the SQUIB (ITEM #9) is oriented with respect to the HOLDER (ITEM #12) as shown in Figure F-2.

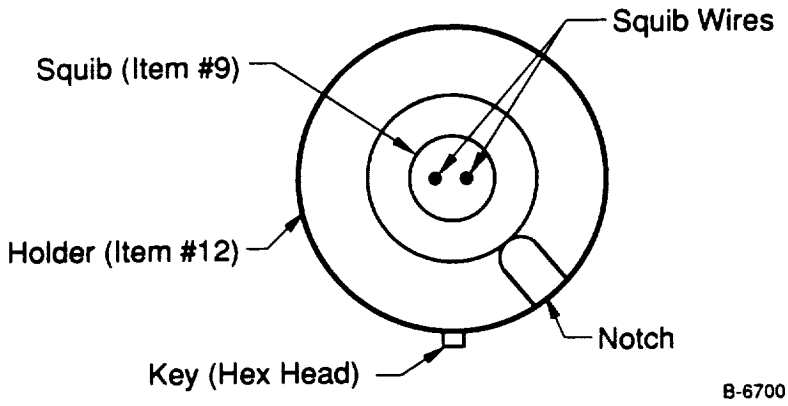


Figure F-2. - SQUIB/HOLDER orientation.

NOTES:

A. **Caution!** The squib is very dangerous and should be handled with care. The squib will produce 150 psi in a 10 cc volume which is enough pressure to remove a finger. The squib wires should be kept shorted until Step #23. Make sure that the black electrical tape remains over the HeNe optical filter during the following steps to prevent accidental triggering.

20) Screw the CAP (ITEM #13) onto the SQUIB RETAINER (ITEM #14) hand tight.

21) Screw a new $CO_2$ CYLINDER (ITEM #10) onto the opposite end of the HOLDER (ITEM #12).

22) Slide the $CO_2$ CYLINDER (ITEM #10)/SQUIB (ITEM #9)/PIN (ITEM #11) assembly into the BODY (ITEM #3) noting the location of the key (HEX HEAD) and key slot.

23) Cut the SQUIB (ITEM #9) wires to 1.5 - 2.0 cm in length.

24) Bend approximately 1.5 mm of the SQUIB (ITEM #9) wires 90 DEG and insert into the horizontal holes in the BINDING POSTS (ITEM #8) and clamp in place by turning the set screw. Make sure that the squib wires are not touching either the CAP (ITEM #13) or the BODY (ITEM #3).

25) Insert the RETAINER (ITEM #7) into the BODY (ITEM #3) noting the location of the cutout for the SQUIB (ITEM #9) wires and the mating notch. Make sure that the squib wires are not touching the RETAINER (ITEM #7).

26) Place the RING (ITEM #6) in the NOZZLE (ITEM #5), making sure the rubber ring is between the RING (ITEM #6) and the NOZZLE (ITEM #5) and screw the NOZZLE (ITEM #5) onto the BODY (ITEM #3).

27) Remove the black electrical tape over the HeNe OPTICAL FILTER (ITEM #1) before experiment.

28) Repeat Step #7 through Step #27 for another experiment. If the battery has to be changed, repeat Step #2 through #27. **Caution!** Be sure to remove any live squib from the assembly before installing a new battery.

NOTE:

A. If the battery has to be removed, the easiest method is to slip a small screwdriver under it and pop it up.

29) An Acrylic Spray was applied to the outside surface of the device to prevent rust and increase wear. Do not apply any Silicon Spray or solvent to the outside surface.

30) To prevent rusting, Silicon Spray was applied to the internal steal and iron parts and to the inside of the nozzle, nose and body. Another application may be required at the test site if evidence of corrosion appears.

APPENDIX G

Large Scale Simulator Installation Procedure

Battery Installation

1) Unscrew nozzle.

2) Remove outer shell retaining screws.

3) Remove outer shell by pulling it away from the cylinder section.

4) While holding simulator vertically, with preheater section pointed upward and cylinder section pointed downward, install a battery into the left most battery clip, with the positive pole up.

5) Install the remaining batteries into the remaining clips from left to right, alternating polarity between batteries

6) Slide outer shell back over heat exchanger section, matching the location of the connector on the simulator with the connector cutout on the shell

7) Fasten the outer shell retaining screws.

8) Screw nozzle firmly into tail end.

Carbon Dioxide Filling

1) Wrap heater around $CO_2$ supply cylinder.

2) Install fill plumbing, consisting of a pressure gauge (2000 psi min), a vent valve, and a flex hose terminated with a male quick connect fitting, onto the $CO_2$ cylinder (Figure G-1).

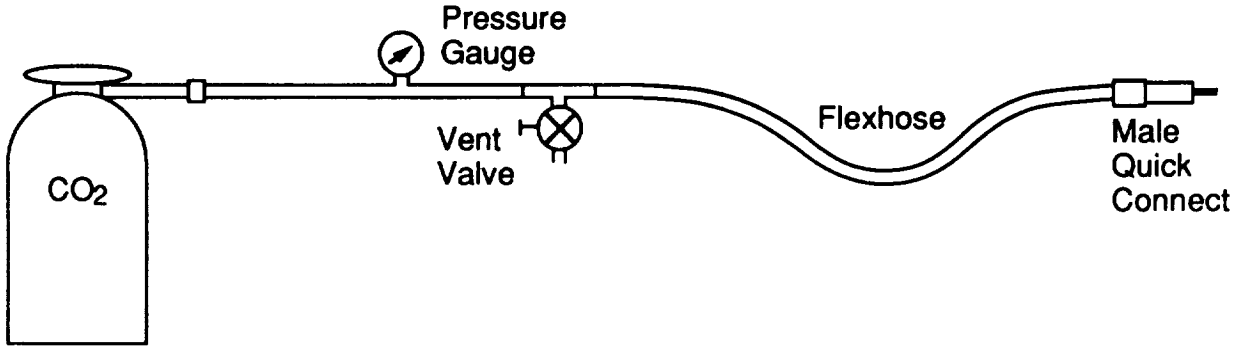


Figure G-1. $CO_2$ Filling Scheme

3) Screw fill fitting into fill port of simulator. Tighten with a wrench until fitting seats firmly.

4) Tape a thermistor to the outside of the simulator cylinder section to monitor bottle temperature.

5) Connect male quick connect of fill plumbing to female quick connect of fill fitting.

6) Open $CO_2$ supply cylinder valve to allow gas to fill.

7) Turn $CO_2$ supply cylinder heater on.

8) Monitor pressure (on gauge) and temperature (from thermistor) until the proper $CO_2$ density is reached as indicated by the chart in Figure G-2.

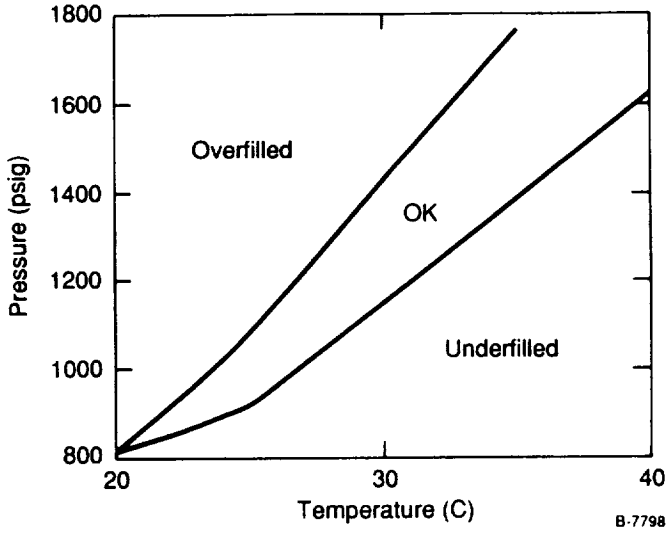


Figure G-2.

9) Turn off $CO_2$ supply cylinder heater.

10) Close $CO_2$ supply cylinder valve.

11) Continue monitoring pressure until pressure drops below 900 psig.

12) Open fill plumbing vent valve to allow line to vent.

13) Disconnect fill line from fill fitting.

14) Remove fill fitting from fill port.

15) Remove thermistor from cylinder section.

Heating/Charging

1) Plug connector of power cord into connector in simulator.

2) Attach ohmmeter to connector leads.

3) Plug end of power cord into 120 VAC, 60 Hz supply.

4) Monitor resistance of connector leads. When resistance drops to 2400Ω, unplug power cord from AC power.

5) Unplug power cord connector from simulator.

6) Simulator is now charged and ready to fire. Be sure that fill port of simulator is pointing vertically.

# APPENDIX H

University of Southampton MSBS Modification Final Report

# UNIVERSITY OF SOUTHAMPTON

## department of aeronautics and astronautics

PROPULSION SIMULATION IN A MAGNETIC SUSPENSION WIND TUNNEL

Keith Garbutt

FINAL REPORT
May 1991

DEPARTMENT OF AERONAUTICS & ASTRONAUTICS
UNIVERSITY OF SOUTHAMPTON

# PROPULSION SIMULATION IN A MAGNETIC SUSPENSION WIND TUNNEL

Final Report
Keith Garbutt, May 1991

CONTENTS


| | PAGE |
|---|---|
| LIST OF SYMBOLS AND ABBREVIATIONS | |
| 1.0 INTRODUCTION | 95 |
| 2.0 PROPULSION SIMULATION AND THE SOUTHAMPTON MSBS | 96 |
| 2.1 THE SOUTHAMPTON MSBS | 96 |
| 2.1.1 ELECTROMAGNETS | 9 |
| 2.1.2 POSITION SENSING | 96 |
| 2.1.3 CONTROL HARDWARE | 96 |
| 2.2 PROPULSION SIMULATION BACKGROUND | 97 |
| 2.3 PROPULSION SIMULATION REQUIREMENTS | 97 |
| 2.4 FUNDING | 97 |
| 3.0 MODIFICATIONS TO THE SOUTHAMPTON MSBS | 98 |
| 3.1 CALIBRATION OF POWER SUPPLIES | 98 |
| 3.1.1 BACKGROUND | 98 |
| 3.1.2 SOLUTION | 98 |
| 3.1.3 RESULTS | 99 |
| 3.2 REPOSITIONING OF AXIAL POSITION SENSING OPTICS | 100 |
| 3.3 MODIFICATIONS TO THE COMPUTER SYSTEM | 101 |
| 3.4 SUSPENSION OF SOFT-IRON MODELS | 102 |
| 4.0 DEVELOPMENT WORK | 104 |
| 4.1 REPRESENTATIVE MODEL | 104 |
| 4.2 SUSPENSION WORK | 104 |
| 4.2.1 PREPARATION | 104 |
| 4.2.2 QUALITY OF SUSPENSION | 104 |
| 4.3 FORCE AND MOMENT CALIBRATIONS | 106 |
| 4.4 OPTIMISATION FOR AXIAL RESTRAINT | 110 |
| 4.5 TUNNEL SPEED MEASUREMENT | 112 |
| 4.6 THRUST TEST STAND | 113 |
| 4.7 PC SOFTWARE | 113 |
| 4.7.1 MSBS DATA LOGGER | 113 |
| 4.7.2 ANALYSIS OF RUN-DATA | 114 |
| 4.7.3 TRANSIENT ANALYSIS | 114 |
| 4.7.4 SOFTWARE FOR STATIC THRUST TESTS | 114 |
| 4.8 INTEGRATION | 115 |

5.0 EXPERIMENTS 117
5.1 SET-UP 117
5.1.1 POSITION SENSING SYSTEM OPTICAL ALIGNMENT 117
5.1.2 CONTROLLER DATA FILES 117
5.1.3 QUALITY OF SUSPENSION 117
5.2 CALIBRATION WORK 118
5.3 ROCKET EXPERIMENTS 119
5.4 ROCKET RESULTS 120
5.5 CARBON DIOXIDE THRUSTER 122
5.5.1 OPERATION 122
5.5.2 INITIAL BENCH TESTS 123
5.5.3 DEVELOPMENT 124
5.6 WIND TUNNEL TESTS 29
5.7 TEST PROCEDURE 125
5.8 INVESTIGATION OF MAXIMUM CURRENT SLEWING RATE 125

6.0 TRANSIENT ANALYSIS 126
6.1 DATA ANALYSIS TECHNIQUE 126
6.2 TRANSIENT HEAVE FORCE AND PITCHING MOMENT 131
6.3 FUTURE DEVELOPMENT OF TRANSIENT ANALYSIS 132

7.0 RESULTS 133
7.1 BENCH TESTS 133
7.2 TESTS IN SUSPENSION 133
7.3 DERIVED EXPERIMENTAL RESULTS 134
7.4 RESOLUTION OF HEAVE AND AXIAL FORCES 134

8.0 DISCUSSION 135
8.1 HARDWARE 135
8.2 CARBON DIOXIDE THRUSTER 135
8.3 CONTROL 136
8.4 DATA ANALYSIS 136
8.5 ROCKETS 137
8.6 RESULTS 137

9.0 CONCLUSIONS 139

APPENDIX 1: ESTIMATED RESPONSE TO A STEP THRUST 140

LIST OF FIGURES 141

FIGURES 143

LIST OF SYMBOLS AND ABBREVIATIONS

| | |
|---|---|
| a | acceleration ($ms^{-2}$) |
| A/D | analogue to digital converter |
| C | current (A) |
| $CO_2$ | carbon dioxide |
| D/A | digital to analogue converter |
| DC | direct current |
| E/M | electromagnet |
| F | force (N) |
| He-Ne | helium-neon |
| i/o | input/output |
| k | calibration constant (N/A, Nm/A) |
| MSBS | magnetic suspension and balance system |
| p | position (m) |
| PACS | photodiode array control system |
| PC | personal computer |
| PDP11 | Digital Equipment computer |
| PSI | Physical Sciences Inc |
| q | dynamic pressure ($Nm^{-2}$) |
| s | displacement (m) |
| SUMSBS | Southampton University magnetic suspension and balance system |
| T | thrust (N) |
| v | velocity ($ms^{-1}$) |
| $\alpha$ | angle of attack (degrees) |

C
FORTRAN
MACRO-11 computer languages

ANALYSE
MAGEN
MAGE2
TRANSIENT computer program names

# 1.0 INTRODUCTION

This report describes research into propulsion simulation in a Magnetic Suspension and Balance System (MSBS), performed at the University of Southampton under contract from Physical Sciences Inc (PSI), over the period April 1989 to May 1991.

As part of a larger investigation into simulation of inlet and exhaust flows in an MSBS, PSI were to supply a model incorporating a simple carbon dioxide thruster. The University were contracted to modify their tunnel hardware and control system to allow suspension of this model, and to perform some basic wind tunnel testing with subsequent data analysis. Ideally the tests would investigate changes in the drag coefficient of a body, caused by the presence of an exhaust plume.

Areas to be addressed at Southampton included data acquisition, control system development, hardware compatibility and calibration techniques. The results of the work at Southampton would then be used by PSI as input to other areas of their propulsion simulation research, and in drawing overall conclusions about suitable techniques and practice.

## 2.0 PROPULSION SIMULATION AND THE SOUTHAMPTON MSBS

### 2.1 THE SOUTHAMPTON MSBS

Research into magnetic suspension systems for wind tunnel testing has been on-going at Southampton University since the late 1950s. The configuration of the present system is largely due the result of work by Britcher (1) and Parker (2), and can be conveniently grouped into a number of sub-systems. A hardware block diagram is presented as Figure 2.1.

#### 2.1.1 ELECTROMAGNETS

The electromagnet array is depicted in Figure 2.2. Its layout is conventional apart from the skew in the lateral magnets, which enables them to produce sideforce during suspension of models at angles of attack from below zero to beyond ninety degrees. The symmetrical arrangement of magnets gives greater field uniformity within the test section, and hence better linearity in force calibrations, and improved performance during large motions.

#### 2.1.2 POSITION SENSING

An optical system is used to sense the position of a suspended model. Laser light sheets are directed across the test section, and the positions of shadows cast by the model are picked up by a number of linear photo-diode arrays. Support electronics allow a shadow position to be made available to the control computer as a digital count of illuminated 'pixels'. Prior knowledge of the sensing system geometry allows the production of look-up tables, used by the controller in real time to decode model position in five degrees of freedom from the shadow positions. More details concerning the position sensing system are available in (2).

#### 2.1.3 CONTROL HARDWARE

The control computer presently used with the SUMSBS is a Digital PDP11/84, and is further discussed in Section 3.3. A 16-bit parallel interface links the computer to the A/D and D/A equipment as well as to the PACS position sensing controller. This equipment provides the analogue signals needed to drive the electromagnet power supplies, and is used to read magnet currents and tunnel speed. The forces and moments experienced by the model in suspension are then derived from the currents using calibration data. The power supplies are

discussed in Section 3.1.

## 2.2 PROPULSION SIMULATION BACKGROUND

For the purposes of this report it is sufficient to point out that propulsion simulation is a frequent requirement in wind tunnel testing, and must be shown to be compatible with new test techniques if they are to become accepted practice. In addition, as a magnetically suspended model is particularly useful for studying base flows, propulsion simulation is a very relevant area for MSBS development work.

## 2.3 PROPULSION SIMULATION REQUIREMENTS

The overriding difference between exhaust simulation in a conventional wind tunnel and in an MSBS is that in the MSBS the representative exhaust gases must be generated on-board the model. This gas generation must be safe and controllable. The flow properties should represent a 'real' exhaust flow for testing to be worthwhile. The model with its gas generator must be capable of being suspended over the required range of conditions throughout the duration of a motor run, and be cost-effective.

## 2.4 FUNDING

This work was funded by Physical Sciences Inc of Andover MA, as part of NASA SBIR 87-1 and represents a part of their more general investigation into MSBS propulsion simulation.

# 3.0 MODIFICATIONS TO THE SOUTHAMPTON MSBS

## 3.1 CALIBRATION OF POWER SUPPLIES

### 3.1.1 BACKGROUND

The current in each electromagnet of the SUMSBS is controlled independently by a Contraves DC Servo Controller. As presently configured, a +/- 20 Ampere current is supplied in response to a +/- 5 Volt input signal from the control system. Current is varied by two-state modulation. The output signal is based on a 5 kHz square wave of amplitude 100 Volts. Duration of the positive and negative signal components is adjusted to give the correct resultant current.

It had been suspected for some time that an inconsistency in supply of current to the electromagnets was affecting operation of the MSBS. Britcher (3) first demonstrated an aberration in current response to a sinusoidal demand. Parker showed that the response to steady demands consisted of a series of line segments, as shown in Figure 3.1.

The cause of the degraded operation of the servo controllers was shown to be the high inductance of the electromagnets. The controllers are designed for operation with industrial DC motors and are rated for a load inductance of 1.0 mH. Operated with the SUMSBS, the loads are 60 mH (main E/Ms) and 135 mH (axial E/Ms). When connected to a pure resistive load, the correct servo controller response was restored.

A number of operational problems have in the past been attributed to the power supply non-linearity. These have included poor dynamic calibration results (4), inconsistent gain requirements, and imperfect following of a changing position demand (2). All of these occur because it is assumed in the control software that E/M current is directly proportional to demand current. There is no feedback of measured current.

### 3.1.2 SOLUTION

A straightforward hardware solution for this problem was deemed unlikely as low inductance is an integral part of the controller design philosophy for minimum losses with the two-state switching technique. More promising was some form of software calibration.

A full look-up table, although easy and effective to implement, would be impracticable on the PDP11/84 control computer. The suspension software uses most of the 64 kB base memory, and the use of overlays to access virtual memory has been shown to be prohibitive in terms of access time.

A compact development of a full look-up table is storage of data for a smaller number of points, with interpolation used to generate intermediate values. This technique is widely used elsewhere in the SUMSBS control software. For example, data for position sensing and control at different angles of attack is generated for each model at ten degree intervals, prior to suspension. Linear interpolation is then used by the control system to generate values for other angles.

To address the power supply non-linearity, the above technique was modified to exploit the line segment structure of the observed current response, as suggested by Thomas (5). Instead of a look-up table with data at regular intervals, the data points are chosen to be the ends of the line segments. Linear interpolation then yields a very good approximation to a point on the line. For each line segment, 3 values describing gradient, offset and applicable current range are stored. This gives typically 15 data items per power supply, instead of the several thousand necessary for a full look-up table.

Fortran software was produced to drive the servo controllers over their full current range and identify the line segments. The responses changed as the system warmed up, and also gradually with time. For these reasons, the calibration process is repeated every few weeks, or before a major testing period. The test is performed after some initial suspension to bring the tunnel hardware to a typical operating temperature. A routine in the control program allowed use of the new data to adjust current demands.

### 3.1.3 RESULTS

Results of the power supply calibration are difficult to quantify, especially because the provision of a magnetising field means that all electromagnets are now typically operating away from the zero current region where the problem was most prevalent. However, quality of control using the calibration has been good, and force/current relationships derived since have been linear.

## 3.2 REPOSITIONING OF AXIAL POSITION SENSING OPTICS

At the start of the propulsion simulation project, the configuration of the position sensing optics was that shown in Figure 3.2. For axial sensing (top diagram) a laser light sheet was directed vertically through the test section across the blunt tail of the suspended model - the shadow cast onto the axial photodiode array giving an indication of its streamwise position. This arrangement was not suitable for use with a model containing a thruster simply because any efflux would obscure or distort the image.

The obvious alternative was to change the system to nose scanning, although this would generate a number of difficulties. The new arrangement would have to be compatible with the propulsive model's nose geometry. A well-rounded nose would use of allow a laser sheet aligned with the model's axis, whereas a sharper nose would necessitate lateral scanning, with the width of the image obtained giving an indication of the model's axial position. After consultation with PSI a hemispherical nose shape was chosen, and the new scanning geometry shown in Figure 3.3 adopted.

The rather tortuous path chosen for the light sheet is a consequence of the lack of space around the SUMSBS test section. Mirror holders had to allow rotation about three axes for alignment purposes, but still have a flat layout to fit into the gaps. Elliptical mirrors were chosen for efficient use of the available space.

The axial scanning laser sheet is directed upwards and backwards across the test section at fifty degrees to the horizontal. This allows positioning of an eight inch model centrally within the electromagnet array, with the mirrors in convenient locations. The rearward tilt retains the capability of the sensing system to position models at high angles of attack.

Hardware purchases to effect the change to nose scanning were limited to mirrors, and new windows for the test section. The mounts were produced in-house. The old combination of laser and lenses to produce the light sheet was re-used. The focal lengths of the lenses dictate a long mounting table, which is attached to the side of the MSBS rig. New hardware to allow a more compact arrangement was ruled out on grounds of cost.

When used in conjunction with its wind tunnel, only the upstream end of the MSBS test section is accessible for launching the model. Hand launching has been almost exclusively practiced at Southampton in recent years, but this conflicted with nose scanning of axial position.

The solution adopted is to disable the axial sensing channel during launch. A keyboard toggle was incorporated into the control software to this effect. The model is launched at zero angle of attack, and restrained manually in the streamwise direction. The operator then adjusts the position of his hand to grip the model either side of the nose and allow the laser sheet to pass unimpeded. With the model held centrally in the field of view of the axial sensor, that channel is enabled with a keyboard command, and the operator removes his hand, taking care not to obstruct the light sheets as he does so. This process has proved less difficult in operation than in description, and no mechanical launch aids have been required.

With the axial sensing geometry finalised, new windows were installed in the MSBS test section. This necessitated repositioning of the static tapping used for tunnel speed calibration.

## 3.3 MODIFICATIONS TO THE COMPUTER SYSTEM

The DEC PDP11/84 computer system used to run the SUMSBS at the start of the project was not thought able to solely fulfill all contractual computing requirements.

Its major limitation is memory. Only 64kB of directly addressable memory is available to be shared between control software and stored run-data. Further memory can be accessed by use of overlays, but only with an unacceptable time penalty. The available memory would be inadequate for storing the quantities of data generated during a thruster firing.

Other limitations include a lack of processing speed which forces control software to be written in Macro-11 Assembler language. No graphics terminal is connected to the system to allow visual data presentation. The 11/84 is the last of the PDP11 family of computers, so no upgrade is available.

The chosen remedy to these problems was the purchase of a fast 80386-based desktop PC with high resolution graphics. This would act as a data logger and presentation device during the propulsion simulation project. A simple speed test was used to confirm that the PC could run suspension-type software in a higher language (C), faster than the PDP11 could run equivalent software in Macro-11. In the future it is intended to use the PC to run the MSBS.

To function as a data logger, the PC needed access to the position and current data flowing from the A/D equipment and the PDP11. This was provided by a simple hardware interface inserted into the sixteen bit parallel line carrying the data. The presence of the PC is invisible to the other equipment. Incoming data is processed by a standard plug-in PC interface card.

Operation of the data logger, as well as the various software tools developed on the PC for use with the SUMSBS, are described in Section 4.7.

## 3.4 SUSPENSION OF SOFT-IRON MODELS

In recent years the SUMSBS has been used almost exclusively to suspend permanent-magnet models. However, for the propulsion simulation project iron was chosen as the structural material. Iron presents no major problems for suspension, and is more easily machinable than the brittle permanent-magnet alloys.

To magnetise the iron model, a steady field component is applied in addition to the field to suspend the model. This had been previously achieved at Southampton 'automatically' as a consequence of the asymmetrical electromagnet geometry, this arrangement being convenient for a system with a low angle of attack capability. To maintain the high angle of attack feature of the present system the magnetising field had to adjust in pitch, so matching the model's orientation.

High angle of attack range magnetising fields were generated in a similar way to Parker's demand distribution generation. Parker had analysed the fields produced by each electromagnet This information allowed a simple magnetising vector to be assigned to each group (Figure 3.4). Given the field strength to

saturate iron - albeit in a more easily magnetisable geometry - from standard texts as a starting value, the problem became one of combining these vectors at different angles of attack.

Initially a software grid search technique was used. The Fortran program MAGEN gives the combinations for lowest total current and lowest peak current to produce a chosen field strength, at ten degree intervals. This data was made available to the control program via a new routine to interpolate for the present attitude and add the magnetising and suspension currents.

An iron model was successfully suspended shortly afterwards, after empirical adjustments to field strength. It became necessary to redistribute the magnetising field away from those electromagnet groups heavily used for suspension. A new version of the magnetising field program MAGE2 was developed. This allows user selection of the magnetising current in one of the four groups, and cycles through the alternatives in the other groups. An appropriate combination is then chosen based on recent suspension experience, and the magnetisation data file modified accordingly. To date iron models have been suspended from -10 to 70 degrees. The upper limit is not fundamental, limited merely by lack of time to adequately set up the system.

Typically, magnetising field strength applied to the model is estimated at 195 * $10^{-4}$ T, compared to the initial value of 210 * $10^{-4}$ T used for early suspension. A strong field was used initially to be sure of sufficiently magnetising the model, and an optimum value later determined as described in Section 4.4.

# 4.0 DEVELOPMENT WORK

## 4.1 REPRESENTATIVE MODEL

To enable further development work prior to delivery of the propulsion simulator from PSI, a model representative of the latest estimates of mass, size and magnetic properties was designed and constructed. A schematic is given as Figure 4.1. The brass weight represents the total of non-magnetisable material carried by the propulsion simulator, and can be traversed to allow investigation of any problems caused by a change in centre of gravity as the propellant gas is exhausted.

Suspension of the new model showed that the MSBS would later be able to cope with the propulsion simulator. Its use allowed data files and control parameters to be developed without endangering a less expendable piece of equipment.

## 4.2 SUSPENSION WORK

### 4.2.1 PREPARATION

Before suspension of the new model, data files were created to be used by th controller in relating position sensor readings to attitude. Coupling factor were generated, to take account of the necessary motion of the model as viewe by the axial sensor during pure pitch or heave motion in model axes. Parker's PIXEL software, which generates the files for different model geometries, was modified to allow for sensing of a hemispherical nose instead of a blunt tail.

### 4.2.2 QUALITY OF SUSPENSION

Initial work with the representative model concentrated on achieving acceptable quality of suspension. As the size and weight of the propulsion simulator marked quite a departure from models previously suspended with the high angle of attack controller, this led to a review of the control software. The review highlighted those aspects of the software which would need to be tuned to give optimum rather than acceptable performance. Some constants relating to the dual-phase advance network were clearly outdated, not having been adjusted since before the hardware was reconfigured for high angle of attack work.

New software, written for the PC to complement its data-logging capability, allowed efficient optimisation of the control constants for each degree of freedom. Four constants per channel were considered, these being overall loop gain, along with time period, phase lag and an internal gain for the dual phase advancer.

During the optimisation process each constant was cycled through a range of values with the model in suspension. After each slight change the model would be commanded to execute a motion impulse in the relevant degree of freedom. The resultant motion of the model was recorded by the PC, with new software allowing instant playback and graphical analysis of the motion transients. The constant was then set to the value giving the subjectively judged 'best' response. Examples of this process are shown in Figure 4.2.

It became clear that the values of the constants needed to give the best response from the dual-phase advancer were angle of attack dependent. Previously a compromise value had been used for all attitudes. In an attempt to achieve the best possible control system performance, optimisation was performed separately for the three angles of attack at which testing was to be performed - zero, ten and twenty degrees.

It would have been relatively easy to incorporate the constants thus determined into a look-up table, and modify the control software to use the correct value depending on attitude. This was prevented by the lack of spare processing capacity on the control computer which resulted from other modifications. Rather than slow the control loop-rate, a look-up table was not used, and different versions of the control program were run for testing at different angles of attack.

Control optimisation was performed initially at zero degrees angle of attack. The next task was to investigate performance at other angles. Parker had previously observed that for the present electromagnet configuration, attitudes around thirty degrees were subject to a high power requirement. This is because the lateral magnets are unable to contribute to lift near this angle. The representative model, and later the propulsion simulator itself, could not be suspended from around twenty-seven to thirty-three degrees angle of attack, using the present control and magnetisation strategies.

As the limiting attitude is approached, members of one or more of the electromagnet groups reach their twenty ampere current limit, resulting in degradation or loss of control. The burden of magnetising the iron model can be shifted to other groups using the program MAGE2 (Section 3.4), but the point is eventually reached where three groups simultaneously approach the limit. Beyond this point it is not possible to magnetise the model sufficiently strongly in its axial direction, and still have current reserves for suspension. An attempt to further increase angle of attack would result in a loss of control.

A different approach not fully investigated is to accept the limit described above, and allow the magnetising field to not exactly match the orientation of the model. It has been possible to move the propulsion simulator model through the thirty degrees limit via a pitch oscillation based around a lower angle. This was possible because the oscillation does not affect the magnetising field direction. With the magnetising field at around twenty degrees, suspension at thirty degrees is just possible.

Off-axis magnetisation has not been pursued, as it is reasoned that even if steady suspension at thirty degrees could be achieved, there would be no reserves remaining to restrain the model as it experienced a thrust impulse. Additionally, blockage of the seven inch test section by an eight inch model at thirty degrees would greatly diminish the value of any aerodynamic results thus obtained.

## 4.3 FORCE AND MOMENT CALIBRATIONS

The requirement for the measurement of forces on the model during propulsion simulation was for axial force data only at zero degrees angle of attack, and for additional heave force and pitching moment data at other attitudes, namely ten and twenty degrees angle of attack. The force/current relationships were derived conventionally using weights applied to the model.

Axial force calibration was performed by attaching a cord to the nose or tail of the model, and positioning the pulley over which the cord subsequently passed so as to apply a pure axial force only (Figure 4.3). This was

considered less complex than trying to apply a pure force in the stream direction, for attitudes other than zero α. For axial calibration with the force applied in the upstream direction, a yoke was used which avoided interfering with the axial sensing laser light sheet.

Heave force and pitching moment calibrations were combined by loading the suspended model in two ways, shown in Figure 4.4 as 'A' and 'B'. The sum of these two loads is a pure heave force, while their difference is a pitching moment about the half-length point. The current changes recorded for loading only at 'A' and only at 'B' were combined accordingly to give pitch and heave calibrations. It should be noted that the heave force calibration was perpendicular to the stream for all angles of attack. This allowed the data analysis to give a direct measurement of lift.

At zero α, axial force experienced in suspension is readily deduced because only the axial electromagnets (group 4) are used to apply such a force to the model. Although the other sets are capable of applying axial force, Parker's demand distribution matrix selects the axial magnets only as the most efficient effectors. As the force/current relationship is linear, only a single calibration constant is required - assuming constant magnetisation - and this is easily derived. The control system provides a constant level of magnetisation unless one or more of the electromagnets reaches its limit.

At other attitudes the situation is more complex, because the different groups must be used in conjunction to produce a pure force in a given degree of freedom. The relevant section of the demand distribution matrix is given below. It represents only one of many possible permutations, but there has not as yet been any advantage perceived in its modification.

| α | E/M Group | | | |
|---|---|---|---|---|
| | 1 | 2 | 3 | 4 |
| 0 | 0.0 | 0.0 | 0.0 | -4.0 |
| 10 | 0.0 | -.83 | -.35 | -2.8 |
| 20 | .03 | 0.0 | -1.45 | -2.52 |

E/M Group 1: Forward Lower, Aft Upper
2: Forward Upper, Aft Lower

3: Lateral E/Ms

4: Axial E/Ms

Some numerical processing is necessary to extract axial force, heave force, and pitching moment data for experiments conducted at attitudes away from zero $\alpha$. From the calibration data we know that application of a force or moment is balanced by a corresponding change in the current in a particular electromagnet. For application of a pure force, with a linear calibration, this can be expressed as

$$\Delta C_x = k_{mx} \Delta F_m \qquad \text{where } x = 1..10$$

C is some current

F is an external force or moment

Most tests will involve changes in axial force, heave force and pitching moment between two conditions. The conditions could be wind on/off, thruster on/off or a combination. Current change in a magnet is now a summation of the effects of the forces and moments:

$$\Delta C_x = k_{ax} \Delta F_a + k_{hx} \Delta F_h + k_{mx} \Delta P_m \qquad \text{where } x = 1..10$$

$F_a$ is axial force

$F_h$ is heave force

$P_m$ is pitching moment

We now have ten equations and three unknowns - five unknowns if side force and yawing moment are non-zero. The axial force, heave force and pitching moment can be extracted by matrix inversion.

Numerous solutions are possible with this over-definition of forces and moments, with considerable scope for cross-checking results. However, as an initial approximation, only three currents were considered simultaneously, giving one solution each to the heave force, axial force, and pitching moment applied by the magnets. This greatly reduced the computation necessary to extract the results, and also reduced the number of calibration constants to be manually derived.

To select the three electromagnets to be used, current traces from the calibration experiments were considered, to see which had the best resolution

of changes in the applied load. Lateral magnets were not used, as they are most relevant for yaw and sideforce investigation. One magnet from each of the other three groups was selected, and calibration constants for heave force, axial force and pitching moment derived for ten and twenty degrees angle of attack.

The tables below summarise the calibration results used in data analysis for this project.

Heave (lift) Calibration:

| α | Aft Lower (A/N) | Fwd Lower (A/N) | Aft Axial (A/N) |
|---|---|---|---|
| 0 | - | - | - |
| 10 | -1.66 | 2.34 | -.365 |
| 20 | -2.39 | 3.30 | -.476 |

Pitch Calibration about mid-length:

| α | Aft Lower (A/Nm) | Fwd Lower (A/Nm) | Aft Axial (A/Nm) |
|---|---|---|---|
| 0 | - | - | - |
| 10 | 7.33 | 8.80 | -1.50 |
| 20 | 6.78 | 10.67 | -1.32 |

Axial Calibration (model axes):

| α | Aft Lower (A/N) | Fwd Lower (A/N) | Aft Axial (A/N) |
|---|---|---|---|
| 0 | - | - | 3.16 |
| 10 | -.258 | 1.11 | 2.92 |
| 20 | -.914 | 2.08 | 2.91 |

Results of the calibration experiments are discussed in Section 5.2.

## 4.4 OPTIMISATION FOR AXIAL RESTRAINT

Leaving the demand distribution matrix unchanged, two control system parameters could be varied in attempting to attain maximum axial force capability. These were

1. Level of magnetisation
2. Distribution of magnetising field generation.

The level of magnetisation used initially for suspension of the propulsion simulator was arrived at empirically. Stronger magnetisation than that suggested in standard texts to saturate soft-iron was required. This was a consequence of model geometry. During attempts to generate maximum axial force on the model for best restraint under a thrust impulse, it became necessary to optimise the level of magnetisation. This level would represent the best balance between use of the electromagnets to magnetise and to restrain, and was found by an experimental technique.

At zero incidence, axial force applied to the model in suspension is countered only by action of the axial electromagnets, whereas all ten electromagnets contribute to magnetisation of the model. The two axial currents are fed with a permanent difference which provides their contribution to magnetisation. The current sum acts to create the restraining force. It was not possible to sufficiently magnetise the model without this contribution from the axial electromagnets. As the force nears the maximum which can be tolerated, one of the magnets reaches its limit. Any further increase in applied force is countered only by increased current in the magnet which is not at its limit.

There is thus a drop in the current difference between the two axial magnets, and hence in the magnetisation of the model. This occurs at the same time as the increase in total current acting for restraint, due to the increased current in the magnet not at its limit. If these changes result in an increase in axial force applied to the model by the magnets it will be controlled, if not it will begin to drift in the axial direction under the influence of the externally applied force.

This was the philosophy used to experimentally optimise the level of magnetisation. An axial force would be applied to the model until it was just becoming uncontrollable. Data logged during this process would then show the

level of magnetisation at which control was lost, ie that at which the peak force was withstood. Future work would then be carried out with the magnetisation at this lower level.

As the new level of magnetisation indicated would be below the starting value, the initial magnetisation had to be greater than the improved level for a useful result to be obtained. Loss of control occurring before a drop in magnetisation would indicate that the initial level was too low.

The above description is summarised in Figure 4.5, showing the balance between magnetisation and restraining current. The axial force is proportional to the product of the state of magnetisation of the model, and the sum of the currents applied to the axial electromagnets. The precise relationship between magnetising field and level of magnetisation is unknown, although it has been shown to be non-linear (Section 6.1).

It was important to consider the other current levels during this process. The drop in model magnetisation would necessitate increased currents in the magnets used for suspension. These magnets would already be operating near their limits (see below). If the incipient loss of control was caused by a non-axial magnet reaching its current limit, then the test would be invalidated.

Distribution of the magnetisation task was initially determined using the MAGEN software (Section 3.4) to determine the most efficient permutation for each attitude. In practice this led to certain E/M groups becoming overloaded even during steady suspension of the propulsion simulator before any firing was attempted. This occurred where the groups chosen for magnetisation coincided with those used heavily for levitation.

The overloaded groups were relieved by a series of empirically determined changes to the magnetisation matrix. The program MAGE2 was used to select more suitable combinations of the four groups. An alternative solution could have been to change the demand distribution matrix at each attitude. This could have reduced suspension currents in the overloaded groups. However this idea was not put into practice, as no advantage could be perceived in redistributing the burden of suspension rather than that of magnetisation.

The changes to the magnetisation matrix were extended to include the task of maximising axial force capability. This was achieved simply by minimising combined suspension and magnetisation currents in those magnets used for axial restraint at the attitude in question. The limiting factor in this process was overburdening the other magnets during steady suspension. It was also decided to ensure that no magnet was within one Ampere of its limit with the model undisturbed, thus preserving a modest capability to respond to disturbances in the other degrees of freedom.

## 4.5 TUNNEL SPEED MEASUREMENT

Previous wind tunnel testing with the SUMSBS has relied on manual recording of tunnel speed, as indicated by a manometer. The manometer was connected to pitot and static tappings in the contraction. A new pressure transducer has been purchased and connected to the same tappings, allowing automated logging of tunnel speed data via a spare channel on the existing A/D equipment.

The transducer is a Setra Systems Model 239, with a unidirectional working range of 3700 $N/m^2$. This range was chosen to match the Mach 0.2 maximum tunnel speed. The calibration between contraction and working section dynamic pressure is known from earlier work by Newcomb (6),

$$q_{true} = 1.017\ q_{ref}$$

The transducer is mounted on the tunnel inlet assembly and supplied with 24 volts by the A/D equipment power supply. A single lead carries power to the transducer and returns the response to the A/D. The MSBS control software running on the PDP11 prompts the A/D to read the pressure transducer output once every program cycle and return the measured voltage. This information is received but not logged by the PDP11, but the PC also has access to returned data and records the tunnel speed signal along with position and current information. The PC data analysis software includes the calibration constants for converting transducer output to dynamic pressure and thence to tunnel speed in metres per second, and this information can be extracted and plotted along with the other parameters.

## 4.6 THRUST TEST STAND

A number of force transducers have been acquired in preparation for MSBS force calibration. One of these has been incorporated into a simple test rig to allow static testing of small thrusters, including the carbon dioxide propulsion simulator.

A schematic of the test stand is shown in Figure 4.6. The model is loosely restrained by three adjustable studs. The transducer is fitted with a conical guide to ensure that the model is aligned with its central axis.

The stand was originally designed for testing with the thruster nozzle pointing vertically upwards only, but as performance of the carbon dioxide model was strongly dependent on attitude, horizontal testing was necessary. This was achieved by mounting the stand horizontally and suspending the model by two loops of thread. These allowed the model to be orientated correctly with the force transducer, without significant friction being present to corrupt thrust data.

To drive the force transducer, a Load Cell Amplifier was designed and built in the departmental Electronics Workshop. This device drives the force transducer with the correct voltage, and amplifies the 200 mV full scale output to an appropriate level for input to the A/D. An audible warning is incorporated to help protect the transducer from damage caused by exceeding the rated maximum force.

Software used with the thrust test stand is described in Section 4.7.4 below.

## 4.7 PC SOFTWARE

The PC has become an important part of the MSBS equipment, with software developed to perform a number of logging, presentation and analysis tasks.

### 4.7.1 MSBS DATA LOGGER

This software uses a standard PC digital i/o card, installed soon after delivery of the computer, to record raw run-data during suspension work with the MSBS. One of the lines between the A/D equipment and the PDP11 indicates

that new data is ready for reading, and this signal is used to interrupt the PC, causing it to scan the i/o card and thus ensuring that all data is recorded.

As presently configured, the PC logs 100,000 words of data on command, and then saves them to disc. A countdown before logging allows the operator to prepare to start an experiment during the logging period, facilitating single-user operation of the MSBS. Seventeen pieces of information are available per program loop, namely 10 currents, 5 position counts with a control flag, and tunnel speed as measured by the pressure transducer described in Section 4.5.

This arrangement allows a complete record of 24 seconds of suspension to be made with the control program running at 242 Hz. Alternatively it is possible to store every *n*th set of data for *n* times 24 seconds. Such a storage capacity has so far proved more than adequate, and has been used for force calibrations and fault diagnosis as well as propulsion simulation data logging.

### 4.7.2 ANALYSIS OF RUN-DATA

The C program ANALYSE decodes the raw data taken by the logger software and allows its presentation and comparison. Some of the seventeen items of data recorded during each loop of the MSBS controller are identifiable, and these are initially used to put the analysis 'in-phase' with the raw data.

A replay of the period of data logging is then started. The ten electromagnet currents and five sensor readings are displayed symbolically on screen, and vary with time as they varied during suspension. At this stage start and end points of events can be marked, as delimiters for a subsequent graph plot. The graph menu can be selected, allowing display of currents, positions, magnetisation level and tunnel speed. Processed graph data can be stored on disc, or a hardcopy made before the replay of events is restarted.

This near-instantaneous availability of large quantities of run-data is a step forward for the SUMSBS, which for some time has been limited by having a small memory, and no graphics capability.

### 4.7.3 TRANSIENT ANALYSIS

A special case in the data analysis task for the propulsion simulation project

is extraction of thrust and drag experienced by the suspended model during a firing. This is complicated by the short duration and unsteady profile of the carbon dioxide thruster. Analysis of transients made up the major part of the data analysis for this project, and is described in Section 6.

### 4.7.4 SOFTWARE FOR STATIC THRUST TESTS

The PDP11 and the PC are used in conjunction during static thruster firings on the test stand Figure 4.6). A/D sampling is initiated by a simple FORTRAN program on the PDP11. This repeatedly requests a reading of the transducer channel, and sends pulses to a frequency meter for a visual confirmation of loop rate. Again the data is intercepted and logged by the PC, giving the same presentation, data storage and hardcopy facilities as with the ANALYSE software.

To ensure acquisition of the thrust data, allowing for possibly unreliable thruster ignition while avoiding the burden of recording large quantities of information, transducer readings are cyclicly stored by the PC in a small buffer. When a significant change is detected, signaling the start of the thruster run, several seconds of data are recorded. The contents of the buffer are then added to the front of the stored data, allowing the full thrust profile to be efficiently recorded, along with a series of zero thrust data both before and after the firing.

The constant used to translate A/D output into force is taken from the transducer's calibration certificate. Its accuracy can be easily tested by placing a laboratory weight, as used for MSBS force calibrations, on the test stand. Data is taken at around 130 Hz during static tests. With the carbon dioxide propulsion simulator, this rate does not pick up all of the percussive noise of squib ignition captured by PSI's 1 kHz sampling rate, but it is adequate for confirmation of thrust profile, and detection of changes due to worn or faulty components within the model.

Results of static tests are discussed in Section 5.5.2.

## 4.8 INTEGRATION

The modifications described above were performed separately over a period of

months, and only brought together towards the end of the project. The only problem encountered during this integration process was that with software additions such as for model magnetisation and power supply calibration, the PDP11 was now unable to maintain the 242 Hz control loop rate. Fortunately, some coding improvements were possible to regain this rate. A reduction in loop rate would have resulted in reduced quality of control and response, as well as requiring considerable setting-up.

As presently configured the control software can just run at 242 Hz on the PDP11. The lack of spare processing power rules out any further enhancements without some sacrifice in loop rate or capability.

# 5.0 EXPERIMENTS

## 5.1 SET-UP

A number of set-up procedures are required before experiments are performed in the SUMSBS. Some are described in other sections of the report, but a summary is appropriate here.

### 5.1.1 POSITION SENSING SYSTEM OPTICAL ALIGNMENT

The laser light sheets used to sense model position in the MSBS must be accurately aligned for suspension in the correct attitude. The optical elements become dirty, and their alignment drifts with time. Periodically, and also on installation/removal of the test section, a lengthy set-up procedure must be performed using apparatus designed by Parker to ensure the correct light sheet geometry.

### 5.1.2 CONTROLLER DATA FILES

A number of data files used by the control system must be individually generated for each new model suspended in the SUMSBS.

### 5.1.3 QUALITY OF SUSPENSION

This is a largely subjective measure, but can be considered in terms of station-keeping, and response to disturbances.

Station keeping is a measure of the model's stillness in undisturbed suspension. When station-keeping is good, no motion can be detected by eye. Examination of position traces will then show motion of between two and eight pixels on each sensor, each pixel measuring position to one thousandth of an inch. This minute motion is inevitable in an unstable system, and is the cue to the controller to make slight adjustments to electromagnet currents to return the model to its required position.

Response in usually evaluated by commanding a position impulse in the degree of freedom being considered, and observing the subsequent motion. Various control parameters are then adjusted. In this work, the target has been a response approaching the classical critical damping case. This does not always represent the quickest return to the undisturbed state, but is compatible with improved station-keeping and steady suspension currents.

The goals of accurate station-keeping and rapid response are to some extent at odds, as the effect of a highly tuned controller is destabilising. For static aerodynamic research, station keeping coupled with good damping would be paramount. Under a constant drag force, the model would be stationary. The suspension currents would be relatively constant during tests, allowing a more accurate measurement of aerodynamic forces and moments.

Set-up for the propulsion simulation experiments represented a compromise. It was known that good control would be required to restrain the model during a thrust impulse, but if drag force changes were to be detected then steady currents would aid accurate measurement.

## 5.2 CALIBRATION WORK

Several types of force calibration were required during the propulsion simulation project. Foremost and simplest was calibration of axial force at zero angle of attack. As only the axial electromagnets are used to provide axial force at this attitude, all that was required was the relationship between applied load, and total axial current. As the experiments would involve thrust and drag forces, this calibration was carried out with the load acting upstream and then downstream. Calibration theory and technique are explained in more detail in Section 4.3.

The calibration results for the carbon dioxide simulator at the three attitudes considered are shown in Figure 5.1A-D. Generally these results are linear - the major source of non-linearities arising from a magnet reaching its current limit, thus causing the other magnets to over-compensate. Other factors degrading the results included system warm-up time, accuracy of pulley alignment and system noise. It should be noted that the maximum axial force achieved agrees closely with the 1lb estimated by Prof MJ Goodyer before the start of the contract.

The heave and pitching moment calibrations both illustrate the transition from a linear to a non-linear calibration as an electromagnet reaches its limit (Figure 5.1A,B). In Figure 5.1C the change in zero-force current between forward and aft calibrations is a consequence of reversing the model, as it

was convenient always to attach the thread to the tail section. A differing zero-current is not a problem as only the gradient is of interest. It is assumed that in a symmetrical system the reversal would not detract from the results.

Figure 5.1D has the data normalised to remove the step change and show the linear calibration result. The gradient is constant over a range of applied forces from -3.7 to +4.5N, then changes as a current limit is reached. At incidence the linear calibration range changes to -3.8 to +3.7N. The loss of positive (resisting a motor thrust) axial force capability with increasing angle of attack is a reflection of the increased suspension currents as thirty degrees is approached. Less current is available to provide axial forces.

## 5.3 ROCKET EXPERIMENTS

During a period when the changes necessary to the MSBS to allow propulsion simulation were nearing completion, but PSI were not ready to deliver the carbon dioxide simulator model, some experiments were performed to evaluate an alternative propulsion simulation technique, using small rockets to provide the exhaust plume.

Small solid propellant thrusters had been considered by PSI in their proposals for NASA SBIR 87-1 (7), but were ruled out on grounds of safety and development cost. However, hobby rockets for model enthusiasts are cheaply and readily available, and were not considered any more dangerous to handle than the explosive squibs used to puncture the $CO_2$ cartridges in the PSI model.

A model of similar dimensions to the carbon dioxide simulator was constructed to contain model rocket motors, and successfully suspended and fired in the SUMSBS. Although these experiments are not strictly relevant to this project report, valuable lessons were learnt. Experience with rockets allowed rapid progress to be made with the PSI model when it arrived. More was achieved in the - by then limited - time available than would have been possible had another form of propulsion simulation not been already attempted.

## 5.4 RESULTS

The rocket experiments were particularly useful in setting up the MSBS to cope with the carbon dioxide thruster, as both propulsion techniques produce an initial thrust level greater than the maximum steady axial force capability of the system. In the case of the rockets the thrust peak of Figure 5.2 is a consequence of the transition from core to end burning of the solid propellant. The carbon dioxide thrust profile has an early peak due to release of the small amount of gaseous $CO_2$ initially contained in the bottle. The profile in Figure 5.2 shows a lower thrust than that advertised by the rocket motor manufacturers - achieved by altering the nozzle to make the thrust peak controllable by the MSBS.

As expected, during the rocket thrust peak the model would accelerate forward, thus initiating a control system response. The axial magnets are commanded automatically to act together so as to restrain the model. The currents in the axial magnets were held at different levels by the amount required for their contribution to the task of magnetising the iron model. Thus, as they responded together to apply a large restraining force to the vigorously thrusting model, one magnet would reach its maximum current, while both were still commanded to increase the axial force. This effect would cause a loss of magnetisation and the appearance of associated control problems in just the same way as experienced during attempts to maximise the axial force capability, as described in Section 4.4.

The solution adopted was to impose a software ceiling on the maximum current of the non-limiting axial electromagnet. This ceiling was placed so that it coincided with the other axial magnet reaching its operational limit. The difference in currents, and hence the strength of the magnetising field, was thus preserved.

Following the optimisation of magnetising field strength, this limit also ensured that the maximum axial force was applied to the model for as long as required. Any further increase in current in the non-limiting magnet would under these conditions have resulted in a drop in the axial force.

Tuning of the axial channel of the control software did not appear to make a great difference to the ability to control a thrusting model. All failures

which occurred with the hardware performing correctly could be attributed to the thrust peak being simply too strong for the equipment, rather than the controller not responding quickly enough. It is shown in Section 5.8 that the speed of response of the magnets is more limited by their own inductance than by minor adjustments to control constants. For this reason it was possible to set the axial channel for moderately 'soft' control, with the advantage of steadier currents which allowed more accurate force measurement.

Ignition of the rockets was electrical, and initiated simply by switching on a mains transformer. The sudden load in the mains electricity circuit occasionally caused one of the position sensing lasers to flicker, with subsequent loss of control of the model. Once identified, this problem was solved by choosing a power point for the transformer some distance from that used for the laser.

During a high thrust period with the maximum axial force being applied, the model was able to accelerate for as long as the thrust exceeded the restraining force. The factor limiting the ability to retain control of the model was now the length of the axial position sensor. Once the model moved sufficiently far upstream that the axial sensor was completely obscured by its shadow, axial position information was no longer available to the control system, and it was unlikely that the model would be brought back under control.

The length of axial sensor available for model motion under high thrust was determined by selection of the 'rest' position of the model before firing. Clearly the further back along the sensor that the model was positioned prior to firing the thruster, the further upstream it could travel before control was lost. The rearward rest position was limited by two factors. Firstly, some further rearward travel had to remain available for axial position overshoot after the forward motion was halted. Secondly, steady suspension at the extreme rearward point demanded changes to the magnetisation matrix because of different suspension current requirements. These tended to reduce the maximum axial force capability so another trade-off was necessary.

Following some initial tests which proved the concept of solid propellant propulsion simulation in an MSBS, a source of motors was discovered not having the inconvenient initial peak in the thrust profile. This source is a local

specialist rocket company, and development is under way with them to produce a rocket motor system better suited for MSBS propulsion simulation testing.

## 5.5 CARBON DIOXIDE THRUSTER

The carbon dioxide propulsion simulator model arrived in Southampton on March 18th 1991. This left little time to gain the necessary experience in its operation, and develop effective test techniques before the end of the contract period.

### 5.5.1 OPERATION

Operation of the model proved straightforward, if a little awkward, but was aided by clear instructions from PSI. The most difficult operation was securing the squib wires to their contacts, which were minute hex-head screws located inside the body tube.

An external switch with which to isolate the firing circuit would have been useful, rather than relying on black tape over the firing window to prevent accidental ignition caused by background light. It was awkward to have to remove this window to access the battery and check its condition.

Only on two occasions did the thruster fire accidentally. In the first case the window and nose section were removed during an attempt to control roll attitude with internal ballast. Background light caused ignition while the model was being held, but no injury was caused. On a different occasion diffuse reflection of a photographic flash set off the thruster while the model was in suspension.

Despite several requests to PSI during development of the new model, no means was provided for adjusting the roll position of the firing window so that it could be aligned with the available slots for directing the triggering laser into the test section. Such an adjustment could have been made possible by changing the preferred roll attitude of the entire model with an internal mass, or by allowing the window and internal light sensor to be rotated relative to the rest of the assembly.

At Southampton the only reliable solution, given the time constraint, was to

attach an external weight to the body of the model, and adjust its position until a satisfactory roll attitude was achieved. This arrangement was clearly unsuitable for aerodynamic tests, although by this stage it was accepted that the experiments performed would be proof-of-concept only.

The laser used to fire the thruster was a 0.95 mW He-Ne device. This was hand-held and directed at the window on the model to trigger its light sensor. This technique was adequate for the present set-up, but more sophisticated control strategies using anticipation of the thruster firing would require a more reliable, automated triggering system.

### 5.5.2 INITIAL BENCH TESTS

The first carbon dioxide thruster firings were bench tests using the new thrust test stand. With the nozzle pointing vertically upwards, some very high thrusts were recorded - overloading the A/D equipment on one occasion. Most later bench tests were performed with the model in the horizontal attitude, as this condition was more representative of wind tunnel tests, and the performance of the thruster was found to be dependent on model attitude.

The thrust profile with the model horizontal was confirmed as matching that recorded by PSI before shipping, an example of a thrust-time curve measured at Southampton being given in Figure 5.3. The shape showed an initial peak related to the squib firing and an initial rush of gas, followed by an almost exponential thrust decay as the contents of the $CO_2$ cartridge were expended. A significant difference between the Southampton and PSI results did exist however, in that the thrust levels recorded were much higher then those obtained at PSI. The maximum was typically 8 N as opposed to 6 N.

The difference in thrust level was thought to be due to lower temperatures in the Southampton MSBS laboratory than at PSI in Andover MA, although no further investigation has yet been carried out into the relationship between ambient temperature and thrust.

Two sizes of pin with which to puncture the $CO_2$ cylinder were provided, the larger pin having a larger central bore to allow the passage of more gas, hence giving a higher thrust. As high thrust was a problem throughout the test series, the large pins were not widely used.

### 5.5.3 DEVELOPMENT

Performance of the carbon dioxide thruster was very sensitive to the condition of some of its internal components, notably the pin used to pierce the gas cartridge, and the squib retainer inside which the pin was housed. Both of these parts had a life of just a few firings, and towards the end of this period tended to give erratic or high thrust levels, as shown in Figure 5.4. To ensure that consistent performance was being achieved in the wind tunnel it was necessary to perform a bench test for every one or two firings in suspension.

Careful handling of the pin and squib retainer was required, particularly when pushing the pin back inside after a firing. A purpose-built tool would have helped move the pin without causing damage. Deformation of the parts and deposit of combustion products gradually impeded pin motion until it could not properly pierce the cartridge cap. Cleaning only partially alleviated this problem.

Experience in operation of the carbon dioxide thruster led to improved consistency of thrust, but at its best the peak would still vary by +/- 25%, with implications on attempts to measure thrust minus drag in the wind tunne.

To reduce thrust levels to a point where the MSBS could control the model, th nozzle diameter was gradually increased. Initially the diameter was 0.1 inches, and initial thrust was typically 8 N, then decaying from 5 N over a period of 1 second (Figure 5.3). Diameter was gradually increased to 0.35 inches before good reliability was achieved in suspension at zero degrees (Figure 5.5), and then to 0.4 inches for tests at ten and twenty degrees angle of attack.

In an attempt to smooth the initial thrust peak, steel wool was packed into the tail of the model, contained by a brass mesh. Presence of the wool appeared to have little effect.

## 5.6 WIND TUNNEL TESTS

Having brought the thrust of the carbon dioxide propulsion simulator down to a more reasonable level, firings with the model in suspension were attempted,

initially at zero angle of attack and with wind off. The success rate of keeping the model in suspension while the thruster was activated was poor at first, but increased with experience. The changes made to achieve greater reliability were concerned with model operation - notably handling of the firing pin - and nozzle size, giving more consistent thrust at a lower level.

MSBS hardware and software were not modified during the test series, although a wrong setting of magnetising field strength was accidentally used for the first three attempts. Previous propulsion simulation experience with the rocket thruster described above had already prompted a number of changes, and no further ideas for immediate improvements were forthcoming during the $CO_2$ experiments. The only MSBS parameter varied during the tests was initial axial position, to try to find the point from which maximum forward travel was possible, without loss of control downstream occurring during recovery.

Having achieved an acceptable success rate at zero degrees, with data recorded for propulsion simulation with wind on and off, attempts were made at the two other chosen attitudes, namely ten and twenty degrees angle of attack. These tests were performed using different optimised software for each attitude, and were successful after the nozzle diameter was increased to 0.4 inches. The ten degree tests gave good data, but at twenty degrees the model was only just controlled during firing and impure motion reduced the quality of run-data recorded.

## 5.7 TEST PROCEDURE

To conduct wind tunnel tests with the carbon dioxide model, the thruster was first loaded and assembled according to the instructions supplied. A bench firing was performed if necessary to confirm that the present set of components were functioning correctly, followed by another reload. With the downstream end of the MSBS test section connected to the wind tunnel fan assembly the model was hand-launched, with the firing window covered with tape to prevent accidental ignition.

After checking the preferred steady roll orientation, the model was retrieved and position of the external weight adjusted before relaunch. This process was repeated as necessary until the tape could be clearly seen through the test

section window used for the firing laser. With practice only one or two adjustments were required.

With the protective tape removed, the model was launched again, and keyboard commands used to select the starting pitch and axial positions. For a wind-on test, the inlet assembly section of the tunnel was connected to the test section at this point, and the pressure transducer plugged in. Care was required to avoid knocking the test section out of position with the inlet assembly, as the positions of its laser windows was critical. This problem has now been alleviated by repositioning some of the windows.

The wind tunnel was then activated, and speed selected. Two speeds were used for wind-on tests; full-speed of around Mach 0.2, and half-speed. Accurate tunnel speed was logged during wind-on tests by the new pressure transducer.

Data acquisition on the PC was then initiated, and once it was confirmed that the twenty-four second logging period had begun, the thruster was fired by pointing a hand-held He-Ne laser at the window. After a successful firing, the equipment would be left undisturbed until data acquisition was complete.

To complete the test the tunnel was stopped, the pressure transducer unplugged, the inlet wind tunnel assembly section disconnected and the model retrieved by hand.

## 5.8 INVESTIGATION OF MAXIMUM CURRENT SLEWING RATE

The maximum axial force attainable to restrain the propulsion simulator at zero degrees angle of attack was around 5 N, and yet a maximum thrust of around 4 N still caused control difficulty. The root of this problem was the finite response time of the MSBS. The delay between the model first experiencing a thrust and starting to move, and application of maximum restraining force, allowed the model to accelerate and begin approaching the axial travel limit.

To ascertain whether the control software was inadequate in its response to the disturbance, or whether the system hardware was causing a delay, the response of the electromagnets to a step change in current demand was

# 6.0 TRANSIENT ANALYSIS

## 6.1 DATA ANALYSIS TECHNIQUE

Recent wind tunnel tests using the Southampton MSBS have been carried out under quasi-static conditions. 'Steady' electromagnet currents have been measured at the test condition, and simple calibrations used to derive the force or moment under investigation.

For the propulsion simulation project, more complex data analysis was required. The model was in motion under the combined influences of thruster and controller for most of its firing, and the analysis requirement stated by PSI was for simultaneous extraction of heave force, axial force, and pitching moment data.

Initially, the simplest case of zero angle of attack was considered, with only axial force to be extracted.

Short duration of firing is a problem because of the response time of the MSBS controller. It takes around half a second for the model to regain its stable position following a disturbance in one or more of the degrees of freedom. Ideally the thruster would fire at a constant force for longer than this period, allowing a steady state to be attained with the thruster on and model still. This would allow the axial force equal to thrust minus drag to be extracted simply as the difference between two sets of electromagnet currents, using a known calibration constant.

Unfortunately the final design carbon dioxide thruster had a decaying thrust profile of short duration, necessitating a special analysis of transient model motion during a thrust impulse. This analysis attempts to use the model's motion history, coupled with knowledge of its inertia and the action of the electromagnet array, to deduce the external forces experienced.

A program TRANSIENT was developed to consider motion in the axial direction, and later extended to include heave force and pitching moment data analysis. Axial position, axial magnet currents, and time data were made available from disc via a special save command in the ANALYSE program. After transient data is extracted, the same graph display and hardcopy facilities as in ANALYSE are

investigated.

A typical response to a step change in current demand is given in Figure 5.6, showing a-45 millisecond delay before the new current is reached. For comparison, Figure 5.7 shows the relevant part of a suspension experiment where the current changes in response to model motion, also with a delay of around 45 milliseconds. The conclusions are that hardware limitations govern the type of thrust profile that the system can cope with, and that a more sophisticated controller could not better the initial response.

A simplified analysis of the response of a suspended model under the action of a step thrust profile was attempted, in order to investigate the effect of variations of thrust level on its motion (Appendix 1). The results show a high degree of sensitivity to step size, due to the delay in application of full restraining current (Figure 5.8). As the peak produced by the carbon dioxide thruster was indeed variable, this goes some way to explaining the range of responses exhibited by the model in suspension.

From these findings it can be suggested that propulsion simulator with a thrust profile showing an increase to its peak value over around fifty milliseconds would result in a reduced axial disturbance and be relatively easily controlled in the SUMSBS.

available. TRANSIENT starts by making second order approximations of model velocity $v$ and hence acceleration $a$ using

$$v_t \simeq 1/2 \left( p_{t+1} - p_{t-1} \right)$$

$$a_t \simeq 1/2 \left( v_{t+1} - v_{t-1} \right)$$

where $p$ is model position, and the $t$ subscripts refer to the present, previous and subsequent data points.

External force on the model is then extracted using Newton's First Law. Figure 6.1 shows force data thus obtained for a thruster firing with wind off, compared to equivalent static test data.

This first approximation was clearly missing some other factors affecting motion of the model, and the software was developed to include the following:

1. Change of zero-force current with position.
The axial current for steady suspension is dependent on axial position as shown in Figure 6.3. This changes the effect of those axial currents applied in an attempt to restrain the model during a thrust transient. The part of the axial current effective in producing axial restraint is thus the difference between the instantaneous value and the present 'zero-force' value, which is position-dependent.

2. Level of Magnetisation
Magnetisation of the model changes during a firing transient if a magnet reaches its current limit. This change will alter the effectiveness of the axial electromagnets in restraining the model. As the precise state of magnetisation of the model is never known, even though the strength of the magnetising field is recorded, the effect of a magnetisation change is hard to quantify. A simple experiment was performed to obtain an approximation to the relationship between magnetising field strength and the force calibration constant. The results are shown in Figure 6.4. From this, the linear approximation

Level of Magnetisation $\propto$ Magnetising Field Strength

was introduced into the TRANSIENT software as a reasonable assumption over the range of magnetisation levels expected. The true relationship may well be non-linear.

3. Position Coupling

For heave, the precise geometry of the position sensing system has not yet been analysed to give a relationship between the heave measure used in the control software, and bodily motion of the model. A coupling coefficient for heave was found experimentally. With the model suspended, heave motions were commanded and the results physically measured to obtain the relationship

$$\text{Axial}_{\text{true}} = \text{Axial}_{\text{measured}} - \frac{\Delta\text{Heave}}{5.45}$$

with all measurements in photodiode pixel counts.

The correction for pitch is derived from that calculated for heave. Pitch is measured by the controller as the height difference of two points on the model, whereas heave is the sum of the two heights. It follows that

$$\text{Pitch Coupling} = \text{Heave Coupling} * \text{Leverage},$$

where

$$\text{Leverage} = \text{Model Length} / \text{Sensing Beam Separation}$$

giving

$$\text{Axial}_{\text{true}} = \text{Axial}_{\text{measured}} - \frac{\Delta\text{Pitch}}{1.93}$$

After inclusion of these corrections, the axial position signal appears to be little changed during large motions, although the noise level is slightly increased.

The effect of these three enhancements on the original results of TRANSIENT applied to a zero angle of attack firing is illustrated in Figure 6.2A. The force trace more clearly approximates, but still does not accurately reflect, a real thrust profile. Better results were obtained from analysis of data taken at ten degrees (Figure 6.2B). At this attitude the more sophisticated three degree of freedom analysis is used. It could be that at zero degrees changes in heave force and pitching moment affect the axial currents, degrading the quality of the extracted force data. Heave and pitch changes

could be caused by loss of propellant mass or by impure axial motion. This suggests that an extension to the zero degrees analysis to include heave and pitch could be justified.

In an attempt to further improve the transient analysis, motion of the model with no externally applied force was investigated. A step motion in axial position was commanded and the resulting data processed. A complete version of TRANSIENT should show no external forces when used to analyse this data. Results from a recent version are shown in Figure 6.5, and are still clearly imperfect.

It was suggested that a damping term was missing from the equation of motion of the model, perhaps due to eddy currents. However, the force errors showed no velocity dependence. It could be that a small damping effect is being swamped by other dominant errors.

The conclusion is that this type of analysis of transient motion needs further development before it becomes an acceptable data extraction tool for aerodynamic testing. The version developed at Southampton is not yet of a sufficient sophistication for 'production' tests. However, it has been applied to the run-data generated.

## 6.2 TRANSIENT HEAVE FORCE AND PITCHING MOMENT

The TRANSIENT software was then adapted for extraction of heave force and pitching moment data, as well as axial force, for test attitudes other than zero angle of attack. This was achieved by making the calibration constants described in Section 4.3 available to the software, and including a simple matrix inversion routine.

For each data point, this routine is used to solve the three simultaneous equations relating changes in electromagnet currents to magnetic forces applied to the model. The validity of this technique was confirmed by analysing the original calibration data and correctly extracting the applied forces and moments.

For axial motion, knowledge of the magnetic forces is used in conjunction with

simple Newtonian dynamics to derive the external axial force. For heave force and pitching moment, time constraints prevented extension of the TRANSIENT software to include dynamic analysis, and only magnetically applied heave force and pitching moment can be extracted. This is not thought to be a major drawback however, as full analysis of the axial channel showed that magnetically applied force represents a close approximation to total external force (Figure 6.6). The largest error occurs during the initial disturbance of the model under a thrust impulse. As the axial analysis is not yet complete during this period, there would be no gain in having equally inadequate heave force and pitching moment data available.

Time also prevented the extensions to the analysis described above, being implemented for attitudes other than zero angle of attack. Again this would have been of questionable value given that the zero degrees case was not yet fully understood.

## 6.3 FUTURE DEVELOPMENT OF TRANSIENT ANALYSIS

It is hoped that further insight will suggest ways of improving the transient software to the point where a thrust profile identical to those observed during static tests can be extracted for a a model in suspension. Analysis of heave force and pitching moment will be brought up to the same level as that for axial force. Extension of the calibration and analysis to all ten magnets and five degrees of freedom is possible, but this would be time consuming and probably would not be justified by the quality of data extracted.

# 7.0 RESULTS

## 7.1 BENCH TESTS

A larger number of bench tests than wind tunnel tests were performed at Southampton, mainly to quantify and track the very variable performance of the carbon dioxide thruster, and less often to confirm the effect of increases in the nozzle diameter. After the first few firings which were conducted with the model vertical, all bench tests were performed horizontally. No attempt was made to investigate changes in thruster performance at ten and twenty degrees angle of attack.

Figures 5.3 and 5.4 showed the thrust difference possible under nominally similar operating conditions. Variation in the thrust profile was reduced as experience in operating the simulator and judging the state of its components was gained, but not to the level where aerodynamic effects could reasonably be resolved from the difference between wind-on and wind-off tests.

The major variation observed was in the level and duration of the initial thrust peak, although some of the apparent changes could be attributable to the relatively slow sampling rate for bench tests of 140 Hz. As discussed in Section 5.8, peak thrust variation has a major effect on the success or failure of a firing in suspension. It was only by reducing the overall thrust to a level where the variations could largely be tolerated, that an acceptable reliability level for control of a suspended firing was achieved.

## 7.2 TESTS IN SUSPENSION

Variations in the initial thrust peak were manifested in the different axial responses in suspension. Typical examples are shown in Figure 7.1. Again, this was in agreement with the response analysis of Section 5.8. In the magnetically suspended tests which failed, loss of suspension was always preceded by the model travelling so far forward as to obscure the axial position sensor, and always a consequence of a high thrust peak.

In some cases a momentary excursion beyond the axial field of view could be survived, in others the model was recovered back into view but was

subsequently lost. An example is shown in Figure 7.2, where the model was out of view from time 937 ms to 955 ms, then partially recovered before control was finally lost. The cases where temporary excursions beyond the sensor field of view were tolerated prompted the question of whether the control software could deal more intelligently with the case of axial motion out of view. However this was felt to be a false area of discussion, as a model kept within view would surely be a more beneficial objective.

Tests were successfully carried out over the required nine data points. These were firings at zero ten and twenty degrees angle of attack and Mach numbers of zero, 0.1 and 0.2.

## 7.3 DERIVED EXPERIMENTAL RESULTS

Forces and moments were extracted from the available run-data using the program TRANSIENT described in Section 6. Figure 7.3 shows derived axial force traces for thruster firings at three different tunnel speeds. The differences between the traces cannot be attributed to an aerodynamic effect such as a change in drag coefficient. The wide range of motor performances observed prevents such a fine measurement.

Figures 7.4A-C and 7.5A-C show heave, pitch and axial results for firings at incidence. The ten degree data gives the truest thrust profile. At twenty degrees the quality of control during firing was poor, and the extracted data reflects impure motion of the model during its recovery by the controller.

## 7.4 RESOLUTION OF HEAVE AND AXIAL FORCES

Heave and axial forces calculated using TRANSIENT measure force components in unconventional axis systems. Heave is measured in wind tunnel axes (lift) and axial force in model axes. The forces measured are independent and can thus be simply resolved into the axis system required.

# 8.0 DISCUSSION

## 8.1 HARDWARE

The MSBS hardware performed well throughout this project, with only one major fault (a power supply failure) needing repair by an outside organisation. A number of minor problems were easily rectified in-house. Hardware modifications to the MSBS, namely repositioning of the axial position sensing optics, and interfacing of the PC, presented no particular problems during implementation or thereafter.

## 8.2 CARBON DIOXIDE THRUSTER

Detailed discussion of the performance of the thruster is a task to be performed by PSI. From the Southampton viewpoint a number of general performance criteria can be addressed.

1. Thrust profile

Thrust profile was the overriding problem throughout the experimentation stage of this project, particularly the high peak thrust level and overall variability of profile. However this entire project must be seen in the context of a proof-of-concept study for tests involving larger, controllable carbon dioxide thrusters. With this in mind, the fact that a thruster was fired in suspension, and data logged and analysed, becomes more significant than the quality of the aerodynamic data obtained.

2. Roll control

Lack of provision of roll control on the propulsion simulator was inconvenient, but also of little consequence overall as it did not prevent the successful firing of the model. Implementation of some form of active or passive roll control on a future model would be simple.

3. Operation and Reliability

Apart from the thrust profile problem discussed above, the propulsion simulator performed well. It was robust enough to survive a few knocks when dropped from suspension, and would always fire when properly set-up. Although it was a little awkward to reload, there were no real problems in operating

and testing the propulsion simulator.

## 8.3 CONTROL

All control problems stemmed from the fact that thrust from the motor having a peak equal to or exceeding the maximum which could be tolerated under steady conditions, was being applied to the model almost instantaneously. A consequence of using a feedback control system was that reaction to this force was necessarily subject to a delay, during which time the model would have started accelerating towards the limit of the axial sensor. The assessment of the effects of thrust profile on MSBS propulsion simulation made in Section 5.8, suggests that hardware rather than software design is the limiting factor with the present equipment.

One way to improve the response to a steep thrust increase given the hardware limitations could be via some form of feed-forward in the control system. This would have to co-ordinate a pre-programmed increase in axial currents with a precisely timed firing of the thruster. The model would start to accelerate downstream just as ignition occurred, and its downstream momentum would also be useful in preventing excessive upstream travel in response to the thrust impulse.

Areas to be addressed in attempting feed-forward with the carbon dioxide simulator would have to include reliability and timing of ignition, computer control of the firing laser, control of the model if ignition fails, accuracy of alignment of the firing laser and roll control of the model.

An alternative is to use a temporary external restraint, to mechanically prevent model motion until the thrust peak has passed, at which time it would be withdrawn.

## 8.4 DATA ANALYSIS

The limitations of the transient analysis software at its present state of development are illustrated by the differences between extracted and bench tested thrust profiles, and by the no-force case described in Section 6.1.

However, the principle of simultaneous derivation of applied electromagnet forces appears a valid notion for unraveling the complex interactions used by the high angle of attack controller. Its main drawback is not the complexity of the calculations, which are ideally suited to computer processing, but the need to extract a number of calibration constants $n$, where

$$n = \text{no. of magnets} * \text{no. of degrees of freedom}$$

These constants must be found by experiment and data analysis for each test condition.

## 8.5 ROCKETS

Use of small rockets for propulsion simulation proved very easy in the SUMSBS. Compared to the carbon dioxide thruster they had the advantages of simplicity, repeatability of thrust profile and reduced cost. Rocket exhaust is clearly a better approximation than a cold stream of carbon dioxide to a real engine efflux, although an analysis with similarity parameters of the type used by Asai (8) amongst others has not yet been attempted.

Further propulsion simulation work is anticipated at Southampton using rockets.

## 8.6 RESULTS

Setting up the system for maximum axial force capability was clearly a trade-off between performance in different degrees of freedom. The calibration results for pitch and heave are degraded by the fact that several magnets were operating close to their current limits in the unloaded case, as part of the attempt to maximise axial force.

No attempt has been made to compare the wind-on and wind-off data and show an effect on drag coefficient caused by the presence of an exhaust jet. It is clear that any such subtleties in the results would be swamped by the variation in thrust levels produced by the carbon dioxide simulator. Other factors, such as the need for external weights on the model for roll control,

and the unsatisfactory transient data analysis, also preclude such a derivation.

# 9.0 CONCLUSIONS

1. The principle of propulsion simulation in a magnetic suspension wind tunnel has been proved viable using a simple thruster on-board a model.

2. Use of iron models with the high angle of attack control system is possible. The use of iron avoids production problems inherent with constructing complex shapes from brittle permanent-magnet alloys.

3. The complexity of the data analysis required for use with future propulsion simulators will depend on their thrust profile.

4. Analysis of motion transients to extract external forces is non-trivial and will need further investigation if step thrust profiles must be used.

5. The acceptable thrust build-up time to enable steady-state testing is hardware dependent, estimated at 50 ms for the SUMSBS.

6. Simultaneous extraction of multiple force and moment components is possible from E/M current data.

7. Small rockets are a promising alternative to carbon dioxide thrusters.

APPENDIX 1: ESTIMATED RESPONSE TO A STEP THRUST

ASSUMPTIONS

1. Max restraining force F = 5 N
2. Model mass m = 0.6 kg
3. Controller delay = 1 program cycle ($1/_{242}$seconds)
4. Current delay = 50 ms
5. Initial thrust T = 4 N

ANALYSIS

The response to the instantaneously applied thrust is assumed to be in two phases. Initially, the thrust is applied and the model accelerates, while the restraining force builds up in response. Assuming a linear build-up, the force acting during this phase can be taken as half the maximum, and the duration of the phase as $t_1$ = 50 milliseconds.

In the second phase the maximum force counters the thrust, and the model is brought to rest. The duration of this phase depends on the velocity attained by the model during the first phase. To find the total axial displacement during the two phases $s_{12}$, Newtonian dynamics give

$$s_{12} = \frac{t_1^2}{2m}\left[(T - F/_2) - \frac{(T - F/_2)^2}{(T - F)}\right]$$

This very simplified analysis is designed only to show the sensitivity of axial motion to peak thrust variations, not to predict axial travel for different cases. Displacements for a range of possible thrust values are given in Figure 5.8.

LIST OF FIGURES

2.1 SUMSBS hardware block diagram
2.2 Electromagnet configuration

3.1 Characteristic power supply response
3.2 Position sensing geometry with old axial layout
3.3 New axial sensing geometry
3.4 Magnetising field vector components

4.1 Schematic of representative model
4.2 Optimisation of responses
4.3 Axial force loading technique
4.4 Heave and pitch combined loading
4.5 Sketch of axial force/currents/magnetisation
4.6 Thrust test stand schematic

5.1 Calibration results for the carbon dioxide model
A: Heave
B: Pitch
C: Axial at incidence
D: Axial at zero degrees
5.2 Hobby rocket motor thrust profile
5.3 Carbon dioxide thruster with 0.1 inch nozzle
5.4 Carbon dioxide thruster with worn/damaged components
5.5 Carbon dioxide thruster with 0.35 inch nozzle
5.6 E/M response to step demand
5.7 E/M response to model motion
5.8 Simplified prediction of axial travel with different step thrusts

6.1 Initial force extraction with TRANSIENT software
6.2 Improved force extraction with modified TRANSIENT software
6.3 Position dependence of 'zero-force' current
6.4 Variation of calibration constant with magnetisation
6.5 Erroneous force extracted from commanded step motion
6.6 Comparison of extracted magnetic and total forces

7.1 Different axial responses in suspension to nominally similar thrusts

7.2 Loss of control despite recovery of model back into axial field of view

7.3 Force traces for three tunnel speeds

7.4 Extracted force and moment data for test at 10 degrees

A: Wind off

B: Mach 0.1

C: Mach 0.2

7.5 Extracted force and moment data for test at 20 degrees

A: Wind off

B: Mach 0.1

C: Mach 0.2

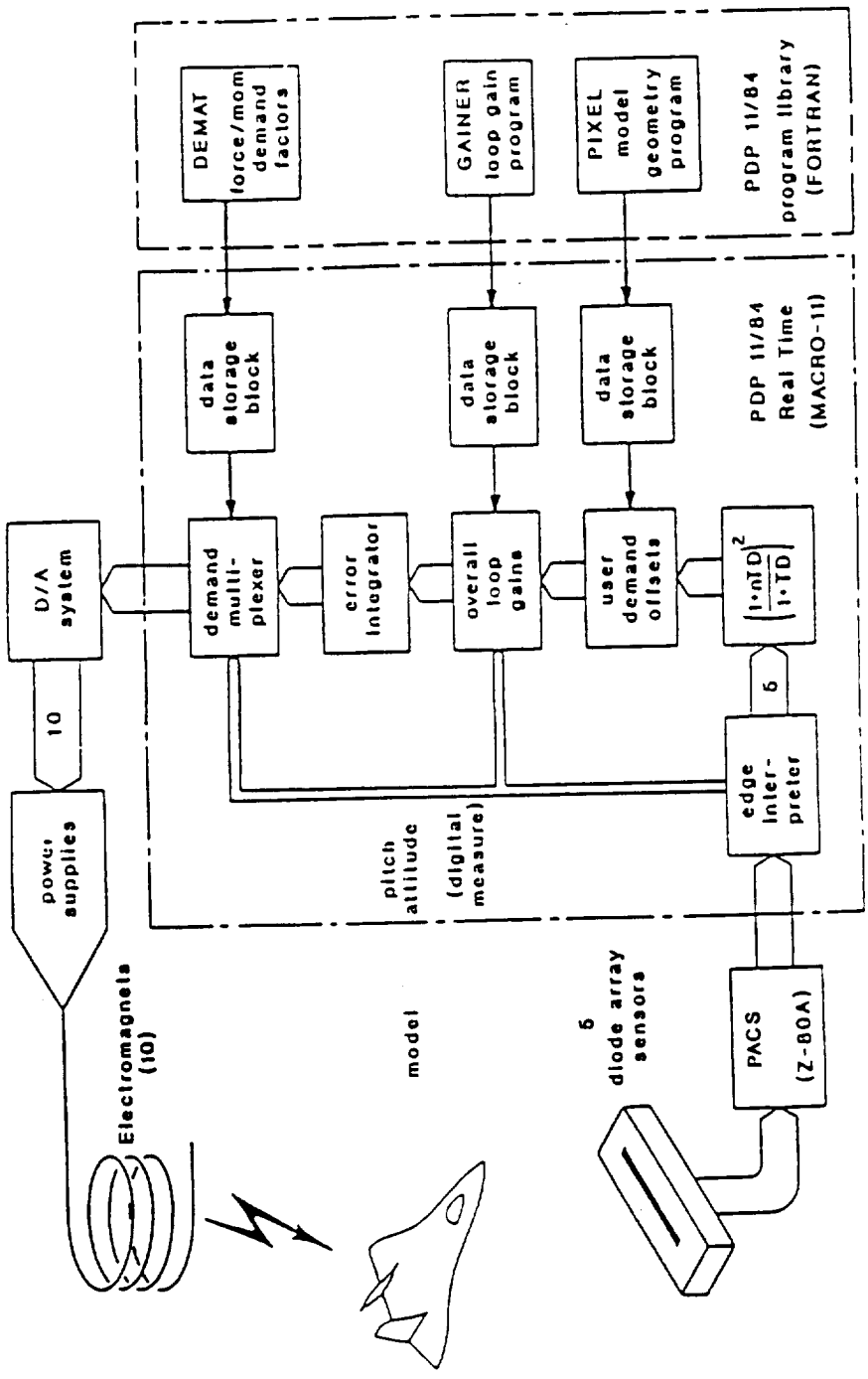


Figure 2.1: SUMSBS Hardware Block Diagram

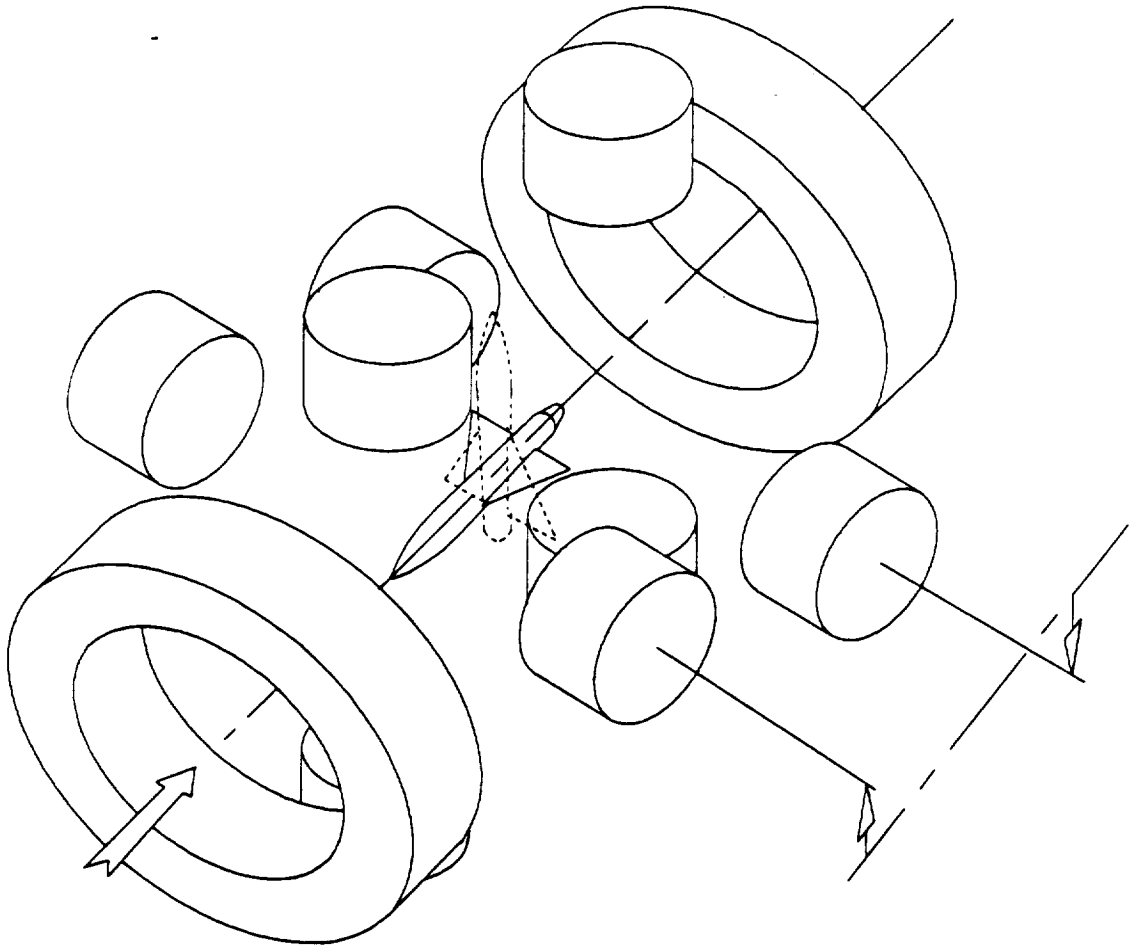


Figure 2.2: Electromagnet Configuration

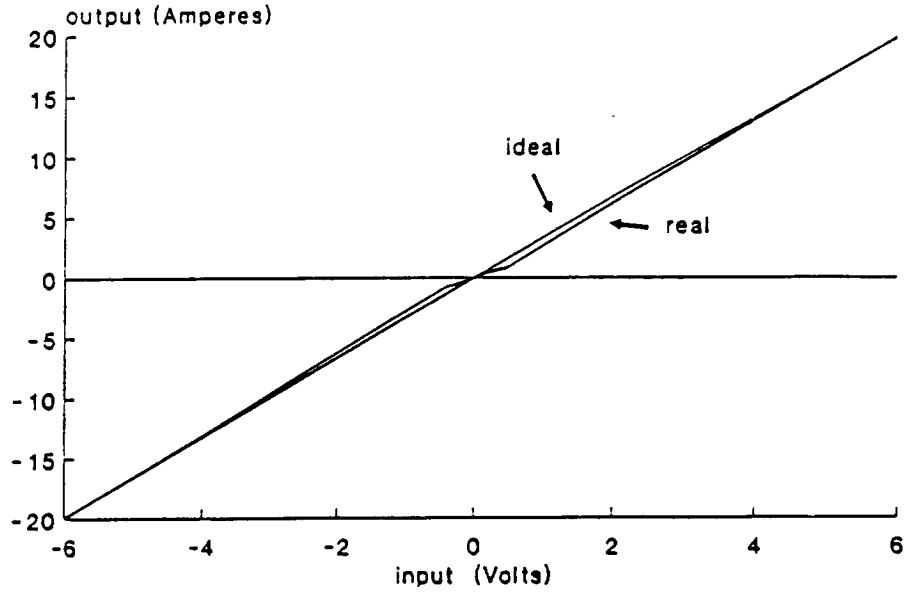


typical input/output characteristics
of power supplies

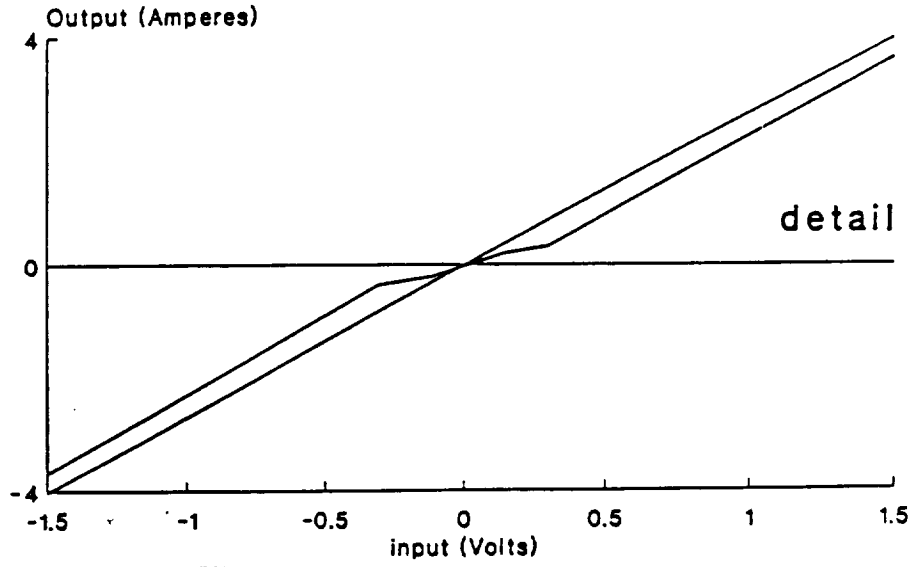


**Figure 3.1: Characterisctic Power Supply Response**

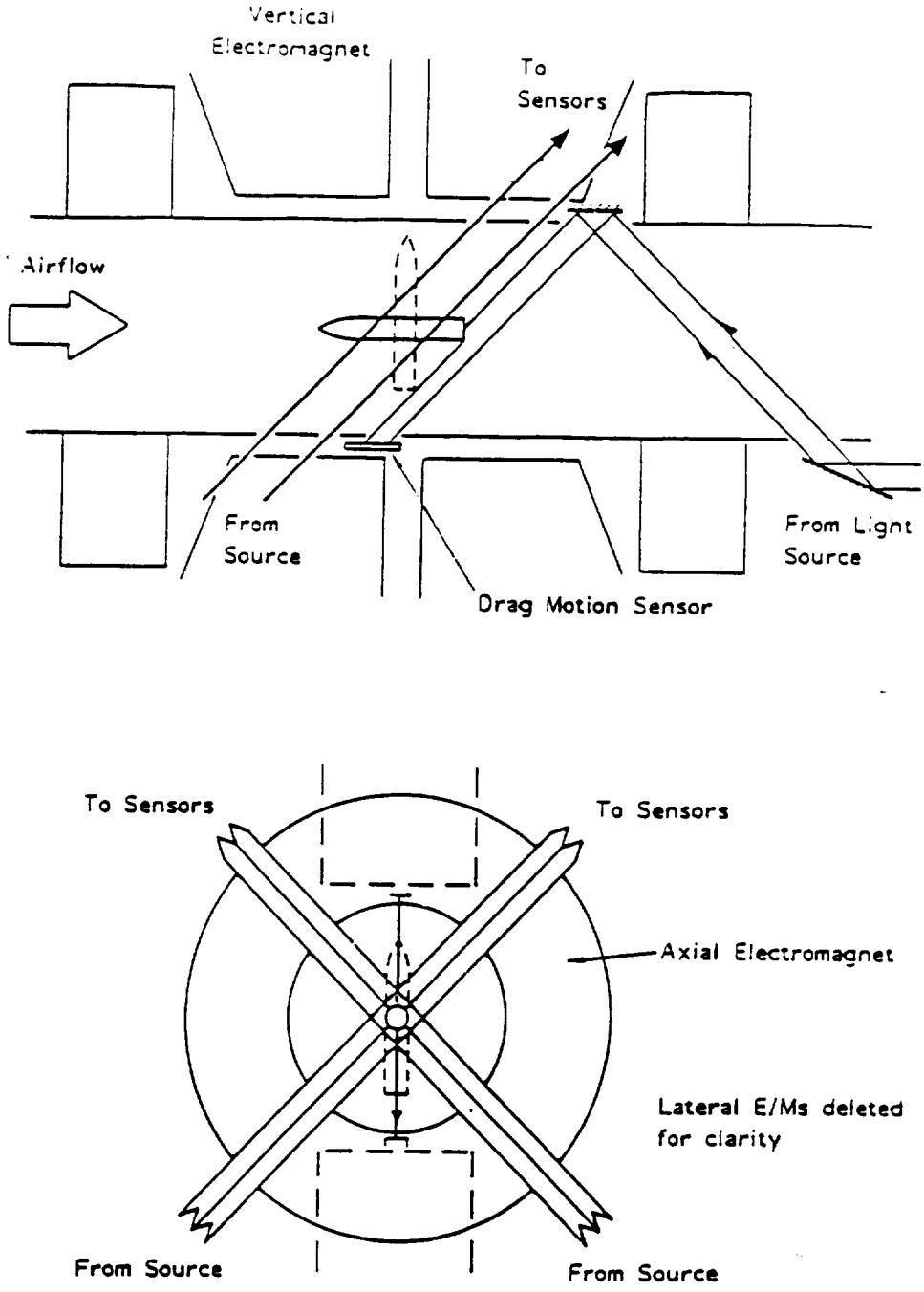


**Figure 3.2: Position sensing geometry with old axial layout**

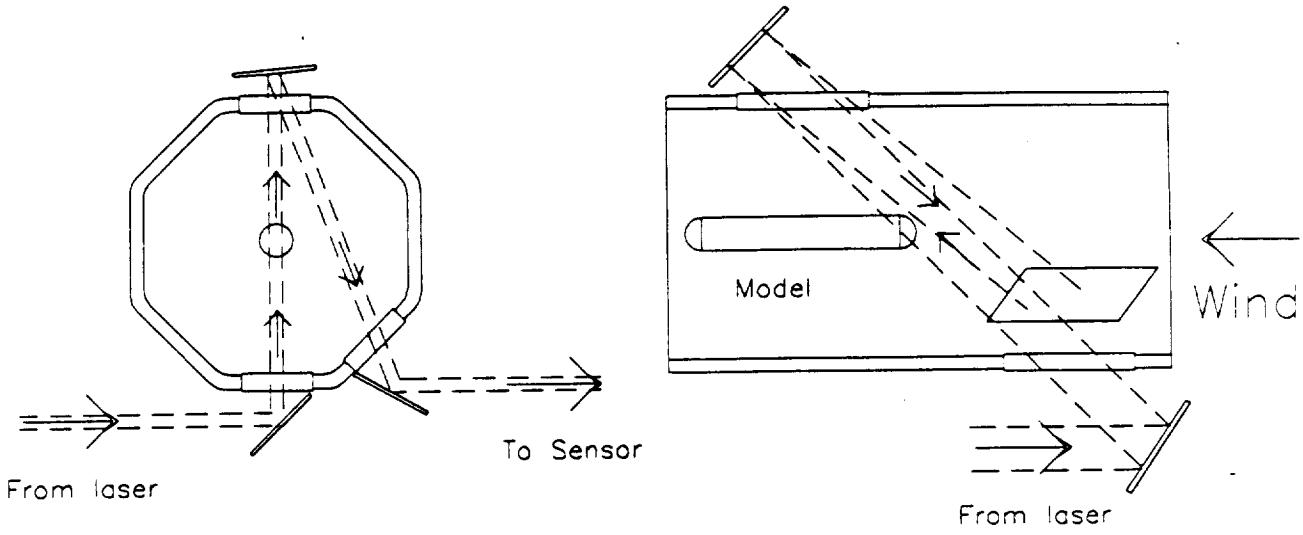


End view

Side view

Figure 3.3: New axial sensing geometry

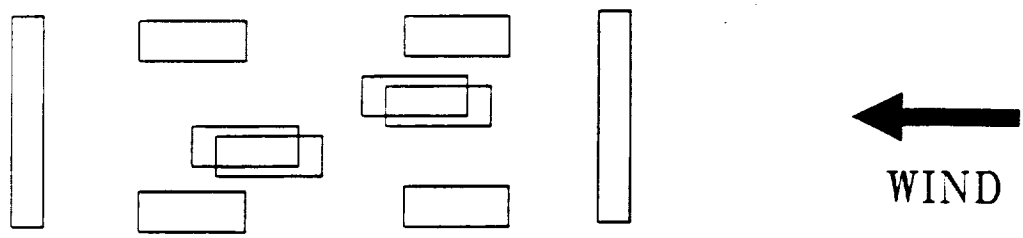


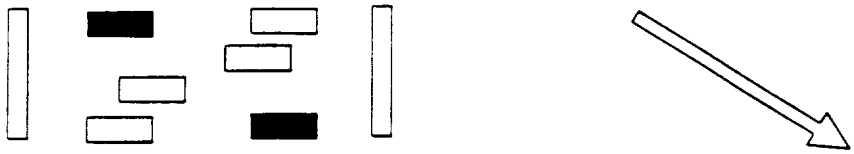

Group 1: -50 degrees, 7.2E-4 T/A

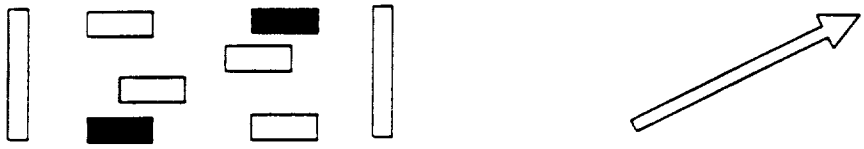

Group 2: 50 degrees, 7.2E-4 T/A

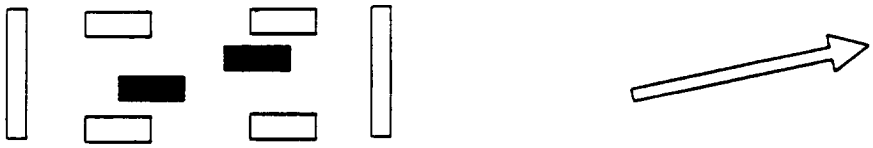

Group 3: 33 degrees, 9.5E-4 T/A

Group 4: 0 degrees, 5.0E-4 T/A

Figure 3.4: Magnetising field vector components

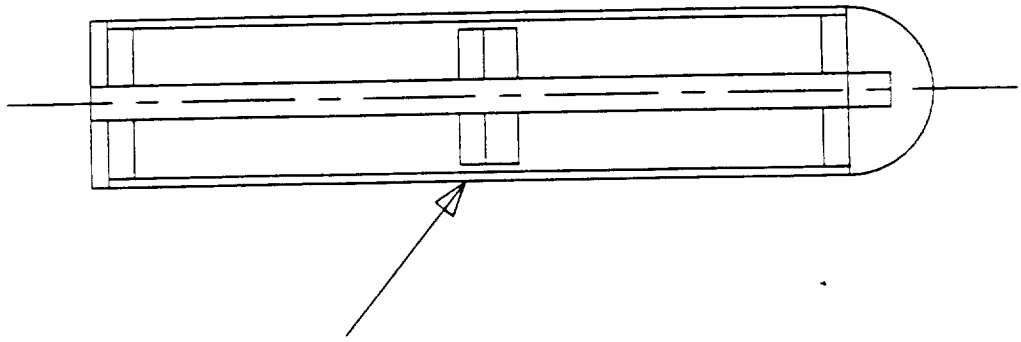


Figure 4.1: Schematic of representative model

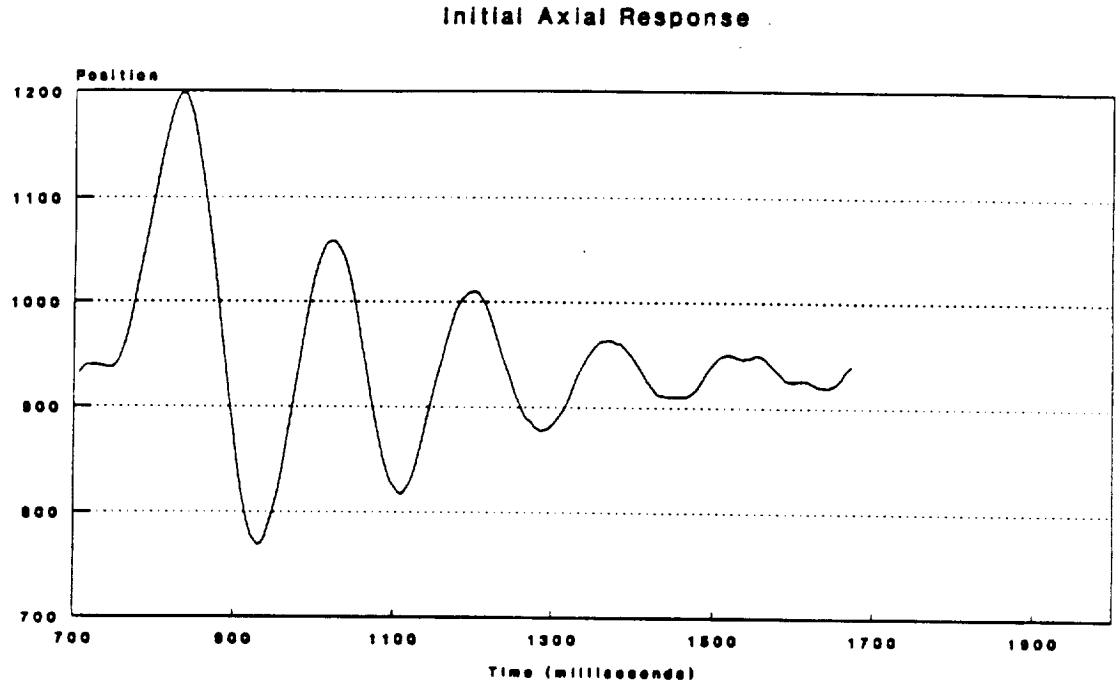


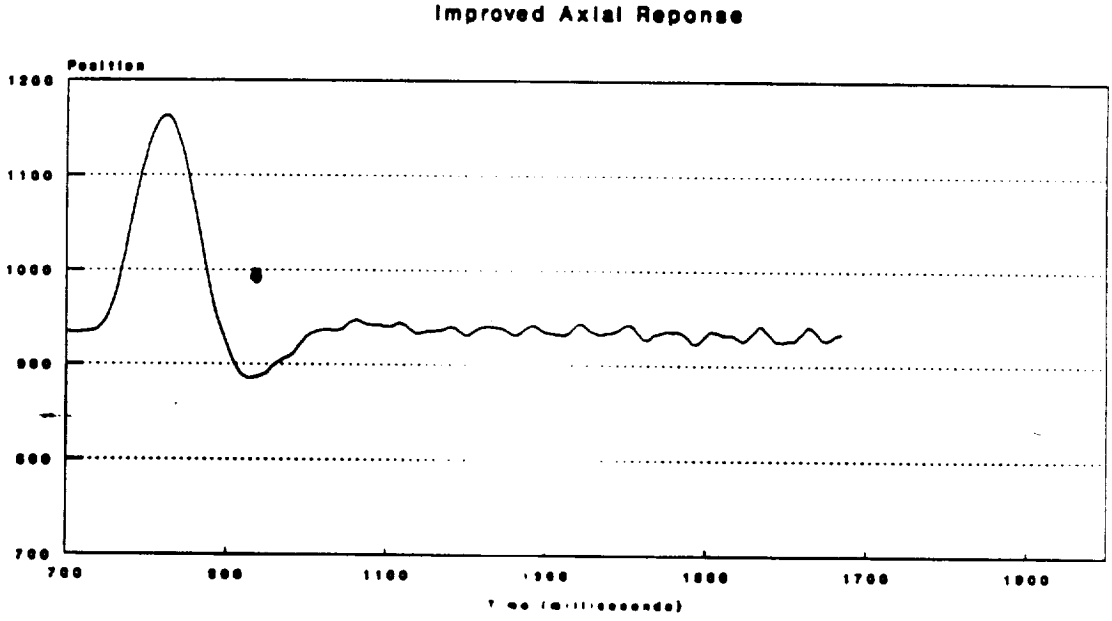


Figure 4.2: Optimisation of responses

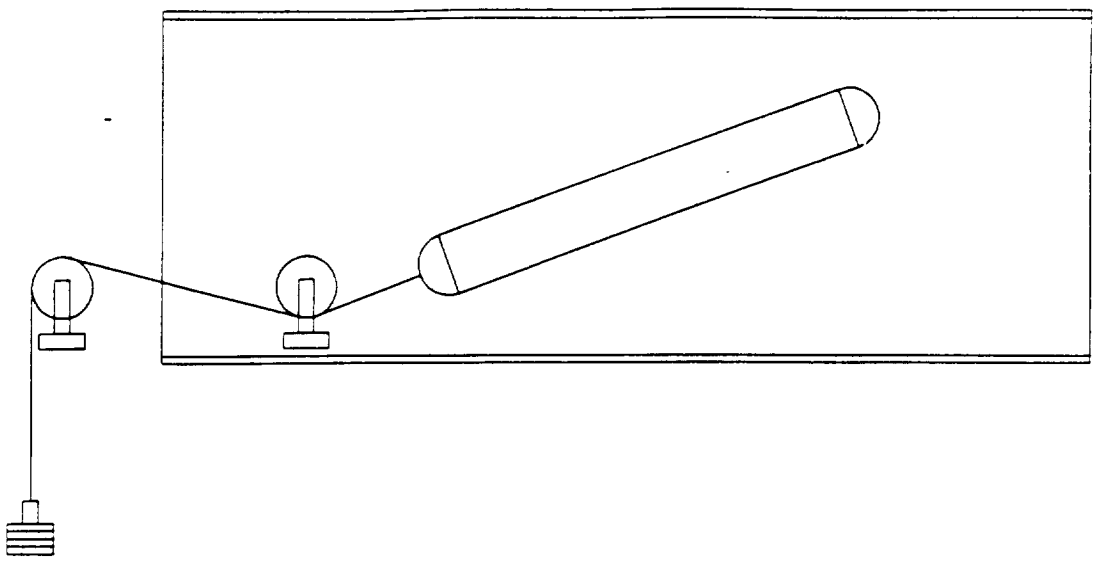

Figure 4.3: Axial force loading technique

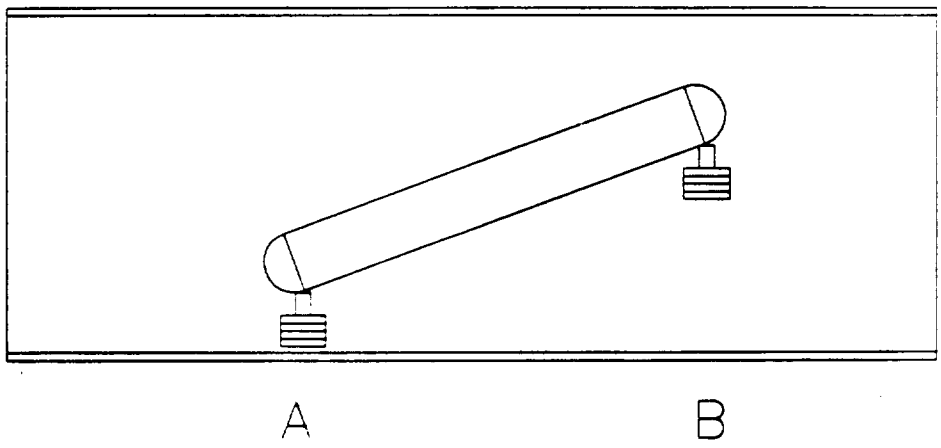


Figure 4.4: Heave and pitch combined loading

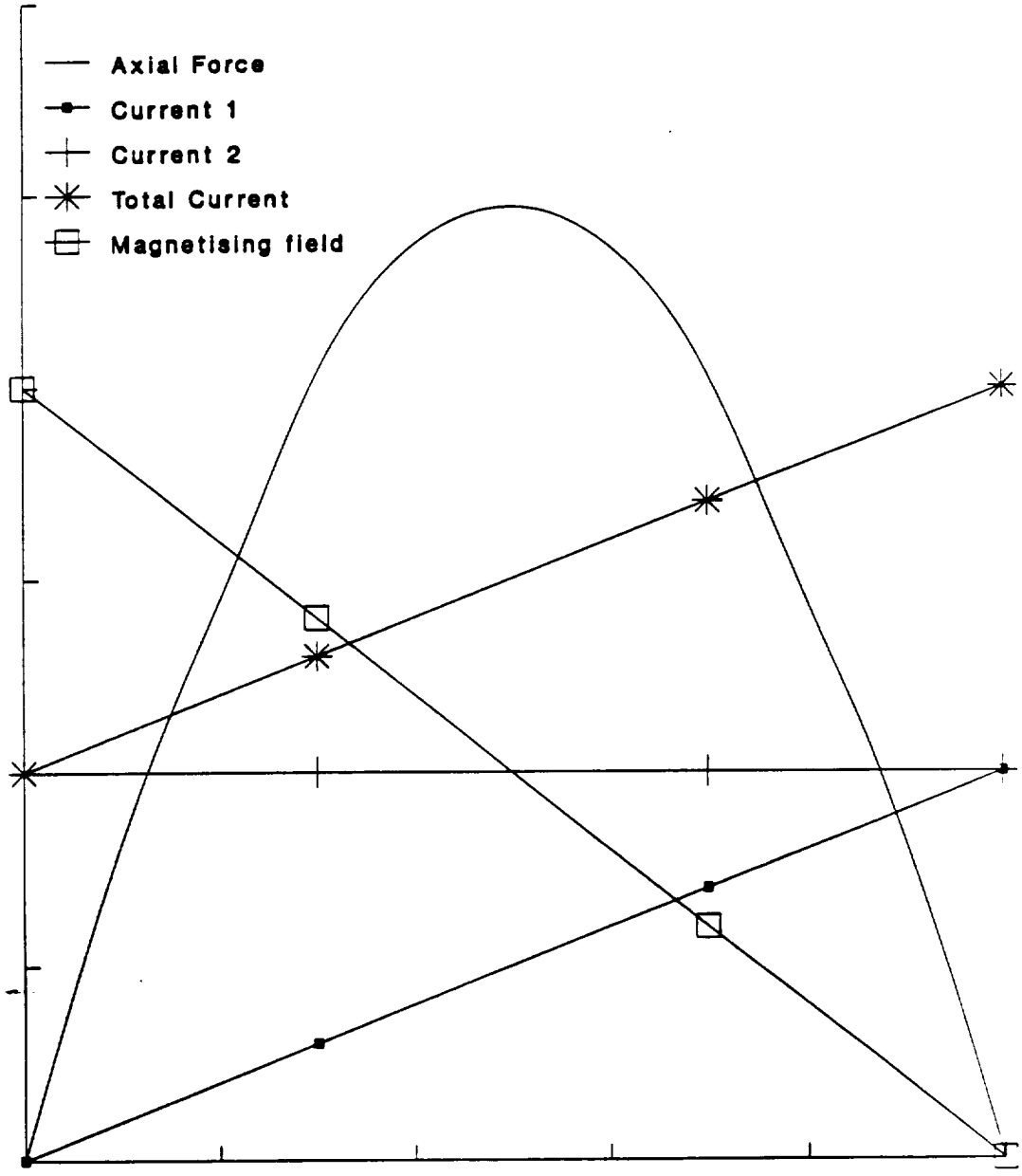


**Figure 4.5: Sketch of axial force change with currents and magnetisation (perceived relationship)**

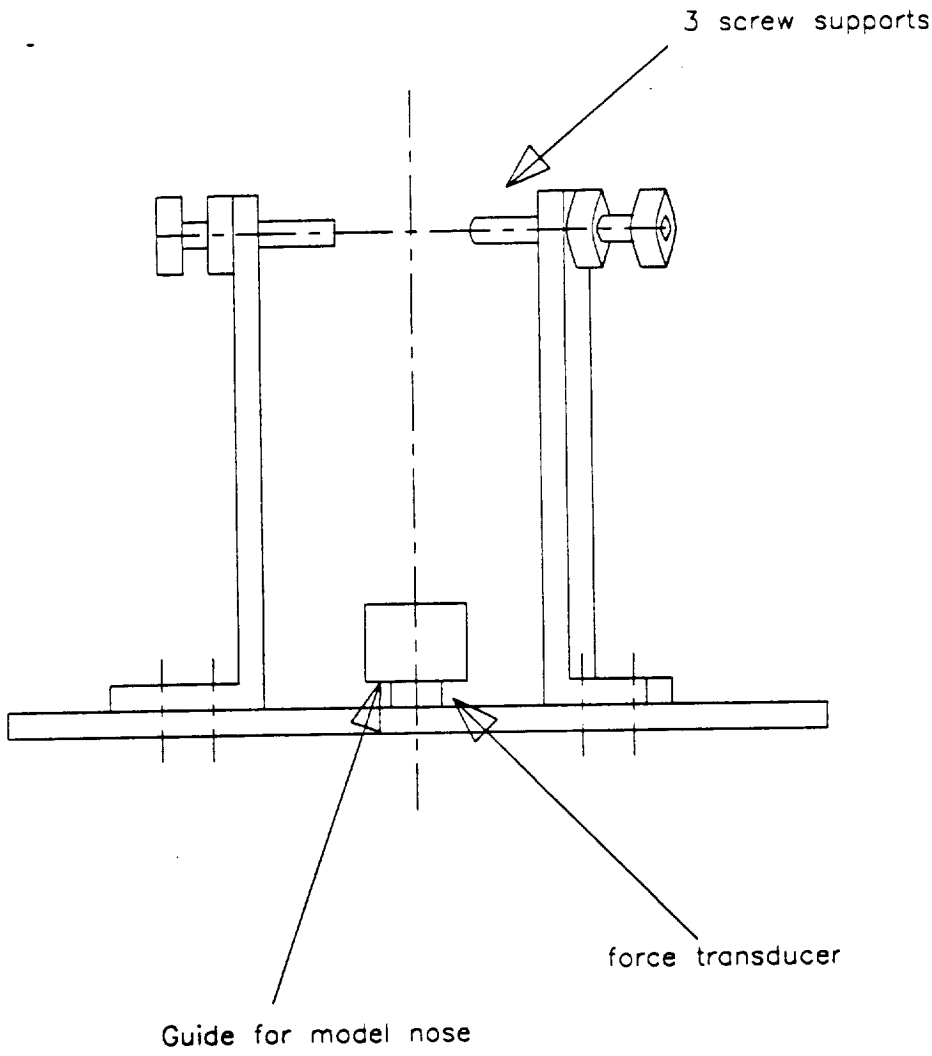


Figure 4.6: Thrust test stand schematic

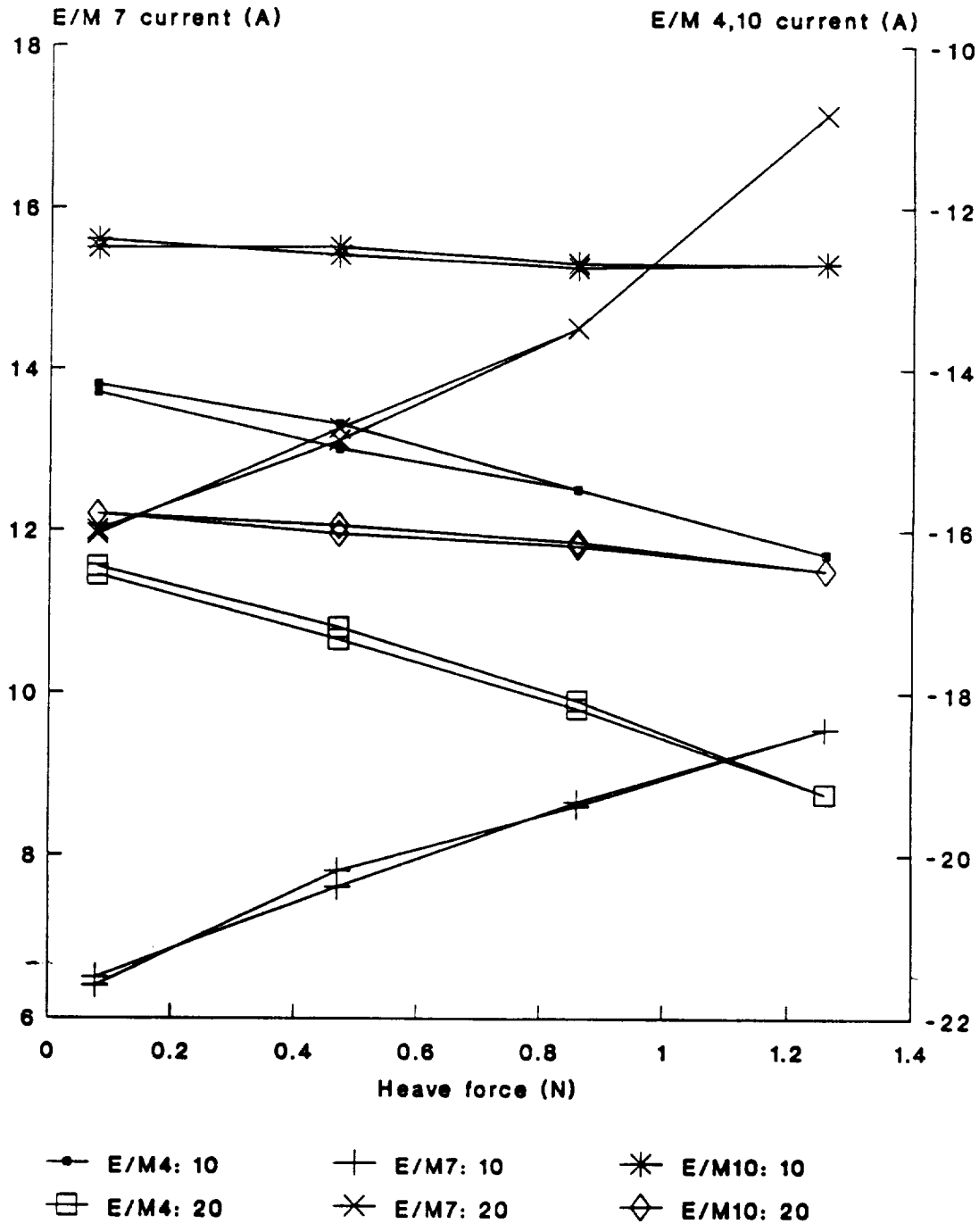


Figure 5.1A: Heave calibration results

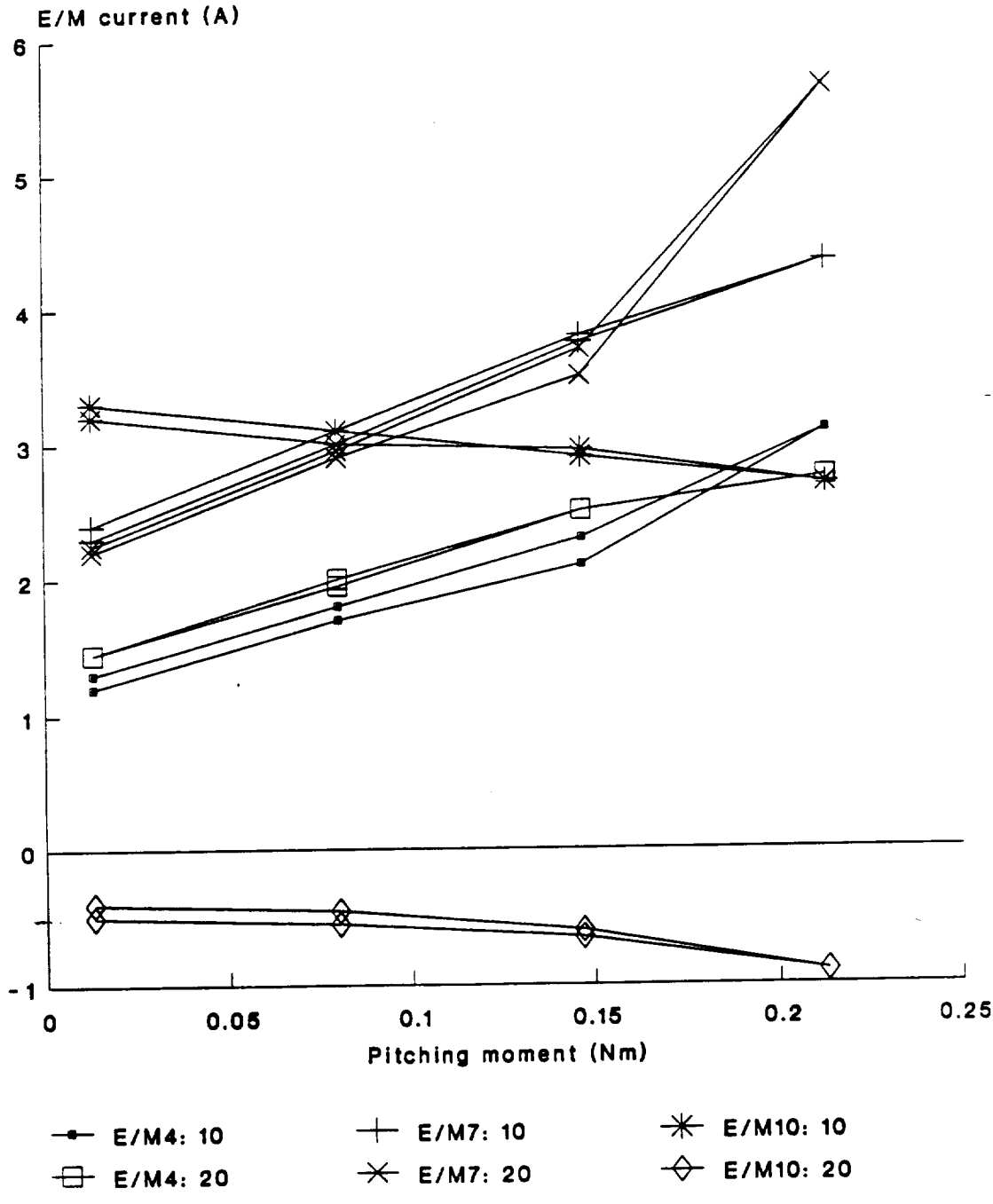


Figure 5.1B: Pitching moment calibration

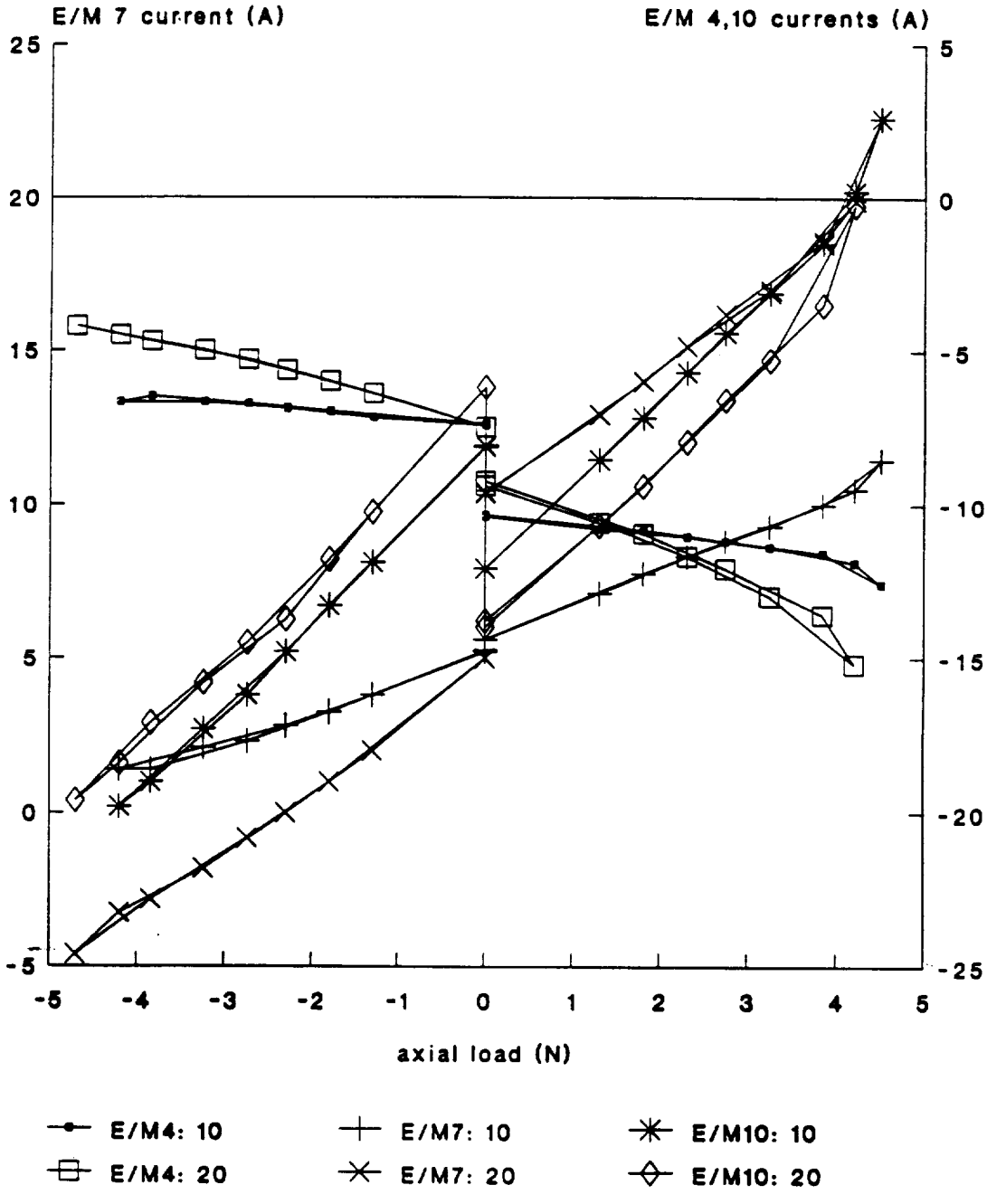


Figure 5.1C: Axial calibrations at ten and twenty degrees

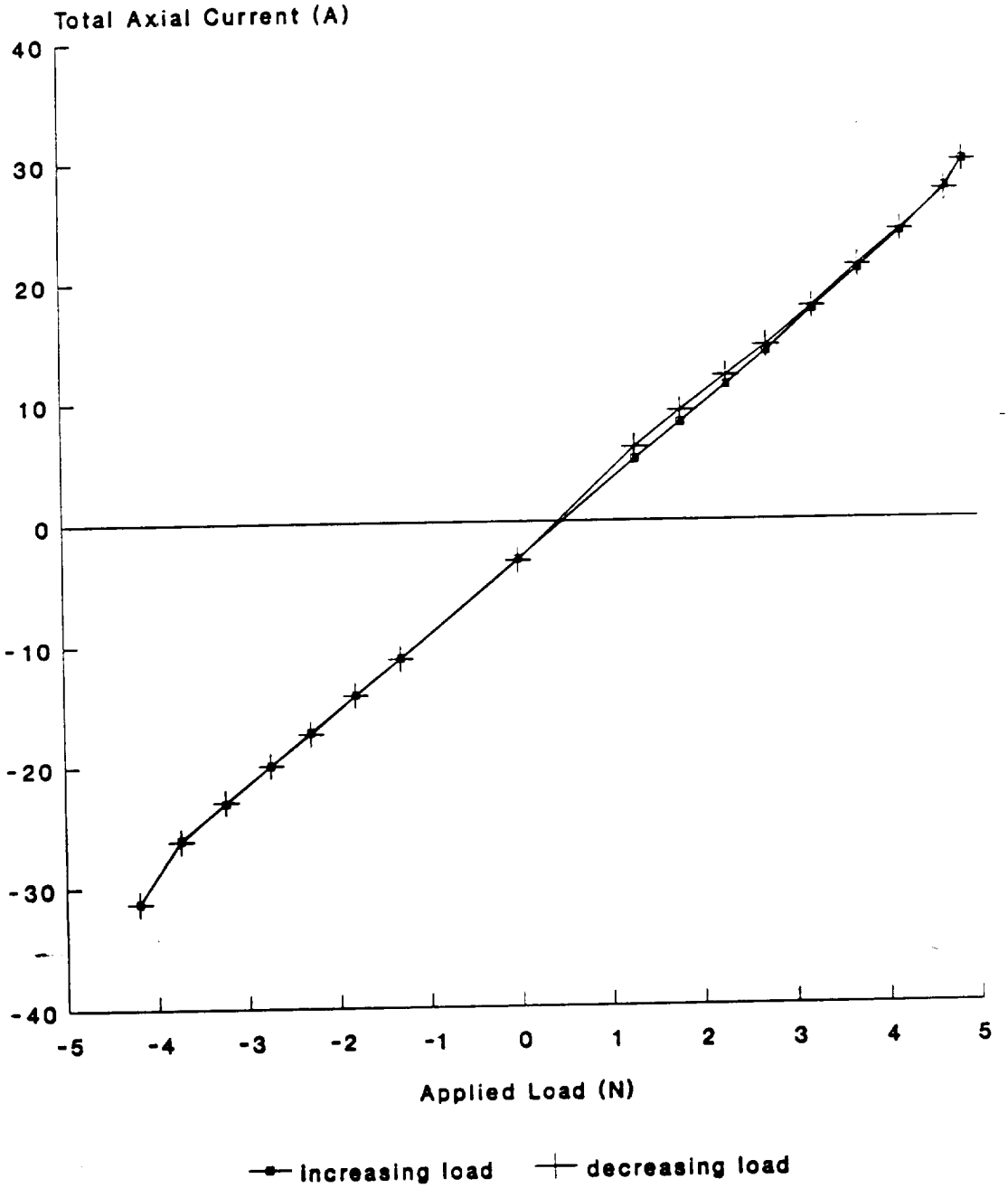


Figure 5.1D: Axial calibration at zero angle of attack

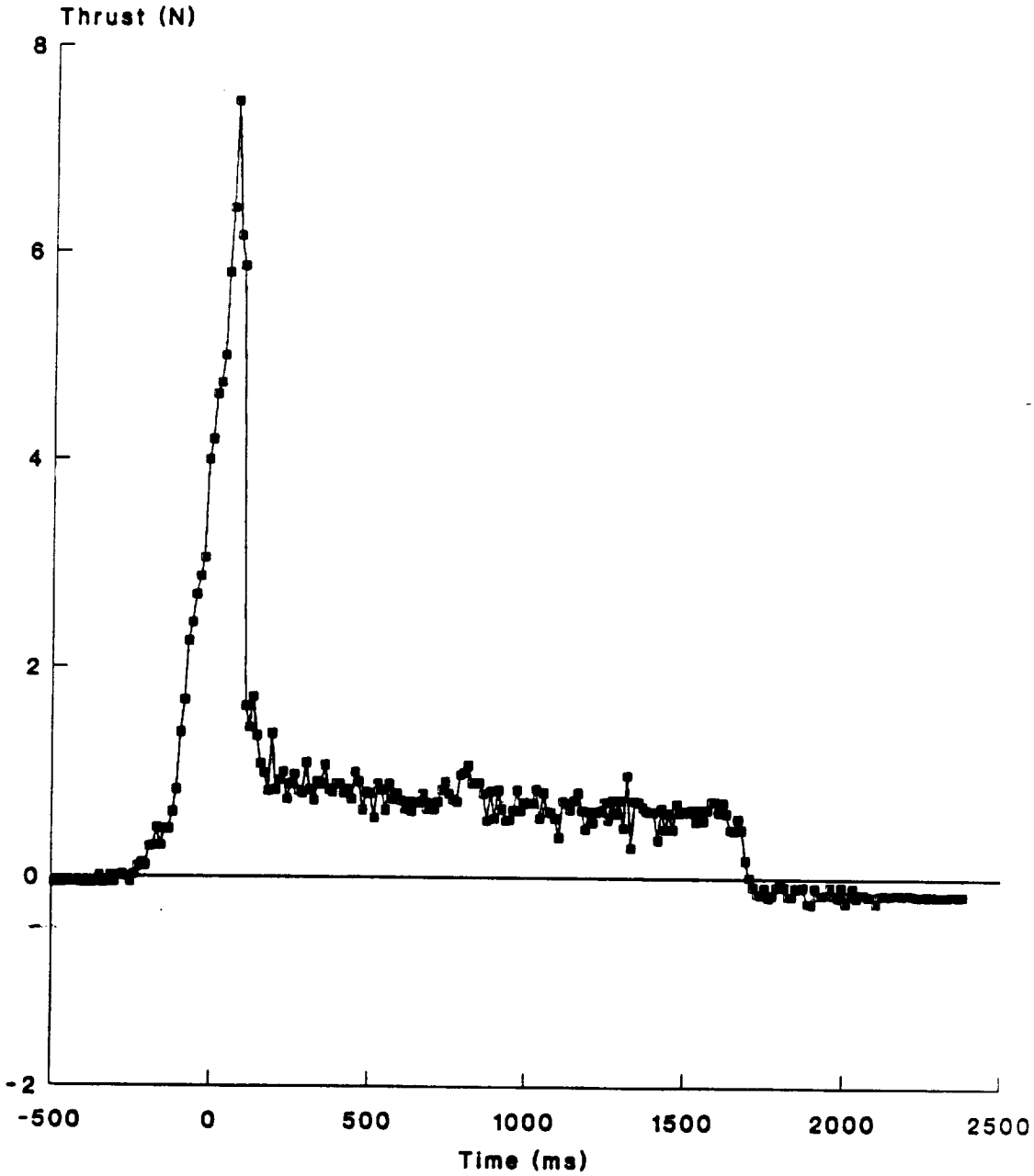


Figure 5.2: Hobby rocket motor thrust profile


Figure 5.3: Carbon dioxide thruster with 0.1 inch nozzle

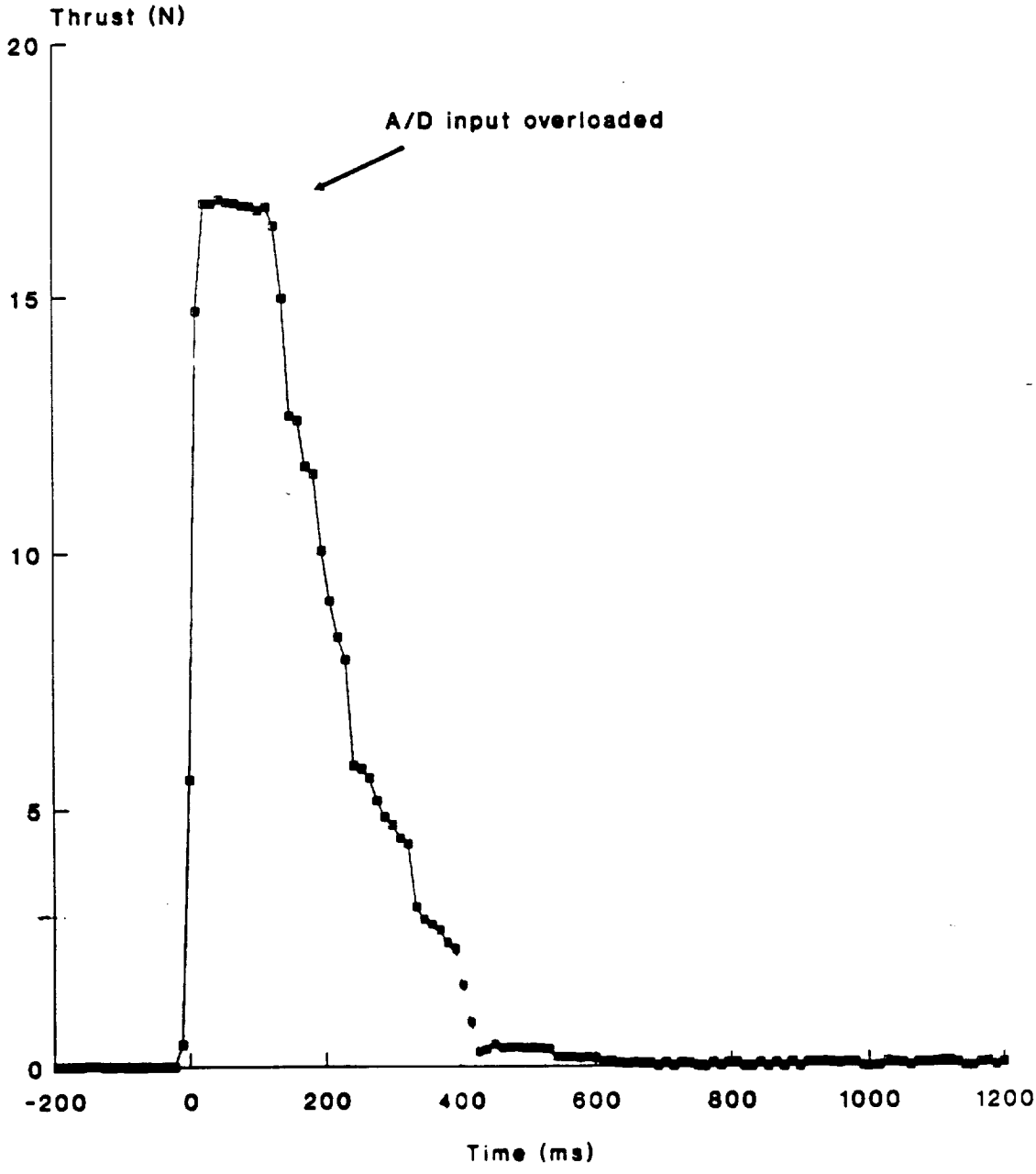


Figure 5.4: Carbon dioxide thruster with worn/damaged components

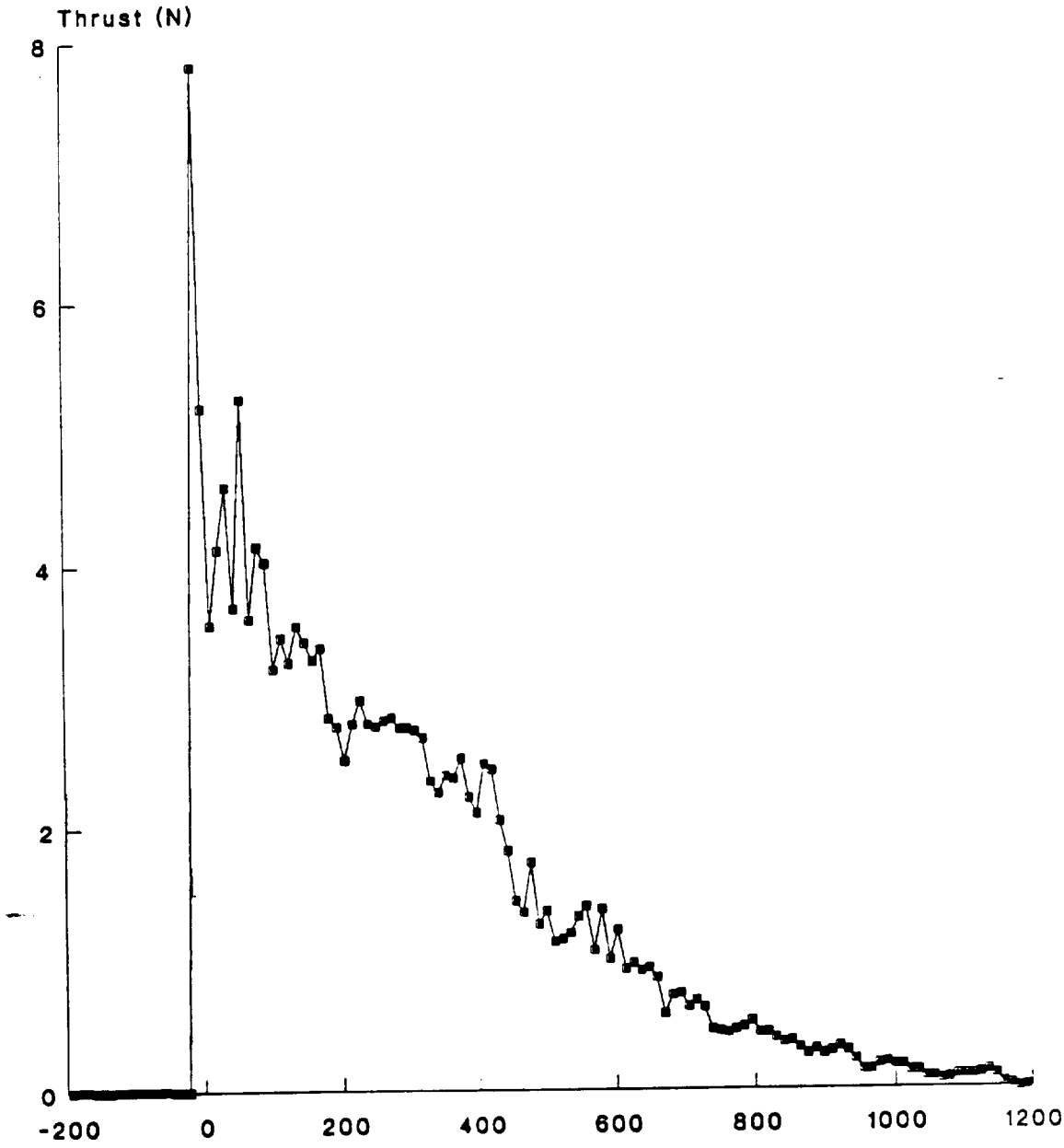


Figure 5.5: Carbon dioxide thruster with 0.35 inch nozzle

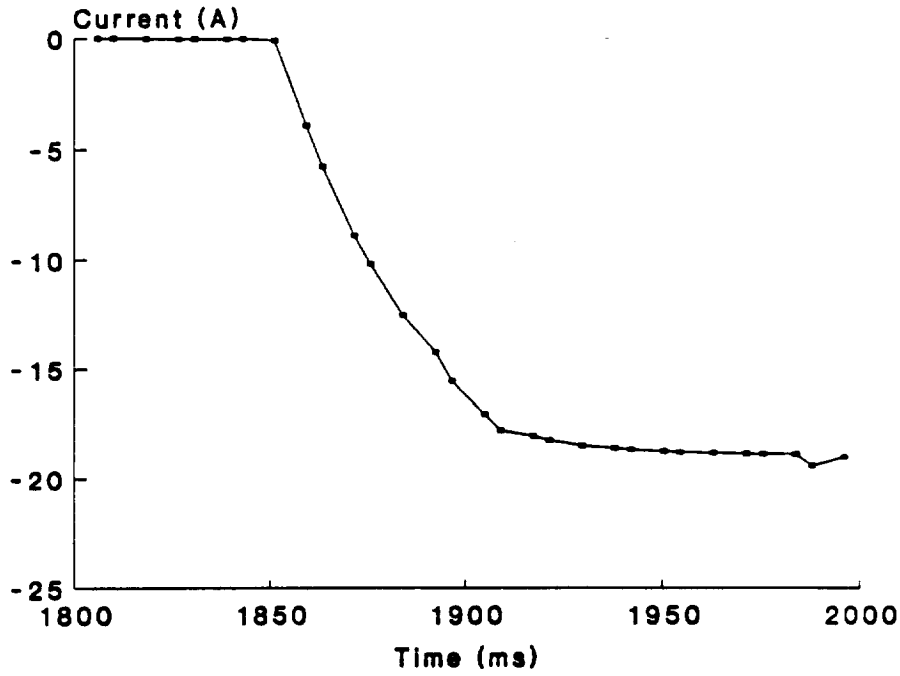


Figure 5.6: Response of axial E/M to demand step

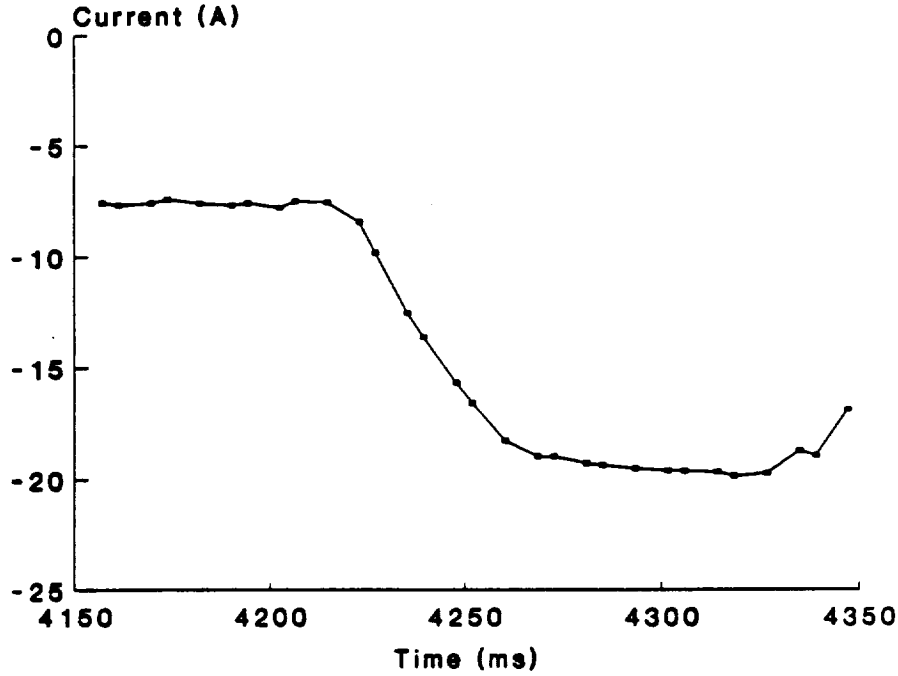


Figure 5.7: Response of axial E/M to model motion

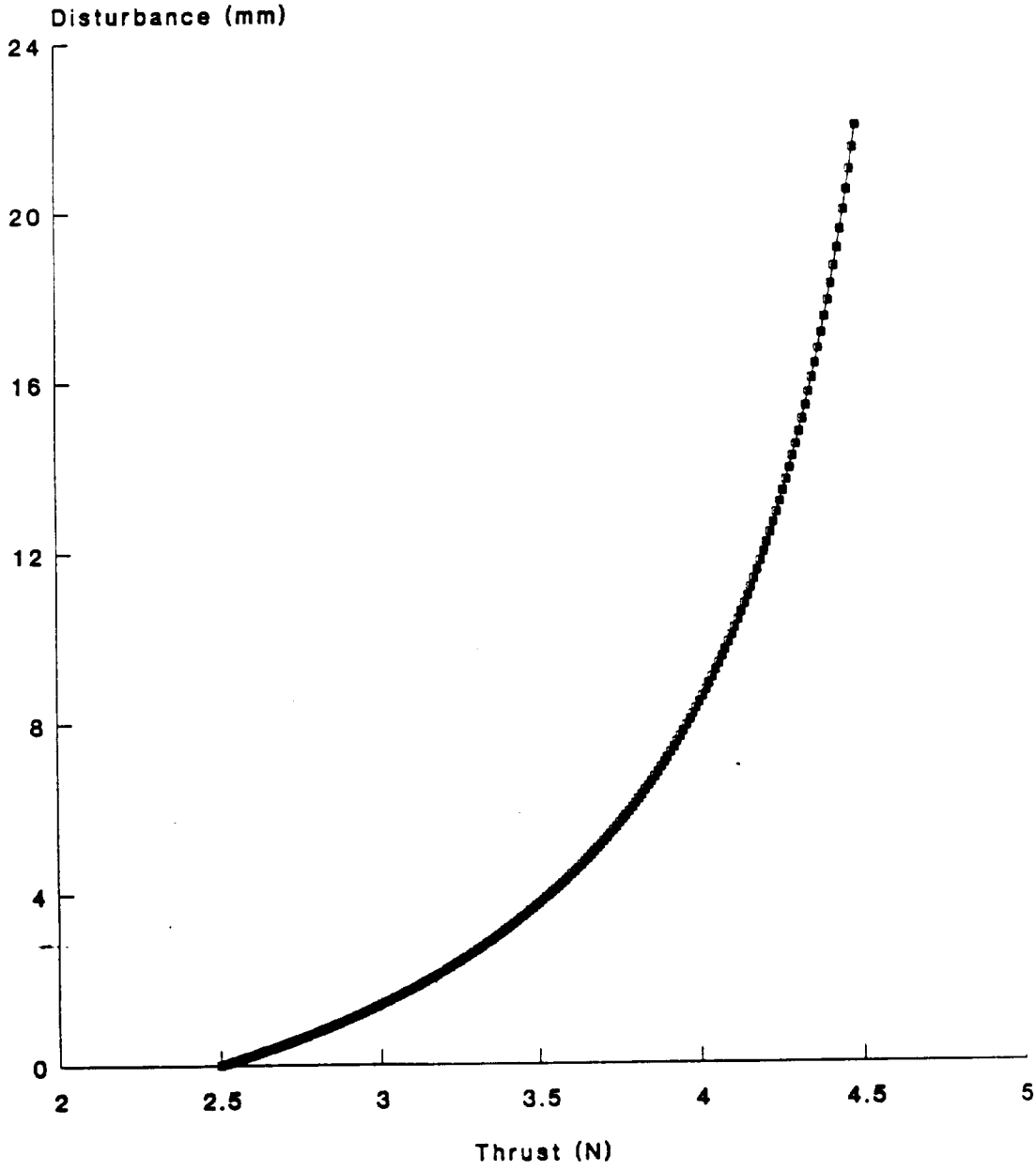


Figure 5.8: Results of simplified prediction of model response to different step thrust impulses

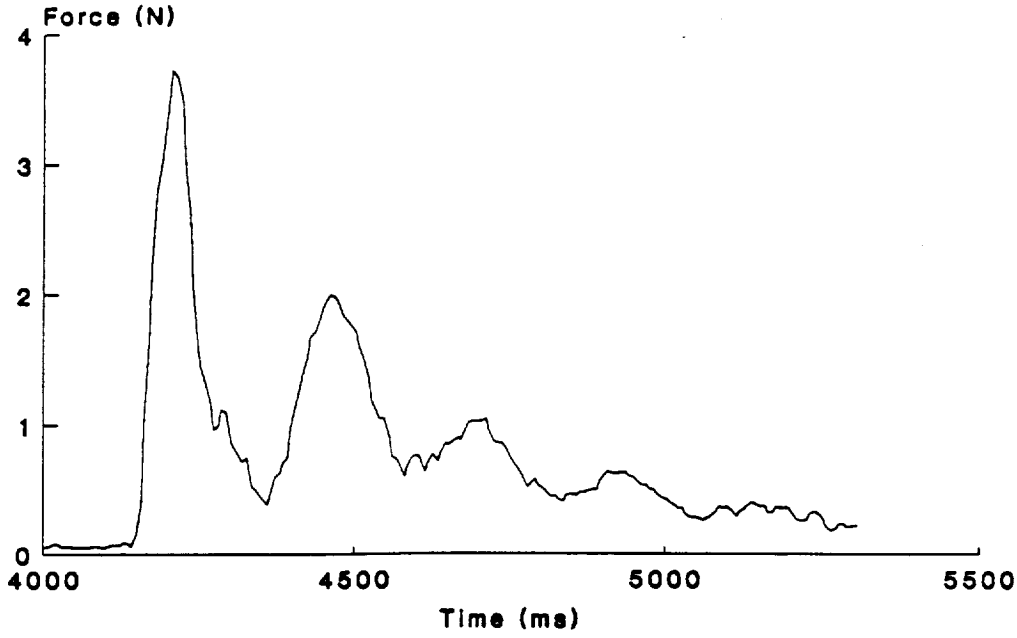


Figure 6.1: Initial force extraction with TRANSIENT

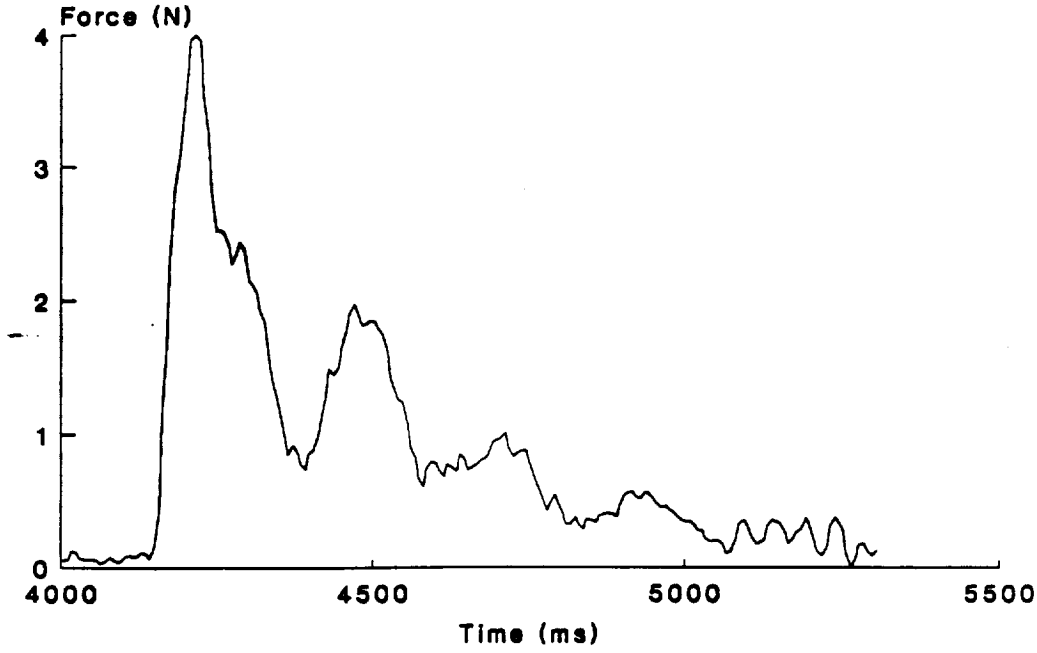


Figure 6.2: Force extraction with modified TRANSIENT

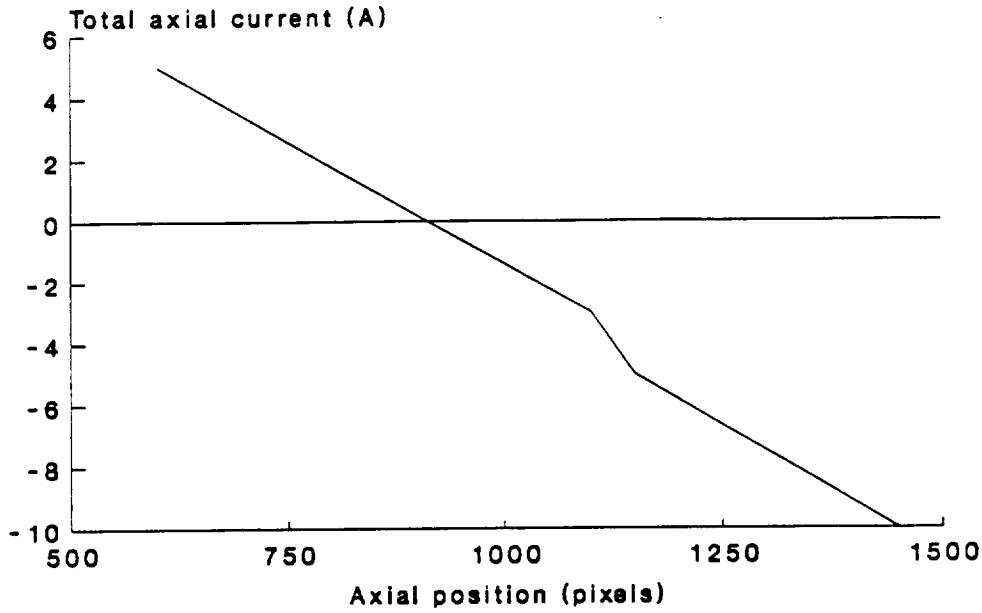


Figure 6.3: Variation of zero-force current with axial position

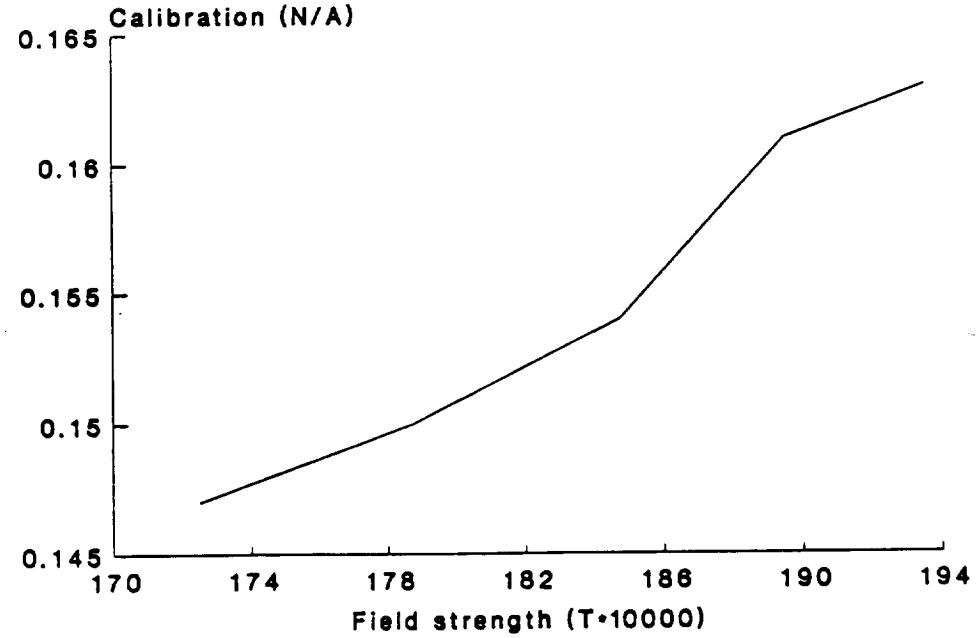


Figure 6.4: Variation of axial calibration constant with magnetisation

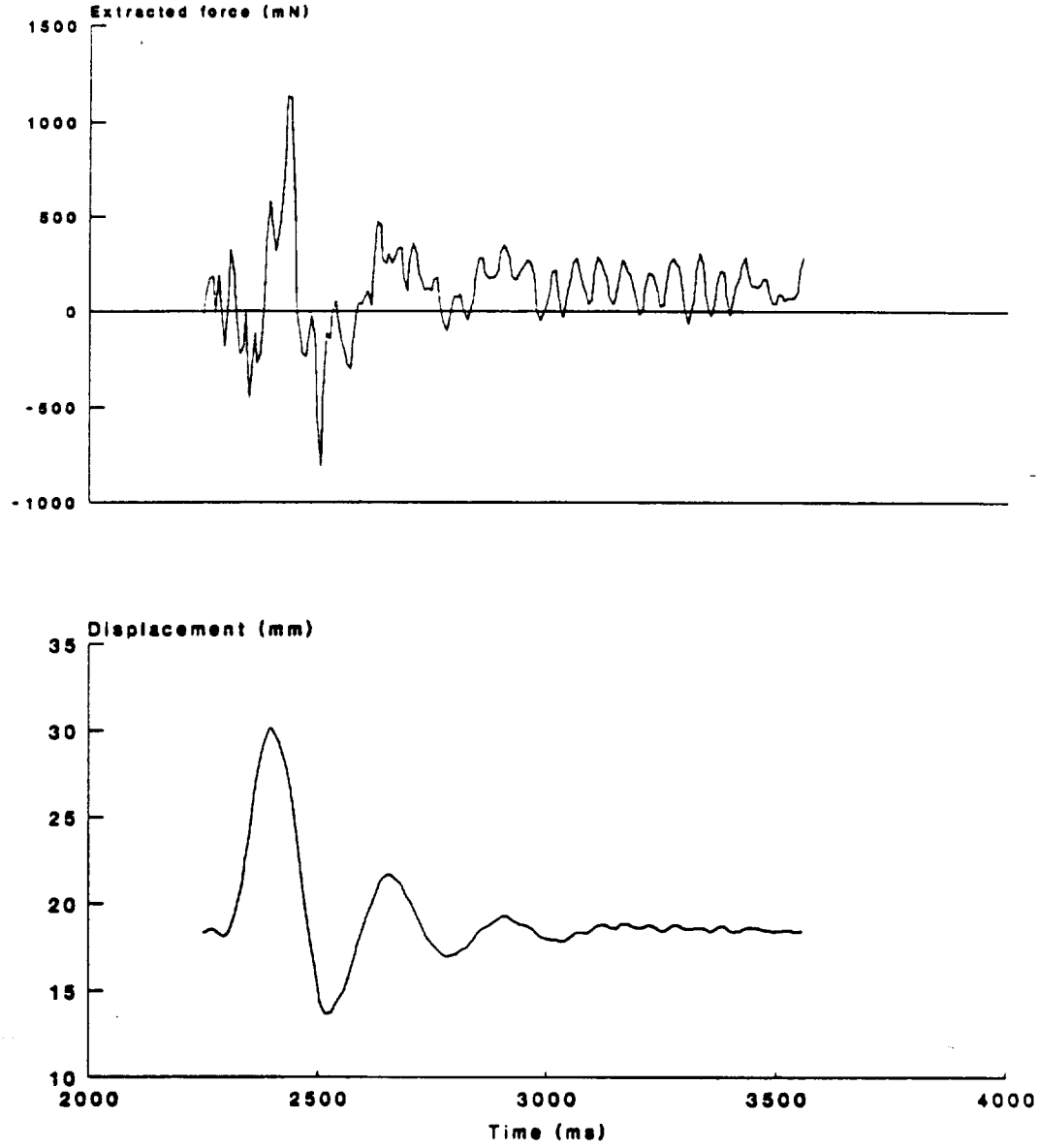


Figure 6.5: Erroneous force data extracted from free motion

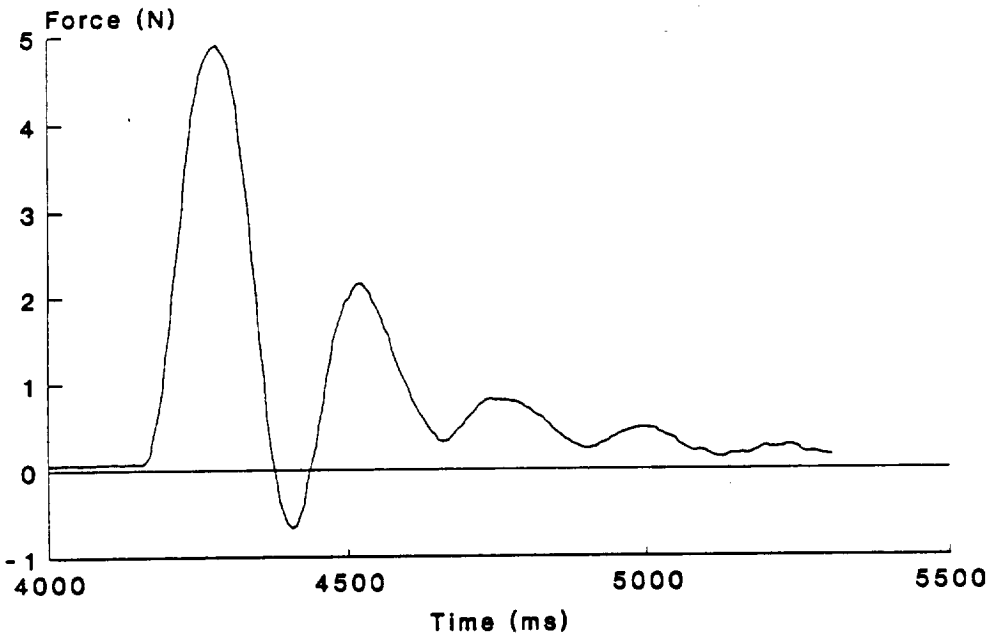


Force generated by axial magnets

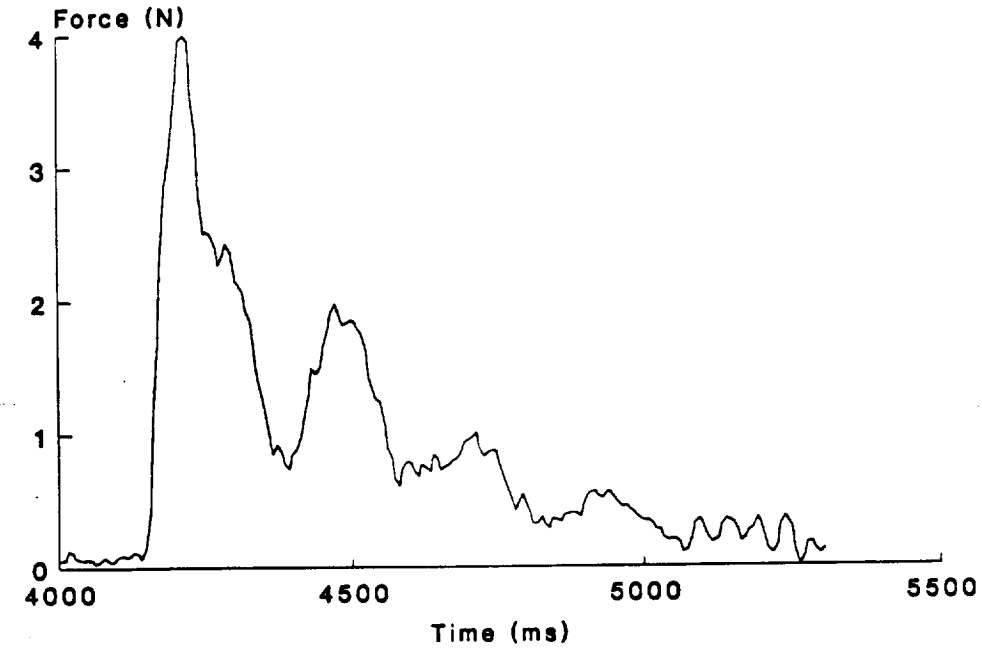


Force including inertial and other effects

**Figure 6.6: Comparison of magnet-only & extracted forces**

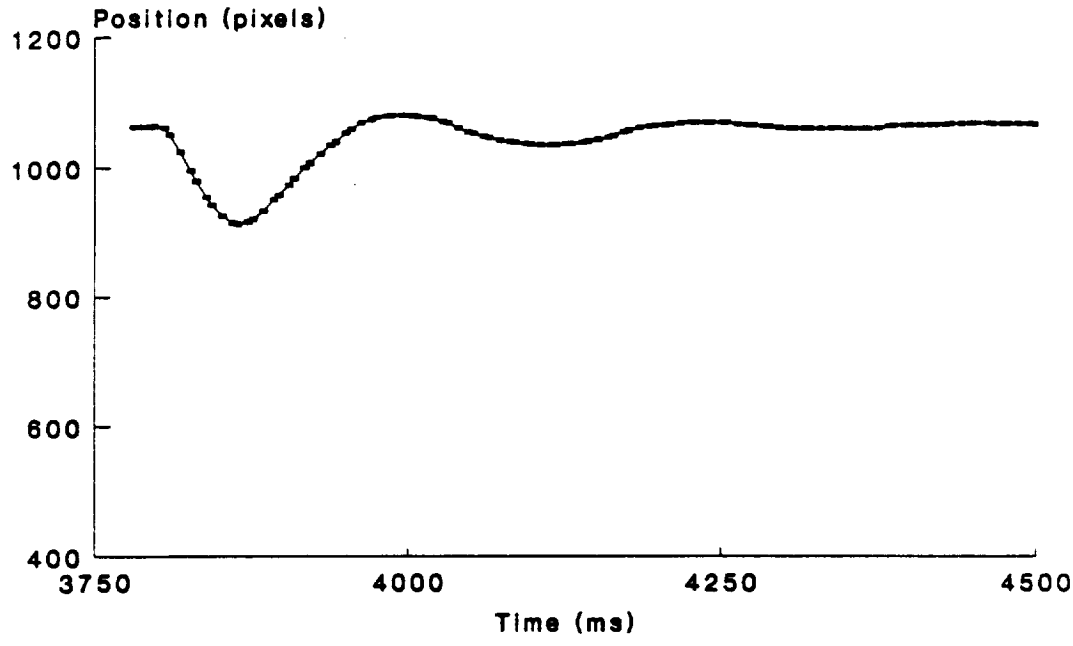


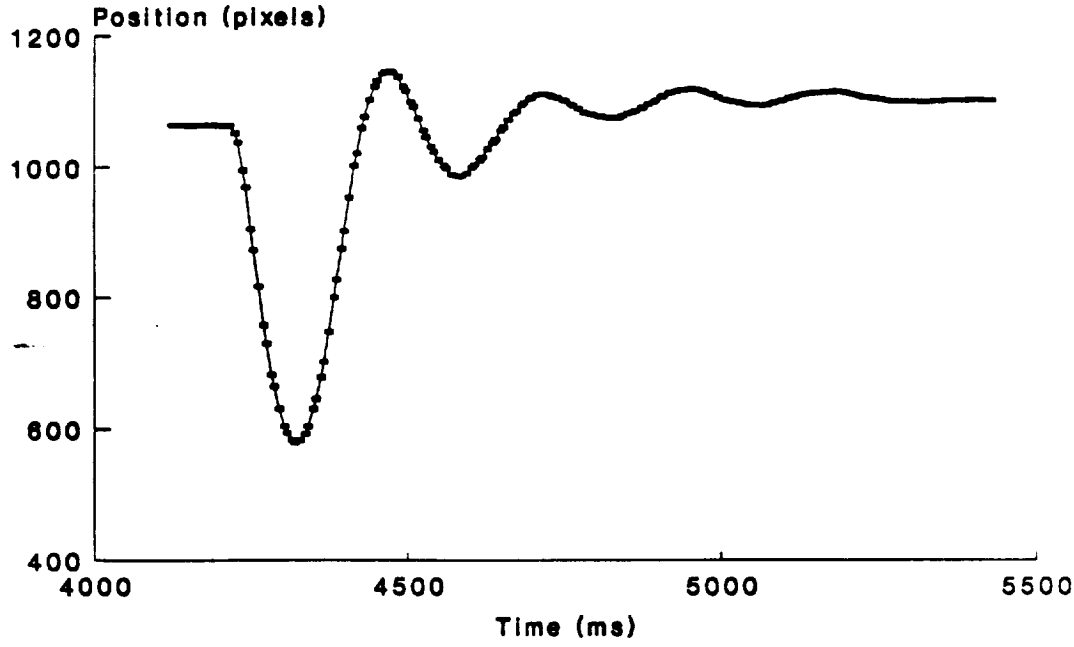


**Figure 7.1: Effect of thrust variation on axial response**

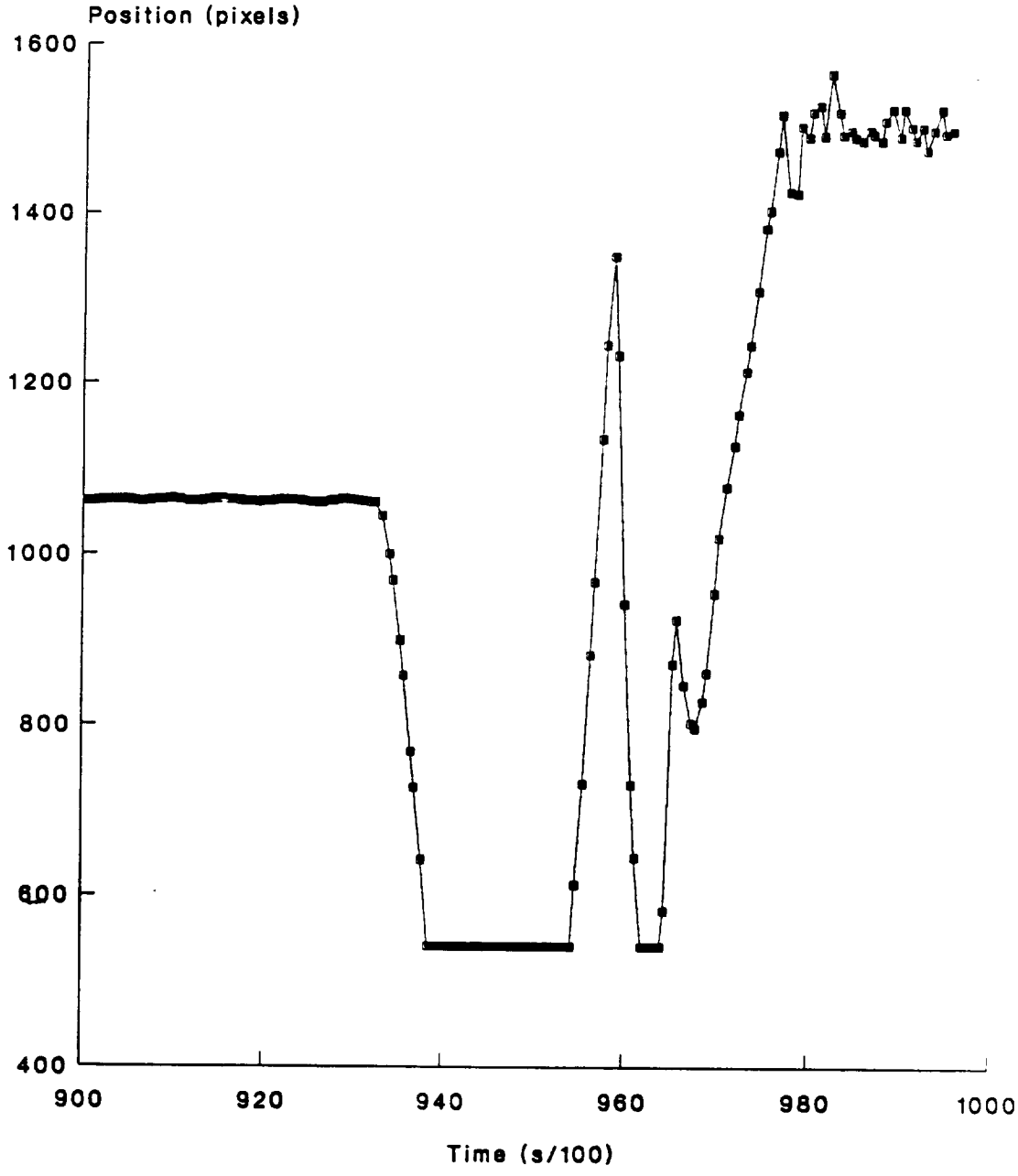


**Figure 7.2: Loss of control despite partial recovery into axial view**

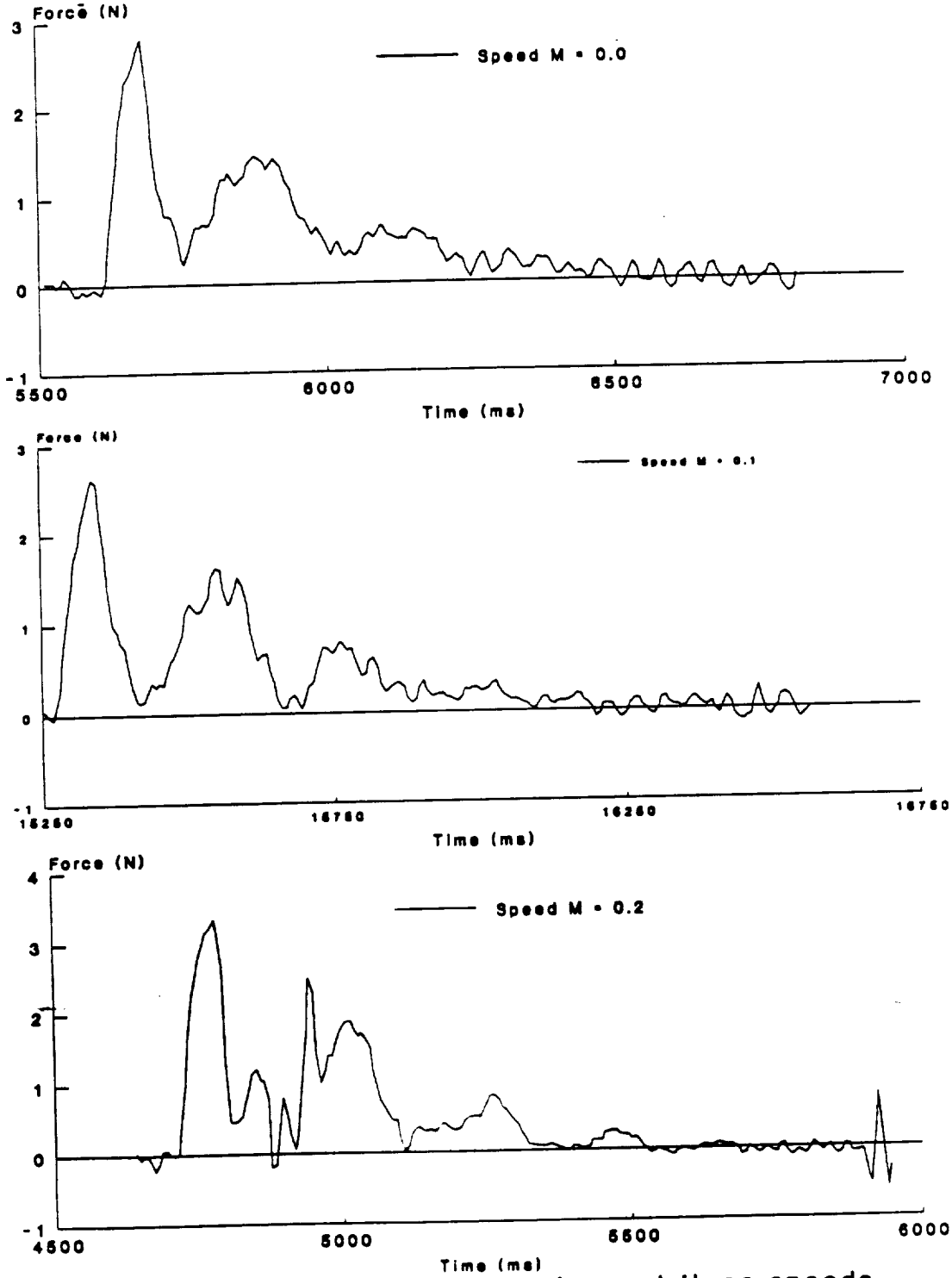


**Figure 7.3: Axial thrust-drag force at three speeds during thruster firing**

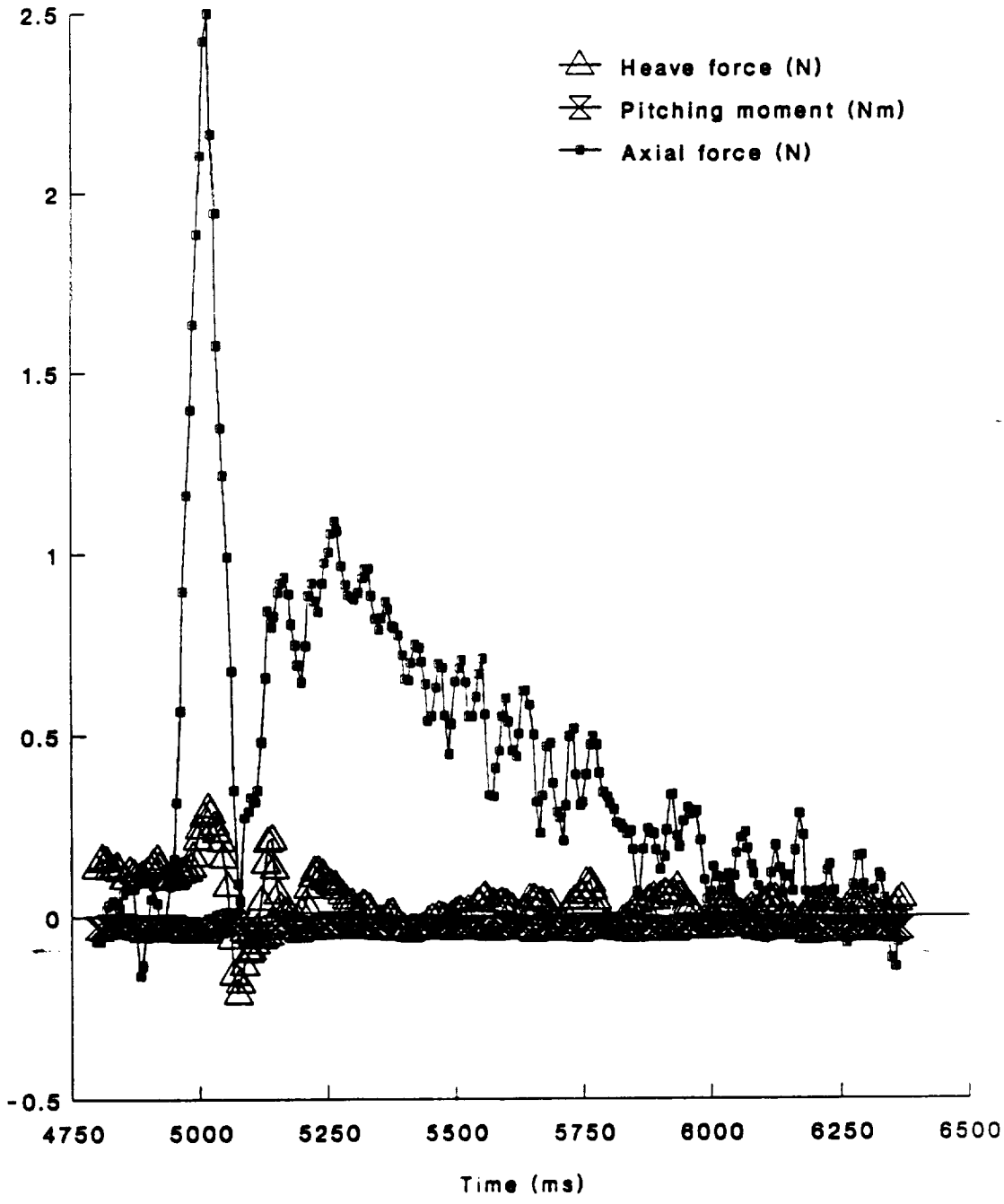


**Figure 7.4A: Force and moment results for 10 degree test wind-off**

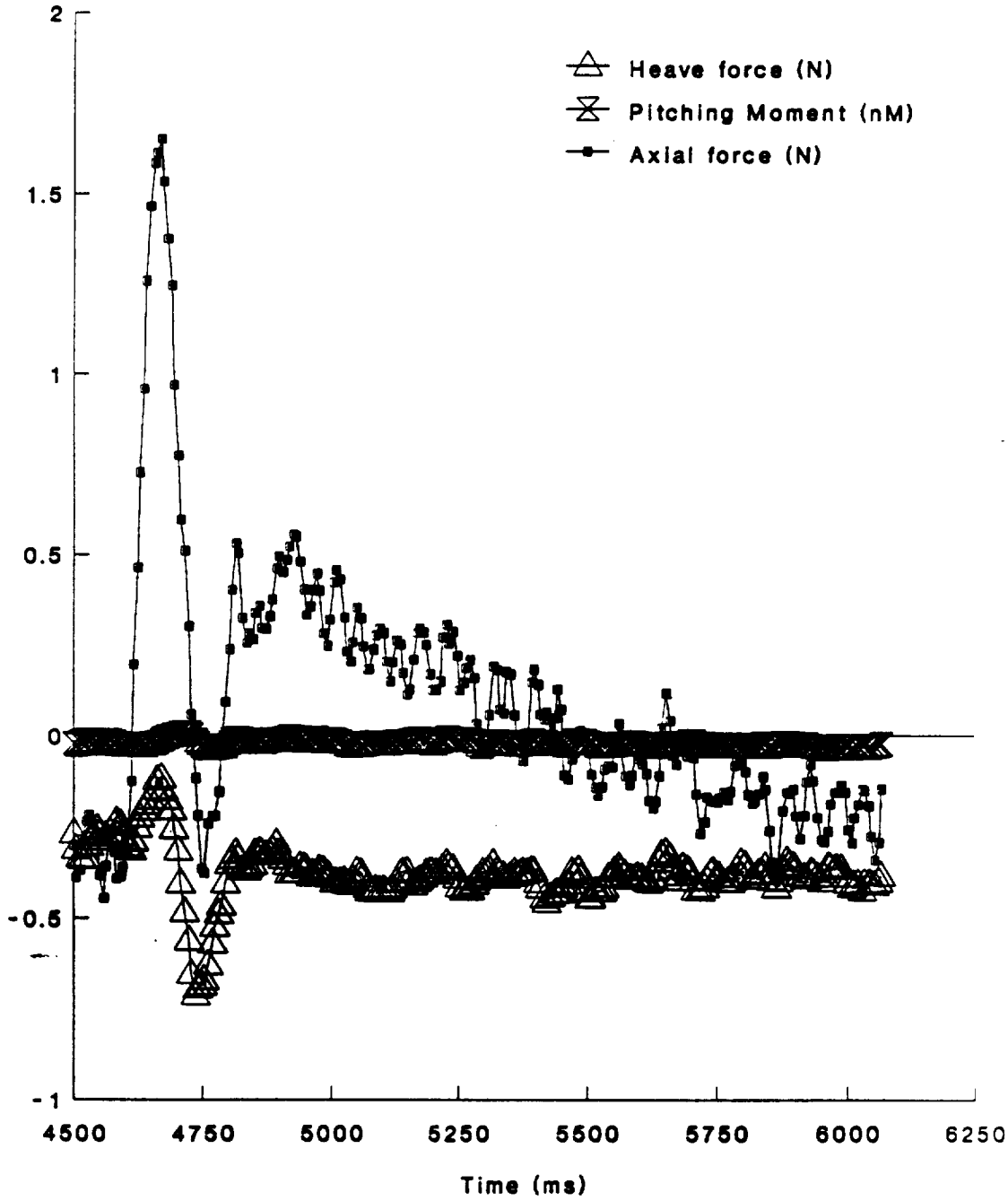


**Figure 7.4B: Force and moment results for 10 degree test at Mach 0.1**

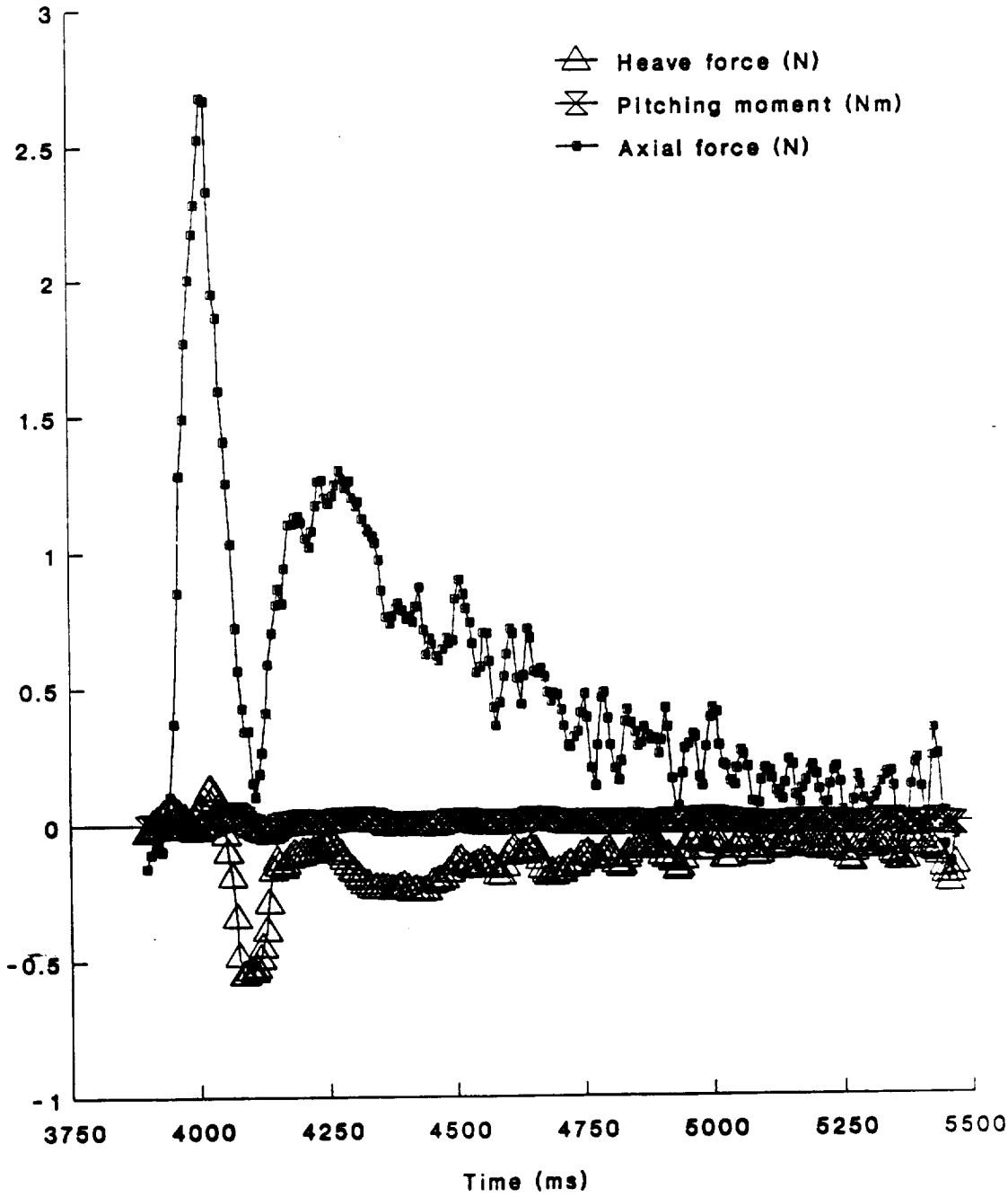


**Figure 7.4C: Force and moment results for 10 degree test at Mach 0.2**

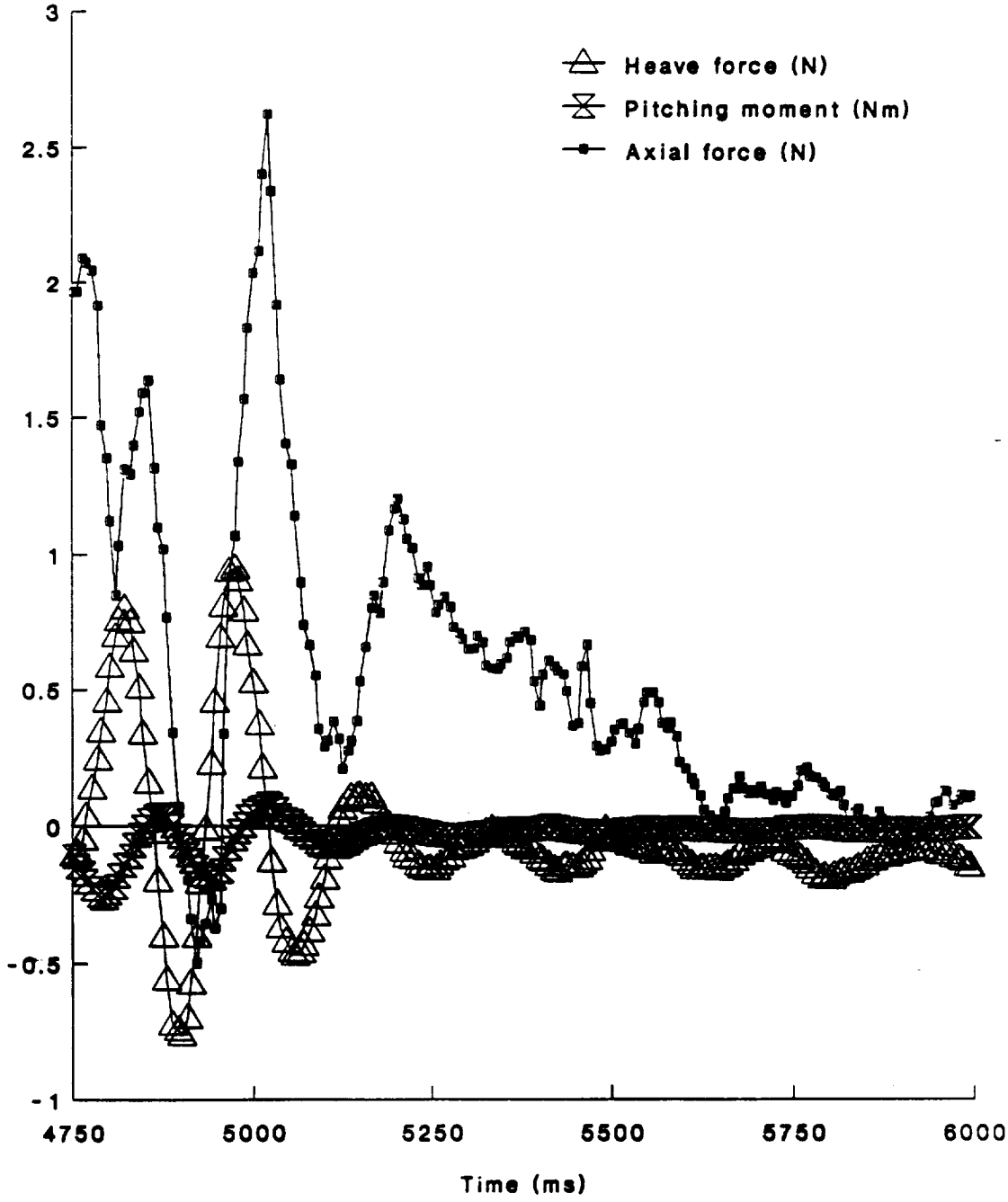


**Figure 7.5A: Force and moment results for twenty degree test wind-off**

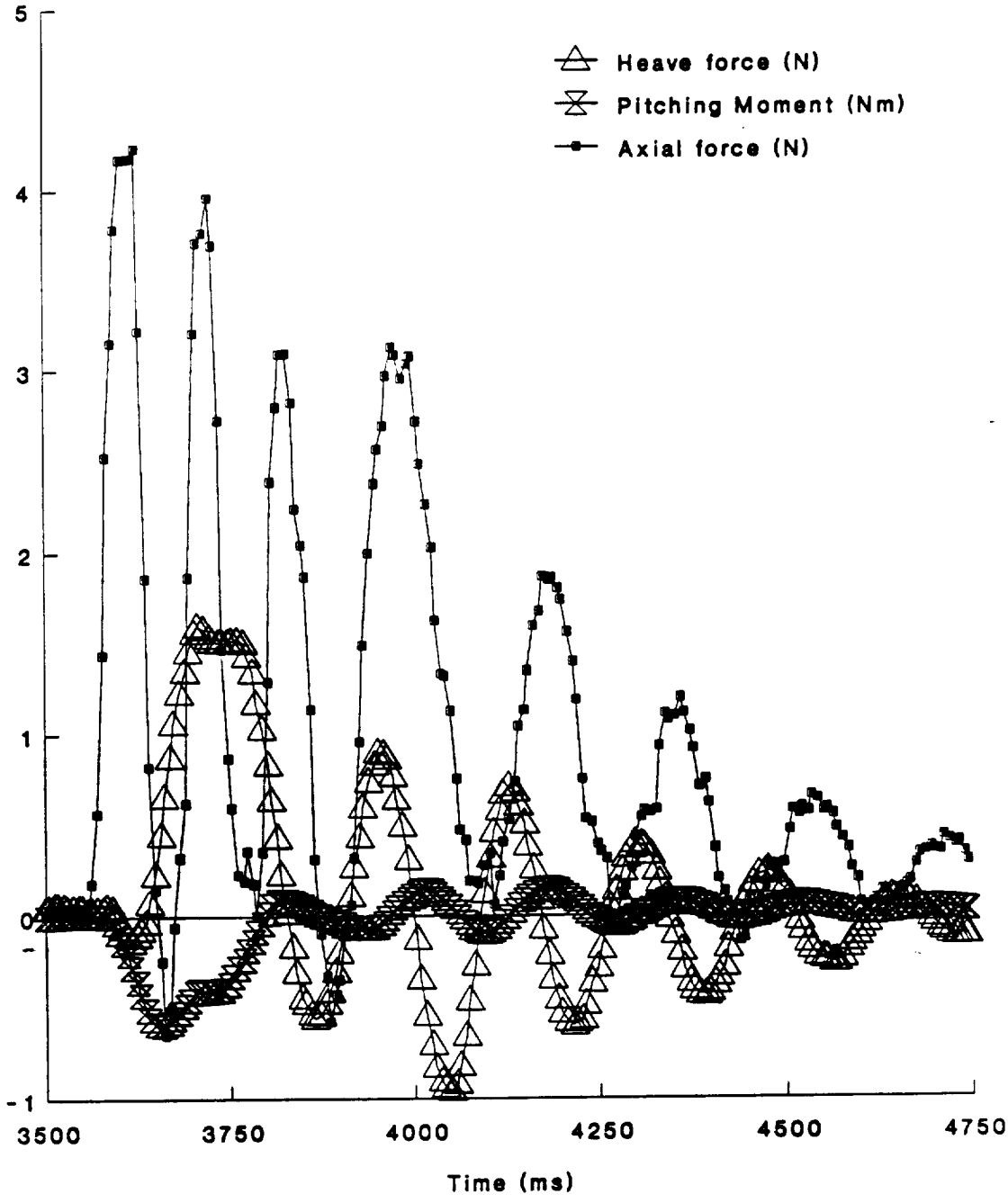


Figure 7.5B: Force and moment results
for twenty degree test Mach 0.1

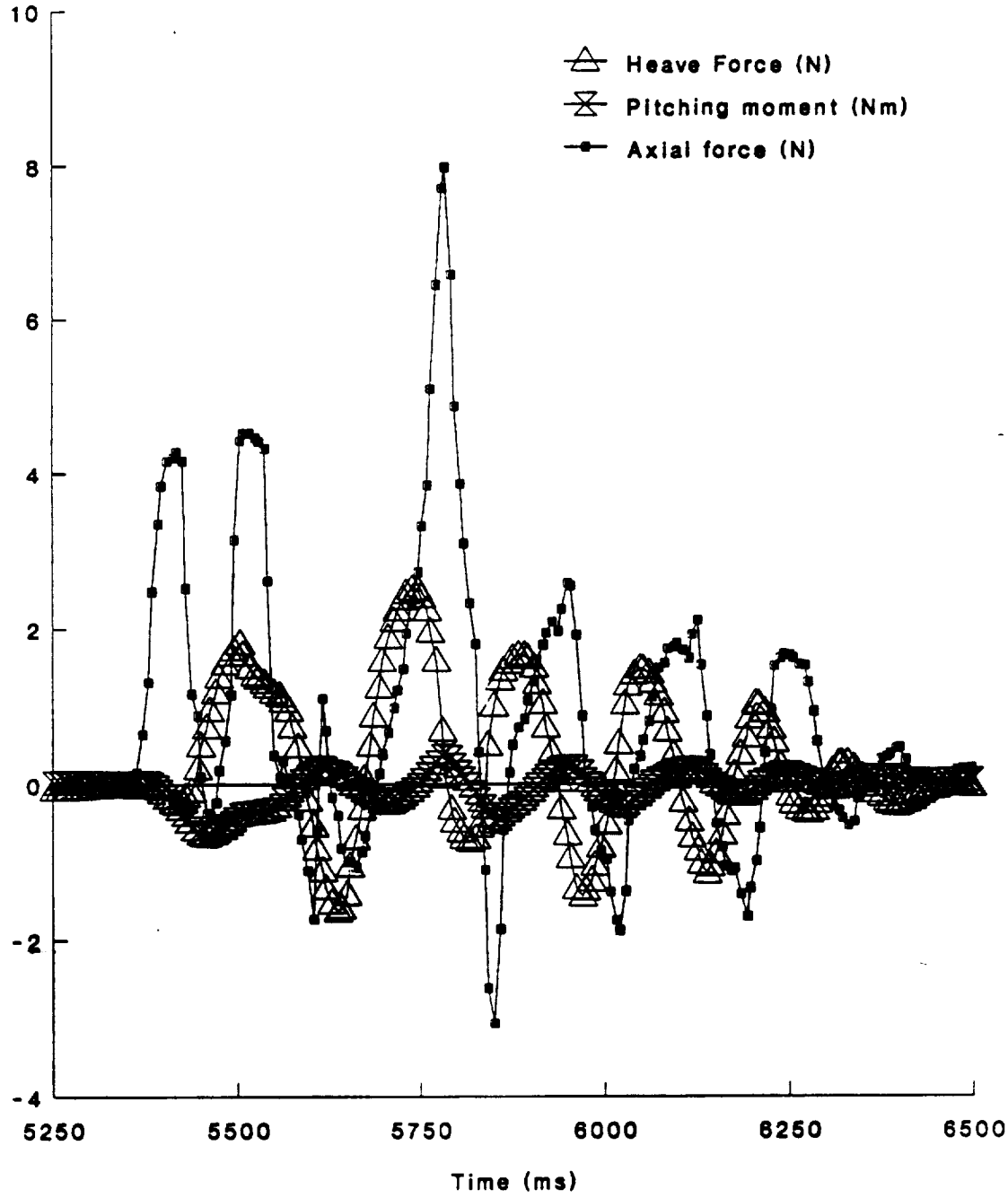


**Figure 7.5C: Force and moment results for twenty degree test Mach 0.2**

# REPORT DOCUMENTATION PAGE

*Form Approved OMB No. 0704-0188*



| 1. AGENCY USE ONLY *(Leave blank)* | 2. REPORT DATE | 3. REPORT TYPE AND DATES COVERED |
|---|---|---|
| | January 1992 | Contractor Report |

**4. TITLE AND SUBTITLE**
Propulsion Simulator for Magnetically-Suspended Wind Tunnel Models

**5. FUNDING NUMBERS**
C NAS1-18845
WU 505-59-54-01

**6. AUTHOR(S)**
P. B. Joshi, M. R. Malonson, G. P. Sacco, C. L. Goldey, K. Garbutt, and M. Goodyer

**7. PERFORMING ORGANIZATION NAME(S) AND ADDRESS(ES)**
Physical Sciences Inc.
20 New England Business Center
Andover, MA 01810

**8. PERFORMING ORGANIZATION REPORT NUMBER**
PSI-2090/TR-1140

**9. SPONSORING/MONITORING AGENCY NAME(S) AND ADDRESS(ES)**
National Aeronautic and Space Administration
Langley Research Center
Hampton, VA 23665-5225

**10. SPONSORING/MONITORING AGENCY REPORT NUMBER**
NASA CR-189560

**11. SUPPLEMENTARY NOTES** SBIR Phase II Final Report
Joshi, Malonson, Sacco, and Goldey: Physical Sciences Inc.
Garbutt and Goodyer: University of Shouthampton, Southhampton, UK
Langley Technical Monitor: Pierce Lawing

**12a. DISTRIBUTION/AVAILABILITY STATEMENT**
For Government Distribution Only

Subject Category 09

**12b. DISTRIBUTION CODE**

**13. ABSTRACT** *(Maximum 200 words)*

In order to demonstrate the measurement of aerodynamic forces/moments, including the effects of exhaust jets, in Magnetic Suspension and Balance Systen (MSBS) wind tunnels, two propulsion simulator models wer developed at Physical Sciences Inc. (PSI). Both the small-scale model (1 in. diameter X 8 in. long) and the large-scale model (2.5 in. diameter X 15 in. long) employed compressed, liquified carbon dioxide as a propellant. THe small-scale simulator, made from a highly magnetizable iron alloy, was demonstrated in the 7 in. MSBS wind tunnel at the University of Southampton. It developed a maximum thrust of approximately 1.3 lbf with a 0.098 in. diameter nozzle and 0.7 lbf with a 0.295 in. diameter nozzle. The Southampton MSBS was able to control the simulator at angles-of attack up to 20 deg. The large-scale simulator was demonstrated to oeprate in both a steady-state and a pulse mode via a miniaturized solinoid valve. It developed a stable and repeatable thrust of 2.75 lbf over a period of 4s and anozzle pressure ratio (NPR) of 5.

**14. SUBJECT TERMS**
Propulsion Simulation, Wind Tunnels, Magnetic Suspension

**15. NUMBER OF PAGES**
177

**16. PRICE CODE**

| 17. SECURITY CLASSIFICATION OF REPORT | 18. SECURITY CLASSIFICATION OF THIS PAGE | 19. SECURITY CLASSIFICATION OF ABSTRACT | 20. LIMITATION OF ABSTRACT |
|---|---|---|---|
| Unclassified | Unclassified | | |